High-Energy Scattering in strongly coupled $\mathcal{N} = 4$ super Yang-Mills Theory

Dissertation

zur Erlangung des Doktorgrades
an der Fakultät für Mathematik,
Informatik und Naturwissenschaften
Fachbereich Physik
der Universität Hamburg

vorgelegt von

Martin Sprenger

aus

Bad Soden am Taunus

Hamburg
2014

Datum der Disputation: 9. Juli 2014

Folgende Gutachter empfehlen die Annahme der Dissertation:

Prof. Dr. Volker Schomerus
Prof. Dr. Joachim Bartels
Prof. Dr. Gregory Korchemsky

Abstract

This thesis concerns itself with the analytic structure of scattering amplitudes in strongly coupled $\mathcal{N} = 4$ super Yang-Mills theory (abbreviated $\mathcal{N} = 4\,\mathrm{SYM}$) in the multi-Regge limit. Through the AdS/CFT-correspondence observables in strongly coupled $\mathcal{N} = 4\,\mathrm{SYM}$ are accessible via dual calculations in a weakly coupled string theory on an $\mathrm{AdS}_5 \times \mathrm{S}^5$-geometry, in which observables can be calculated using standard perturbation theory. In particular, the calculation of the leading order of the n-gluon amplitude in $\mathcal{N} = 4\,\mathrm{SYM}$ at strong coupling corresponds to the calculation of a minimal surface embedded into AdS_5. This surface ends on the concatenation of the gluon momenta, which is a light-like curve. The calculation of the minimal surface area can be reduced to finding the solution of a set of non-linear, coupled integral equations, which have no analytic solution in arbitrary kinematics. In this thesis, we therefore specialise to the multi-Regge limit, the n-particle generalisation of the Regge limit. This limit is especially interesting as even in the description of scattering amplitudes in weakly coupled $\mathcal{N} = 4\,\mathrm{SYM}$ in this limit a certain set of Feynman diagrams has to be resummed. This description organises itself into orders of logarithms of the energy involved in the scattering process. In this expansion each order in logarithms includes terms from every order in the coupling constant and therefore contains information about the strong coupling sector of the theory, albeit in a very specific way. This raises the central question of this thesis, which is how much of the analytic structure of the scattering amplitudes in the multi-Regge limit is preserved as we go to the strong coupling regime. We show that the equations governing the area of the minimal surface simplify drastically in the multi-Regge limit, which allows us to obtain analytic results for the scattering amplitudes. We develop an algorithm for the calculation of scattering amplitudes in the multi-Regge limit and apply it to the special cases of the 6- and 7-gluon amplitude. Our results show that for the cases under study the factorisation of the amplitude as predicted by Regge theory is also preserved in the strong coupling limit.

This thesis is based on the following publications:

- J. Bartels, V. Schomerus and M. Sprenger, *Heptagon Amplitude in the Multi-Regge Regime*, arXiv:1405.3658, submitted to JHEP.
- J. Bartels, J. Kotanski, V. Schomerus and M. Sprenger, *The Excited Hexagon Reloaded*, arXiv:1311.1512, submitted to JHEP as erratum to JHEP 1101 (2011) 069.
- J. Bartels, V. Schomerus and M. Sprenger, *Multi-Regge Limit of the n-Gluon Bubble Ansatz*, JHEP 1211 (2012) 145.

Contents

1. Introduction **6**

2. $\mathcal{N} = 4$ super Yang-Mills **12**
2.1. Field theory 12
2.2. AdS/CFT 12
2.3. Amplitudes at strong coupling 14
2.3.1. Finding the correct prescription 14
2.3.2. General solution for AdS_3 18
2.3.3. General solution for AdS_5 23

3. The multi-Regge limit **27**
3.1. Definition 27
3.2. Kinematical identities 29
3.3. Cross ratios in the multi-Regge limit 31
3.4. Weak coupling results 32

4. The Y-system in the multi-Regge limit **39**
4.1. Cross ratios and Y-functions 39
4.2. The multi-Regge limit of the Y-system 40
4.2.1. The 6-point case 40
4.2.2. The 7-point case 41
4.3. Large phases and residue contributions 44
4.3.1. The 8-point case 45
4.3.2. The n-point case 46

5. Calculating amplitudes in the multi-Regge limit **50**
5.1. Excited states and Bethe ansatz 50
5.2. An alternative Y-system 53
5.3. Numerical evaluation of the Y-functions 55
5.4. Regge regions 56

6. The 6-point amplitude **58**
6.1. Equations for the 6-point case 58
6.2. The remainder function R_6 in the Euclidean regime 59
6.3. Regge regions 60
6.4. The remainder function $R_{6,--}$ 61
6.4.1. Crossing solutions 62
6.4.2. Symmetries of the Y-system and endpoint conditions 62
6.4.3. Calculation of the amplitude 66
6.4.4. Comparison with weak coupling 68

7. The 7-point amplitude **70**
7.1. Cross ratios . . . 70
7.2. Regge regions . . . 71
7.3. Predictions from weak coupling . . . 72
7.4. Contributions to the remainder function . . . 74
7.4.1. The remainder function in the Euclidean regime . . . 75
7.5. Region $P_{7,--+}$ . . . 75
7.5.1. Continuation of the driving terms . . . 76
7.5.2. Crossing solutions . . . 76
7.5.3. Calculation of the remainder function $R_{7,--+}$ . . . 78
7.6. Region $P_{7,---}$ . . . 81
7.6.1. Continuation of the driving terms . . . 81
7.6.2. Crossing solutions . . . 82
7.6.3. Calculation of the remainder function $R_{7,---}$ . . . 85
7.7. Region $P_{7,-+-}$ . . . 87
7.7.1. Continuation of the driving terms . . . 87
7.7.2. Crossing solutions . . . 87
7.7.3. Calculation of the remainder function $R_{7,-+-}$ . . . 88
7.8. Comparison with weak coupling predictions . . . 88

8. Conclusions and outlook **90**

A. Acknowledgements **92**

B. Determination of the phases ϕ_s for the 7-point amplitude **93**

C. Residue structure for the large cross ratios in the MRL **95**

D. Kernels and S-matrices **97**
D.1. Kernels . . . 97
D.2. S-matrices . . . 98

E. Conformal Gram relations **99**

F. The remainder function $R_{7,+--}$ **101**

G. Zusammenfassung **104**

1. Introduction

Quantum field theory is the pillar on which modern physics rests. It is an indispensable tool from condensed matter physics to cosmology to particle physics and its success in describing nature has only recently again been demonstrated in the discovery of a Higgs-like boson at the LHC [1,2]. But still, eighty years after quantum field theories have first been studied, no four-dimensional, interacting quantum field theory has ever been solved exactly. The lack of exact solutions is partly explained by that fact that standard methods for the perturbative computation of observables using Feynman diagrams work nicely in principle, but quickly become cumbersome beyond the simplest examples, making it difficult to generate exact data. However, the final result is often much simpler than intermediate expressions. The prime example for this is the Parke-Taylor formula [3], describing a colour-ordered n-gluon maximally helicity violating (MHV) scattering amplitude[1] at tree level, which, written in spinor helicity variables, is given by

$$A_n^{\text{tree}}(1^+,\dots,i^-,\dots,j^-,\dots,n^+) = \frac{\langle ij\rangle^4}{\langle 12\rangle\cdots\langle n1\rangle}. \tag{1.1}$$

This formula is valid for any number n of gluons. The simplicity of this one-line formula is to be compared with the effort of calculating and summing up $\mathcal{O}(n!)$ Feynman diagrams, every single one being more complicated than the final result. This formula begs for another, simpler description.

Over the last decade new powerful methods were developed that allow the calculation of scattering amplitudes without resorting to Feynman diagrams. In fact, the proof of the Parke-Taylor formula Eq.(1.1) is by now textbook material (see, for example, [4]). This progress is mostly due to calculations performed in a special theory, $\mathcal{N}=4$ supersymmetric Yang-Mills theory with gauge group $SU(N)$, which we abbreviate as $\mathcal{N}=4\,\text{SYM}$. This theory is conformally invariant even at the quantum level and is currently the best candidate for being a completely solvable quantum field theory, at least in the planar limit $N\to\infty$. In fact, the scaling dimension of certain operators in $\mathcal{N}=4\,\text{SYM}$ can by now be calculated efficiently using integrability techniques at all values of the coupling constant [5–10] and it would be desirable to understand how this success can be lifted to more complicated observables.

After scaling dimensions, scattering amplitudes are the simplest quantities characterising a theory. They are of course richer objects than operator dimensions because they are functions of the kinematical invariants and not just numbers, but they still depend solely on on-shell degrees of freedom. Another observable closely related to scattering amplitudes are form factors, which are basically scattering amplitudes with operator insertions and therefore mixtures between off-shell and on-shell degrees of freedom. While

[1] MHV amplitudes describe the scattering of n outgoing gluons with $n-2$ gluons having positive helicity and 2 gluons having negative helicity. Accordingly, amplitudes with k gluons having negative helicities are called N^{k-2}MHV.

these observables are studied, as well (see for example [11–20]), it is fair to say that the main focus still lies on the determination of scattering amplitudes. Correlation functions, being completely off-shell objects are even more complicated and are not part of this review. It should be noted that $\mathcal{N}=4$ SYM is not realised in nature, of course, but it is certainly a non-trivial gauge theory and understanding any four-dimensional gauge theory non-perturbatively would be a great success. The hope connected with the programme of solving $\mathcal{N}=4$ SYM certainly is that the obtained results and the techniques developed along the way have validity beyond this particular theory.

The way research on scattering amplitudes developed over the last years typically proceeded along the following steps: a difficult calculation was performed, a simple result was obtained and once the result was understood properly, the result became almost obvious. An example of this, similar in spirit to the Parke-Taylor formula, is a calculation performed by Bern, Dixon and Smirnov [21]. In [21], the authors calculate the 4-gluon MHV amplitude at three loops by standard methods and find that the amplitude exponentiates. More precisely, generalising their result to the n-gluon MHV amplitude they find that

$$\log M_n(\varepsilon) := \log \frac{A_n}{A_n^{\text{tree}}} = \sum_{l=1}^{\infty} a^l \left(\frac{\gamma_K^{(l)}}{(l\varepsilon)^2} + \frac{\gamma_{col}^{(l)}}{l\varepsilon} \right) \sum_{i=1}^{n} \left(\frac{\mu^2}{-(p_i+p_{i+1})^2} \right)^{l\varepsilon} + \gamma_K(a) F_n^{(1)} + C_n(a) + \mathcal{O}(\varepsilon), \tag{1.2}$$

In this expression, μ is the renormalisation scale of the coupling constant $a = \frac{\alpha_s N}{2\pi} \left(4\pi e^{-\gamma}\right)^{\varepsilon}$ and the $C_n(a)$ are functions with a fixed transcendental weight (for explicit expressions see [21]). Furthermore, $\gamma_K^{(l)}$ and $\gamma_{\text{col}}^{(l)}$ are the l-loop coefficients of the cusp and collinear anomalous dimension, respectively. Most notably, all kinematical dependence in the IR-finite piece is stored in $F_n^{(1)}$ whose coupling dependence is determined solely by the overall factor of the cusp anomalous dimension $\gamma_K(a)$, which is known to all orders in perturbation theory [22]. This finite piece can therefore be determined from a one-loop calculation.

The BDS ansatz is remarkable since not only the IR-divergent part, but also the finite pieces of the amplitude exponentiate and it was conjectured that this is the answer to all loop orders. As it turns out, this conjecture is wrong as was shown by an explicit Wilson loop calculation [23], a calculation at strong coupling [24] and considerations in the multi-Regge limit [25]. However, it was soon found that $\mathcal{N}=4$ SYM has a dual conformal symmetry. This is another conformal symmetry, unrelated to the space-time conformal symmetry of $\mathcal{N}=4$ SYM, which is not obvious from the Lagrangian and which was found both in weak [26] and strong coupling [27] calculations. Once the presence of this symmetry was understood it became clear that scattering amplitudes have to satisfy an anomalous Ward identity for dual conformal symmetry [28] for which the finite piece of the BDS ansatz provides the solution to the anomalous part. This allows us to write any MHV amplitude as

$$A_{n,\text{MHV}} = A_{n,\text{MHV}}^{\text{tree}} e^{A_{\text{BDS}}+R}, \tag{1.3}$$

where the *remainder function* e^R must be a function of dual conformal invariants, so-called cross ratios. Those are only available for more than five gluons, which in turn means that the BDS ansatz in fact gives the full answer for the MHV amplitude for four and five gluons, again nurturing the hopes that scattering amplitudes in $\mathcal{N}=4$ SYM indeed can be solved completely. In hindsight, it is therefore clear that the BDS ansatz is, up to the remainder function, the only possible solution consistent with dual conformal symmetry,

nicely showing the transition of very difficult calculations becoming almost trivial in the course of a few years.

The main goal then is, of course, the determination of the remainder functions. For the simplest case, namely the 6-point MHV amplitude, the remainder function is by now known to four-loop order [29–31]. Reference [31] nicely shows the current state of art of the field as no reference to any loop integration is made in the calculation. Rather, the answer is fully fixed by understanding the class of functions that can appear in the result, as well as using certain kinematical limits. Whether this programme can easily be lifted to higher loop orders is still an open question, but it certainly shows the superiority of these modern approaches over standard QFT methods.

It is important to note that the study of scattering amplitudes in $\mathcal{N} = 4$ SYM certainly goes beyond just simplifying calculational methods, it has led to conceptual insights. As a specific example, let us mention colour-kinematics duality [32]. Roughly speaking, this duality relates L-loop integrands in gravity theories with two L-loop integrands of a gauge theory in a specific way, see for example [4] for a proper description. While this duality is so far only proven at tree level [33] (steps towards a proof at one-loop level are presented in [34, 35]), it shows that gravity amplitudes might be conceptually much simpler than is expected from a standard Feynman graph analysis and no more difficult than amplitudes of a gauge theory. In fact, this relation to gauge theory can be used to improve the power-counting analysis of supersymmetric gravity theories which is typically too pessimistic when using Feynman graphs [36]. It also provides a tool for performing high-loop integrals in gravity theories, which might settle the interesting question whether $\mathcal{N} = 8$ SUGRA is a finite theory or not [37–39].

Scattering amplitudes at strong coupling

The enormous progress described in the previous paragraphs, however, is not limited to weak coupling calculations. Through the AdS/CFT-correspondence [40], we have access to the strong coupling regime of $\mathcal{N} = 4$ SYM, which, in fact, is the main focus of this thesis. As we will explain in much more detail in chapter 2, AdS/CFT relates strongly coupled $\mathcal{N} = 4$ SYM with a weakly coupled string theory on an $\mathrm{AdS}_5 \times \mathrm{S}^5$ background, which is amenable to a standard perturbative treatment. Specialising further to the planar limit of $\mathcal{N} = 4$ SYM, the theory is related to the supergravity limit of classical string theory on this particular background, which means that observables in strongly coupled $\mathcal{N} = 4$ SYM are determined by classical calculations on the string side of the correspondence. In this framework, scattering amplitudes have first been studied in [27] and a solution is developed in a series of papers [41–44] which relate a scattering amplitude of strongly coupled $\mathcal{N} = 4$ SYM to the area of a minimal surface which is embedded into AdS_5 and ends on the concatenation of the gluon momenta on the boundary of AdS_5. Using integrability, the area of this minimal surface can be calculated through the solution of a set of complicated non-linear, coupled integral equations. These particular equations have the form of a thermodynamic Bethe ansatz which usually appears in quantum integrable models. In fact, it is known that the sigma model describing classical string theory on $\mathrm{AdS}_5 \times \mathrm{S}^5$ is classically integrable, i.e. that an infinite amount of conserved charges exists [45], supporting the suspicion that $\mathcal{N} = 4$ SYM is integrable for every value of the coupling constant. In a similar way to the scattering amplitudes, form factors were studied in strongly coupled $\mathcal{N} = 4$ SYM in [24] and progress towards a full solution is made in [46,47].

It should be remarked that $\mathcal{N} = 4$ SYM is not the only theory whose strong coupling

behaviour can be described by a gravity dual. Another well-studied example is ABJM theory [48], which is a three-dimensional Chern-Simons theory arising from the duality with a string theory on $\mathrm{AdS}_4 \times \mathbb{C}\mathrm{P}^3$. However, very little is known about scattering amplitudes at strong coupling in this theory, mostly because it is not clear how to realise a fermionic T-duality at strong coupling in a similar way to $\mathcal{N} = 4$ SYM (see for example the discussion in [49]).

If we want to move from high-loop order calculations at weak coupling to an all-loop order ansatz, the strong coupling expressions derived from AdS/CFT will provide strong constraints on a possible ansatz and it is therefore vital to carefully study strong coupling amplitudes. In the same way, the solution to the operator dimensions in $\mathcal{N} = 4$ SYM was only found after taking into account strong coupling input.

While a full solution for scattering amplitudes at strong coupling exists as mentioned before, this is not the end of the story: the strong coupling description consists of a set of implicit integral equations which do not allow an analytic solution for arbitrary kinematics. This makes a comparison with weak coupling results very difficult. In this thesis, we therefore try to solve a simpler problem by specialising to a special high-energy regime, called the multi-Regge limit (abbreviated MRL).

Other kinematical choices are, of course, possible. For example, in [50–52] the external momenta are restricted to a two-dimensional subspace, which in the strong coupling picture corresponds to a minimal area embedded into an AdS_3-subspace of the full AdS_5. Furthermore, the limit in which the boundary polygon becomes regular is studied in [53–56]. Another natural kinematical limit to consider is the collinear limit, which gives rise to an OPE-like expansion for light-like Wilson loops [57–60]. From this approach, first all-loop proposals emerged [61–63] based on integrability techniques for the GKP string [64, 65] which, for example, helped to constrain the four-loop remainder function for the 6-point amplitude in [31].

The multi-Regge limit

The multi-Regge limit is by definition the limit for a $2 \to n-2$ particle amplitude in which the rapidities of the outgoing particles are strongly ordered. This is the natural generalisation of the well-known Regge limit $s \gg -t$ for four-particle scattering. This limit has received a lot of attention as it describes high-energy scattering in QCD and is therefore of phenomenological importance, see for example [66]. The multi-Regge limit is special as it naturally reorganises the perturbative expansion. In fact, even if calculations are performed at weak coupling α_s, loop integrals can lead to large compensating factors such that the dominant part of the n-loop contribution is proportional to $\alpha_s^n \log^n s \sim \mathcal{O}(1)$, where s is the energy involved in the scattering process. Since this is not a small parameter, these contributions have to be resummed. Summing the dominant diagrams leads to the so-called leading logarithmic approximation (abbreviated LLA). The resummation of all dominant diagrams works out in such a way that the answer looks like an effective particle with t-dependent spin, a so-called Reggeon, is exchanged. Remarkably, if one allows for several Reggeons to be exchanged, their evolution is described by the Hamiltonian of an integrable spin chain [67–69]. This is already true for multi-colour QCD. How this spin chain integrability relates to the integrability seen in $\mathcal{N} = 4$ SYM is a very interesting and still open question.

The multi-Regge limit has also been studied in $\mathcal{N} = 4$ SYM, both employing methods similar to those in QCD and using the modern methods developed in the last years. The

class of functions governing the multi-Regge limit is identified in [70]. It is a special class of harmonic polylogarithms and this basis turns out to be restrictive enough to easily determine the expansion in the coupling constant at a given logarithmic accuracy. Such an expansion can provide strong constraints on a general ansatz for an amplitude and was indeed used to bootstrap the four-loop remainder function in the 6-point case. Furthermore it is shown in [71] that this class of functions can be used to analytically determine the coefficients in the Mueller-Navelet dijet cross section to any loop order in LLA. In LLA, QCD and $\mathcal{N} = 4$ SYM give the same results, showing that the methods developed in $\mathcal{N} = 4$ SYM can have direct impact in phenomenological applications. If and how this analysis extends to NLLA in either QCD or $\mathcal{N} = 4$ SYM is an open problem.

Further studies in the multi-Regge limit include the study of the Wilson line picture [72] and the study of the multi-Regge limit in colour-kinematics duality [73, 74]. In this thesis we will focus on results obtained in [25, 75] which are based on the factorisation of amplitudes in the multi-Regge limit. By studying the BDS ansatz in various kinematical regimes which are defined by the signs of the Mandelstam invariants, it is shown in [25] that the BDS ansatz does not have the correct analytic structure starting from six gluons to be compatible with the expected factorisation of the amplitude. Practically, this means that another term has to be present to fix the analytic structure, which is just the remainder function mentioned before. From this framework it is furthermore possible to derive a dispersion relation-like expression for the remainder function [76]. Physically, these contributions arise from a Regge cut generated by the bound state of two Reggeons. Finding the strong coupling equivalent of these Regge cut contributions will be a main aspect of this thesis. Since they will play a major role in our investigations, we will describe these factorisation-based methods in some detail in chapter 3.

As remarked before, due to the necessary resummation of the large logarithms, every logarithmic order contains all-loop information in the coupling constant, albeit in a very specific way. Hence it is a very natural question to ask how much of the all-loop information as obtained from a weak coupling calculation in the multi-Regge limit survives as we go to the strong coupling regime. This is the central question of this thesis and will guide us through the following chapters.

Organisation of this thesis

Some comments on the organisation of this thesis are in order. As explained in the last sections, the results we find are ultimately results about the structure of a gauge theory at strong coupling. However, the methods which lead us to these results are purely string-theoretic. We therefore focus on the description of the string theory side and introduce the gauge-theoretic description along the way to an extent which allows a comparison with our results. In detail, this thesis is organised as follows:

- In chapter 2 we provide a self-contained introduction to the calculation of scattering amplitudes via AdS/CFT, showing the relation to the calculation of minimal surfaces and a review of the integrability techniques that lead to the set of integral equations governing the amplitudes.

- Chapter 3 then introduces the multi-Regge limit. After a proper definition and the introduction of the kinematical invariants we use, we derive some necessary kinematical identities and briefly review the methods and results from weak coupling to which we want to compare our results in later chapters.

- In chapter 4 we then combine the two subjects and study the equations governing the strong coupling amplitudes in the multi-Regge limit. We find that the integral equations simplify drastically and allow us to obtain analytic results for the scattering amplitudes. The results we find provide a clear path towards an explicit algorithm which determines the amplitudes in the multi-Regge limit. These results are originally obtained in [77].

- This algorithm is worked out in detail for a general number of gluons in chapter 5. We will find that there exists a set of Bethe ansatz equations which determine the amplitude. In order to find the correct solution of the Bethe ansatz we have to perform numerical calculations which are also explained.

- Following [78–80] this algorithm is then applied to the calculation of the 6- and 7-point amplitudes in chapters 6 and 7, respectively. Our results are nicely consistent with gauge theory calculations at weak coupling, which we review, as well.

- We conclude in chapter 8 and highlight opportunities for future work. Technical details are collected in several appendices.

2. $\mathcal{N} = 4$ super Yang-Mills

2.1. Field theory

The theory under investigation in this thesis is maximally supersymmetric $\mathcal{N} = 4$ Yang-Mills theory with gauge group $SU(N)$. Its field content is fully fixed by extended supersymmetry [81] and consists of a vector field A_μ, 4 Weyl fermions $\psi_{aA}, \bar{\psi}^{\dot{a}}_A$ with $a, \dot{a} = 1, 2$ and $A = 1, \ldots, 4$ and 6 real scalars ϕ^{AB} with antisymmetric superscript. In total these are $2 + 6$ bosonic and $4 \cdot 2$ fermionic degrees of freedom. All fields are in the adjoint representation of $SU(N)$, which means that we can write them as matrices $X = t_a X^a$ with t_a, $a = 1, \ldots, N^2 - 1$, being a set of traceless anti-Hermitian $N \times N$ matrices which generate the fundamental representation of the gauge group $SU(N)$. The Lagrangian of this theory can be obtained by dimensional reduction of ten-dimensional $\mathcal{N} = 1$ super Yang-Mills theory, which results in

$$\begin{aligned}\mathcal{S} =& \frac{1}{g^2_{YM}} \int d^4x \,\mathrm{Tr}\left(-\frac{1}{4} F_{\mu\nu} F^{\mu\nu} - \left(D_\mu \phi_{AB}\right)\left(D^\mu \phi^{AB}\right) - \frac{1}{2}\left[\phi_{AB}, \phi_{CD}\right]\left[\phi^{AB}, \phi^{CD}\right] \right. \\ & \left. + i\bar{\psi}^A_{\dot{a}} \sigma^{\dot{a}a}_\mu D^\mu \psi_{aA} - \frac{i}{2}\psi^a_A \left[\phi^{AB}, \psi_{aB}\right] - \frac{i}{2}\bar{\psi}^A_{\dot{a}} \left[\phi_{AB}, \bar{\psi}^{\dot{a}B}\right] \right), \end{aligned} \tag{2.1}$$

with two free parameters, g_{YM} and N, the covariant derivative D_μ and some matrices $\sigma^{\dot{a}a}_\mu$, see [82] for details. This theory has the remarkable property that the coupling constant g_{YM} does not run [83, 84], which implies that the classical conformal symmetry of the theory is maintained also at the quantum level and the theory is ultraviolet finite. Since this is a massless gauge theory, it still contains infrared divergences which we will discuss later on.

From the Lagrangian Eq.(2.1) we could in principle deduce the Feynman rules and start calculating scattering amplitudes or other observables. However, as already explained in the introduction, research of the last ten years shows that there are much smarter ways to perform calculations, which include different choices of variables, the use of symmetries and knowledge about the class of functions governing a given observable. As we will not perform any perturbative field theory calculation in this thesis, we refrain from going into more details. Recent reviews of this beautiful subject include [4, 82].

2.2. AdS/CFT

The framework which allows us to go beyond pure field-theoretic weak coupling calculations in $\mathcal{N} = 4$ SYM is the AdS/CFT-correspondence [40, 85, 86]. Let us therefore briefly introduce the main ideas, for detailed reviews we refer the reader to [87, 88].

AdS/CFT is a duality between a string theory and a field theory and arises from the study of D-brane solutions. Let us therefore consider type IIB string theory with a stack of N D3-branes in flat ten-dimensional Minkowski space. The excitations of this theory

contain open strings which end on the branes, as well as closed strings from the excitations of the flat space. Furthermore, the open and closed strings can interact, so that the total effective action for this setting in the low-energy limit schematically reads

$$S = S_{\text{brane}} + S_{\text{bulk}} + S_{\text{int}}, \tag{2.2}$$

where S_{bulk} describes the massless excitations of the closed strings, which is just type IIB supergravity. S_{brane} describes the low-energy limit of the world-volume theory on the D3-branes which is $U(N)$ $\mathcal{N} = 4$ SYM with higher-derivative corrections. Finally, S_{int} describes the interaction between the two systems. However, taking the low-energy limit in which all dimensionless quantities are held fixed while $\alpha' \to 0$, Maldacena shows in [40] that the interaction part of Eq.(2.2) vanishes and the bulk and the brane sectors decouple. Furthermore, this limit suppresses all higher-derivative terms in the world-volume theory and we end up with pure $U(N)$ $\mathcal{N} = 4$ SYM.

On the other hand, the branes can be interpreted as solitonic solutions of the classical supergravity equations of motion. In fact, the solution for the case at hand is known and the backreaction of the stack of branes on the metric is given by

$$ds^2 = H^{-\frac{1}{2}} \eta_{\mu\nu} dx^\mu dx^\nu + H^{\frac{1}{2}} \left(dr^2 + r^2 d\Omega_5^2 \right), \text{ where } H = 1 + \frac{R^4}{r^4} \tag{2.3}$$

and $R^4 = 4\pi g_s \alpha'^2 N$, with the string coupling constant g_s. For large r this reduces to flat ten-dimensional space. To see what happens close to the branes, we make a change of variables $z := \frac{R^2}{r}$ and find

$$ds^2 = \frac{R^2}{z^2} \left(\eta_{\mu\nu} dx^\mu dx^\nu + dz^2 \right) + R^2 d\Omega_5^2 \tag{2.4}$$

in the limit $r \ll R$, which is the metric of the product space $\text{AdS}_5 \times \text{S}^5$. One can then wonder which excitations an observer at infinity would see in the low-energy limit. Firstly, the massless excitations for $r \gg R$ contribute, which is just the field content of type IIB supergravity. However, excitations from the region $r \ll R$ are highly redshifted due to the redshift factor calculated from Eq.(2.3) and an observer at infinity would measure the energy

$$E_\infty = E_0 \sqrt{\frac{g_{tt}(r)}{g_{tt}(\infty)}} \cong E_0 \frac{r}{R}. \tag{2.5}$$

Therefore, massive excitations from the region $r \ll R$ survive the low-energy limit and an observer at infinity would see the full spectrum of type IIB string theory on $\text{AdS}_5 \times \text{S}^5$. As it turns out, the two regions $r \lesseqgtr R$ decouple because of the gravitational potential close to $r \sim 0$.

We see that in both interpretations of the brane system, we find a decoupled system of type IIB supergravity. Since we started from the same situation and just interpreted the D-brane system differently, this result suggests that we should also identify the other decoupled systems, which gives rise to the idea that $\mathcal{N} = 4$ SYM is equivalent to type IIB string theory on $\text{AdS}_5 \times \text{S}^5$. This is a remarkable idea as it postulates the equivalence of a field theory with a theory of quantum gravity.

Keeping track of the parameters in the above considerations, one finds the following correspondence,

$$g_{YM}^2 = g_s, \quad R^4 = 4\pi g_s N \alpha'^2. \tag{2.6}$$

In its strongest form the AdS/CFT hypothesis proposes the equivalence of the two models for any value of g_s and N. However, arbitrary values of g_s and N include very quantum regimes of either theory and it is difficult to make any progress beyond comparing static elements such as the symmetry groups or the mapping of states. But even classical limits lead to very non-trivial statements. Using Eq.(2.6) we see that the limit

$$N \to \infty, \text{ with } \lambda := g_{YM}^2 N \text{ fixed}, \tag{2.7}$$

where λ is called 't Hooft coupling, identifies the planar limit of the field theory with a free string theory. Taking the $\lambda \to \infty$ limit, we end up with the identification of the infinite coupling limit of planar $\mathcal{N} = 4$ SYM with the SUGRA approximation of classical string theory on $AdS_5 \times S^5$, which is the weakest form of the hypothesis. This is a very interesting regime, as it provides access to the strong coupling regime of a field theory which is not accessible from standard perturbation theory. Turning this around, the AdS/CFT duality relates a non-perturbative string theory with a perturbative field theory, which might actually serve as a non-perturbative definition of string theory. Of course, this virtue of the duality also reflects the enormous difficulty in proving it - we have to face non-perturbative effects on at least one side of the correspondence. In the $N \to \infty$ limit progress is made using integrability techniques (for a review see [89]), some of which we will review below. In this thesis, we will use AdS/CFT as a computational tool, which provides the strong coupling analogue of scattering amplitudes and compare our results to weak coupling field theory computations. In fact, one might interpret our results as a non-trivial check of the hypothesis in its weakest form.

2.3. Amplitudes at strong coupling

2.3.1. Finding the correct prescription

We now want to find the description of a gluon scattering amplitude in strongly coupled $\mathcal{N} = 4$ SYM via AdS/CFT. The results presented below are derived in a series of papers [24, 27, 41–44] and we closely follow those references and the review [90] in this section.

We start from the brane picture of AdS/CFT, in which $\mathcal{N} = 4$ SYM arises as the world-volume theory on a stack of N D3-branes. The matter content of the theory is represented by open strings attached to the branes, where the branes on which the open string ends determine the colour indices of the corresponding gluon in the low-energy limit. To calculate a gluon scattering amplitude we therefore face the problem of calculating the scattering of open strings which end on D3-branes. Since we are calculating the scattering amplitude of massless particles in a gauge theory, we will necessarily find IR-divergences. We therefore introduce an IR-regulator by moving the brane on which the strings end[1] a finite distance from the stack of the remaining D3-branes. We then take the large-N and the decoupling limit for the remaining branes on the stack, which generates the $AdS_5 \times S^5$ background, as discussed before. We remain with a probe D3-brane embedded into the background

$$ds^2 = \frac{R^2}{z^2}\left(\eta_{\mu\nu} dx^\mu dx^\nu + dz^2\right), \tag{2.8}$$

[1] To be more general, one should consider the possibility that the strings end on different branes. In this case, one would move all k branes to which a string is attached away from the stack, effectively breaking $SU(N+k) \to SU(N) \times U(k)$. However, the central results can be obtained already for the case $k = 1$, which we therefore use in the main text.

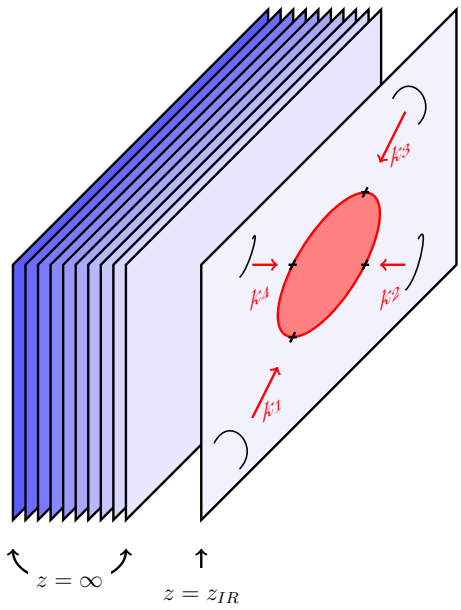

Figure 2.1.: Initial setup for the calculation of a colour-ordered amplitude at strong coupling. We separate one D3-brane from the stack to regulate IR-divergences and scatter strings on this brane, giving rise to a world-sheet with the topology of a disk with vertex operator insertions.

with a fixed z-coordinate $z = z_{IR}$ and we neglected the S^5-part of the metric. As the branes are originally located at $z = \infty$, z_{IR} is a large but finite quantity and removing the IR-regulator would correspond to sending $z_{IR} \to \infty$. The asymptotic states we scatter then are the open strings attached to the IR-brane. From a world-sheet perspective we have the topology of a disk with vertex operator insertions on the boundary. Each ordering of the vertex operators corresponds to a colour-ordered amplitude. This setup is shown in figure 2.1.

A crucial observation is that for any value of the field theory momentum k of a particle we are scattering, the proper momentum of the corresponding string $k_{\text{Str}} = k\frac{z_{IR}}{R}$ is very large. This means that all inner products $k_{i,\text{Str}} \cdot k_{j,\text{Str}}$ become large, which corresponds to the regime of high-energy, fixed-angle string scattering. This regime is studied in flat space in [91,92] with the result that the string scattering amplitude in this kinematical situation is dominated by a saddle point of the classical action. As shown in [91, 92] this result is largely independent of the string states which are scattered and the particular string theory under consideration, since the dominant terms come from the universal bosonic part. Classically, these bosonic terms just describe the area of the world-sheet, which the saddle point then extremises. We therefore see that the leading contribution to the amplitude we want to calculate is given by a minimal area. We now perform a coordinate transformation

$$\partial_\alpha y^\mu = i\frac{R^2}{z^2}\epsilon_{\alpha\beta}\partial_\beta x^\mu, \tag{2.9}$$

which formally looks like a T-duality transformation, but of course the x^i are not periodic directions. We furthermore invert the radial coordinate, $r := \frac{R^2}{z}$, after which the metric

reads

$$ds^2 = \frac{R^2}{r^2}\left(\eta_{\mu\nu}dy^\mu dy^\nu + dr^2\right), \tag{2.10}$$

which again is an AdS_5 space with the same radius as before but the IR-brane is now located at $r_{IR} = \frac{R^2}{z_{IR}}$, close to the boundary of the AdS_5 space. Since this dual AdS_5 space again has an $SO(2,4)$ isometry group which is not the isometry group of the original AdS_5 space, this coordinate transformation hints at a hidden symmetry[2], which we now know to be dual conformal symmetry. At the time of publication these results, together with similar observations at weak coupling [26], were the first hints of the covariance of amplitudes in $\mathcal{N} = 4$ SYM under dual conformal symmetry[3].

To find the boundary conditions in the new metric, recall that a T-duality interchanges Neumann and Dirichlet boundary conditions so that the boundary of the world-sheet will be located at fixed values in the four T-dualised directions. Furthermore, T-duality interchanges momentum with winding, so that the boundary condition that the original coordinates X^μ carry momentum k_i near the operator insertions translates into the statement that the boundary of the world-sheet gets shifted by an amount

$$\Delta y^\mu = 2\pi k_i^\mu, \tag{2.11}$$

every time an operator with momentum k_i is inserted. This naturally introduces the dual variables y_i which parametrise the positions of the cusps of the boundary curve and are defined by the relations

$$k_i = y_{i-1} - y_i, \tag{2.12}$$

with adjacent y_i being null-separated, $(y_{i-1} - y_i)^2 = 0$. These intuitive arguments can be verified explicitly by following [95], as is nicely shown in [96]. This shows that the correct boundary conditions for our problem in the new variables are such that the minimal area ends on the contour of the concatenated momenta of the scattered particles. This contour is closed because of momentum conservation and every edge is light-like since we are scattering massless gluons. Furthermore, colour-ordering is reflected in the way the gluon momenta are attached to each other. An example of such a contour is shown in figure 2.2. We have reached a remarkable conclusion. The leading contribution to a gluon scattering amplitude in $\mathcal{N} = 4$ SYM is given by the area of a minimal surface, which is embedded into AdS_5 and ends on the boundary of AdS_5 on a closed polygon with light-like edges,

$$\text{Amp.} \sim e^{-\frac{\sqrt{\lambda}}{2\pi}\text{Area}(k_i)}, \tag{2.13}$$

where the full coupling dependence is in the prefactor of the exponent. Note again that this is the leading contribution for any scattering amplitude and that information such as the helicity of the gluons are subleading in $\sqrt{\lambda}$. The first subleading order would give rise to a λ-independent prefactor in Eq.(2.13), which can be zero (as it must, for example, for the case of amplitudes with all gluons having the same helicity). To find this prefactor, one would have to include quantum effects in the calculation. First steps in this direction are made for Wilson loops in [97].

[2] In fact, in [93] it is shown that some of the dual conformal generators correspond to the non-local conserved quantities that appear due to the integrability of the original sigma model [45].

[3] We only consider bosonic coordinates in the main text. However, by defining a suitable transformation for the fermionic directions of the superstring sigma model, this result can be lifted to account for dual superconformal symmetry, as well [93], [94].

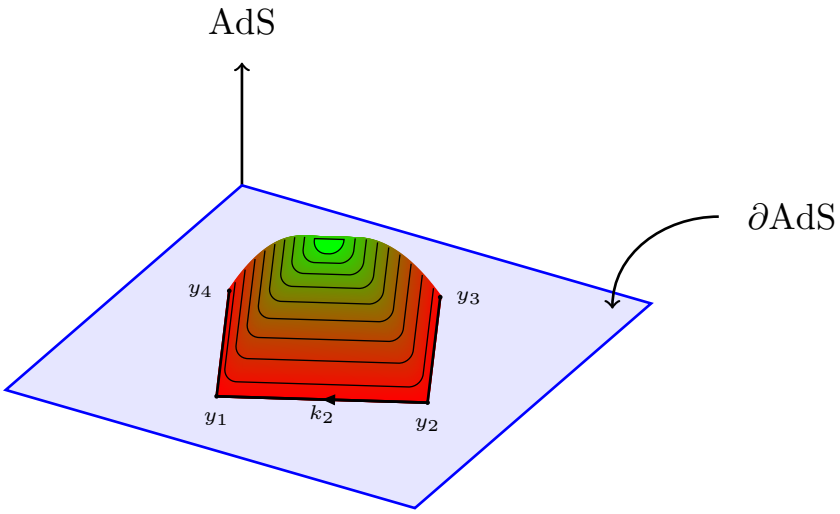

Figure 2.2.: Final setup for the calculation of a colour-ordered amplitude at strong coupling, which is given by the area of a minimal surface embedded into AdS_5, ending on the concatenation of the gluon momenta on the boundary of AdS_5.

The prescription Eq.(2.13) is formally the same as the one given for the calculation of the expectation value of a Wilson loop via AdS/CFT [98, 99]. Note, however, that the boundary in the case of the scattering amplitude lives in the dual AdS_5 space, not in the original AdS_5 space. This shows that at strong coupling amplitudes are equivalent to the expectation value of a light-like Wilson loop in a dual AdS_5 space. After this result was first obtained in [27], a similar result was verified also in weak coupling calculations [26] and by now the equivalence between scattering amplitudes and light-like Wilson loops is expected to hold at any value of the coupling [100, 101], with caveats explained in [102]. Furthermore, this amplitude $\leftrightarrow$ Wilson loop duality was extended to a triality which also includes correlation functions of local operators in the limit where all insertion points become light-like separated [103–108].

While we found a very nice geometric prescription of how to determine an amplitude in strongly coupled $\mathcal{N} = 4$ SYM, it turns out to be very difficult to obtain explicit results. In [27], the 4-point amplitude is obtained. To compare their result with the BDS ansatz, the authors employ the strong coupling analogue of dimensional reduction, which amounts to considering a Dp-brane with $p = 3-2\varepsilon$. This introduces a regularisation parameter ε, as well as an IR-cutoff scale μ, which appears since the analytic continuation of the coupling constant λ to an arbitrary dimension is no longer dimensionless, see [27] for details. Using these parameters the exponent of Eq.(2.13) for the 4-point amplitude is given by

$$-\frac{\sqrt{\lambda}}{2\pi}\text{Area} = \left(-\frac{1}{\varepsilon^2}\frac{1}{\pi}\sqrt{\frac{\lambda\mu^{2\varepsilon}}{(-s)^\varepsilon}} - \frac{1}{\varepsilon}\frac{1}{2\pi}(1-\log 2)\sqrt{\frac{\lambda\mu^{2\varepsilon}}{(-s)^\varepsilon}} + (s \leftrightarrow t)\right) + \frac{\sqrt{\lambda}}{8\pi}\log^2\frac{s}{t} + \frac{\sqrt{\lambda}}{4\pi}\left(\frac{\pi^2}{3} + 2\log 2 - \log^2 2\right). \tag{2.14}$$

Noting that at strong coupling, the leading term for the cusp anomalous dimension is given by $\gamma_K = \frac{\sqrt{\lambda}}{\pi} + \dots$ [85], this result nicely matches the BDS ansatz Eq.(1.2) evaluated

at strong coupling. In [24], a large number of light-like edges is used to mimic a space-like Wilson loop for which the result at strong coupling is known [98,99]. In fact, the result of this calculation is not in accord with the BDS ansatz and was one of the first hints that the BDS ansatz fails for a large number of gluons at the time of publication. However, other than these two results, analytic solutions for the minimal area problem are hard to obtain and the general solution of the problem is found using integrability techniques, as we will show in the following. Before closing, let us remark that the above results have been generalised to include fundamental particles by incorporating a D7-brane in the background [96, 109, 110], to amplitudes at finite temperature by adding a black hole in the background [111, 112] and to β-deformed $\mathcal{N} = 4$ SYM in [113].

2.3.2. General solution for AdS_3

In this section we will present the general solution of the minimal area problem for the case in which the minimal surface can be embedded into an AdS_3-subspace, following [90]. This is a simpler problem, but will contain the relevant ideas for the solution of the general case.

We start by embedding AdS_3 into $\mathbb{R}^{2,2}$ as the surface

$$\vec{X}.\vec{X} := -X_{-1}^2 - X_0^2 + X_1^2 + X_2^2 = -1. \tag{2.15}$$

In terms of these coordinates, the world-sheet equations of motion and Virasoro constraints in conformal gauge are given by

$$\partial\bar{\partial}\vec{X} - \left(\partial\vec{X}.\bar{\partial}\vec{X}\right)\vec{X} = 0,\ \partial\vec{X}.\partial\vec{X} = \bar{\partial}\vec{X}.\bar{\partial}\vec{X} = 0. \tag{2.16}$$

The boundary curve on which the minimal surface shall end is determined by the N positions x_i of the cusps, with adjacent cusps being null separated, $x_{i,i+1}^2 = 0$. Due to the two-dimensional geometry of the boundary the polygon has to have an even number of edges $N = 2n$, because we demand it to be closed. The polygon can then be specified by n light-cone coordinates x_i^+ and n light-cone coordinates x_i^-, where the first cusp is at the position (x_1^+, x_1^-) and we alternately change the x^+- or x^--component. The second cusp, for example, is at (x_1^+, x_2^-), the third at (x_2^+, x_2^-) and so on. Below we will introduce a regularised area Eq.(2.24), which is invariant under dual conformal symmetry. Therefore, it can only depend on conformal cross ratios,

$$\chi_{ijkl}^{\pm} := \frac{x_{i,j}^{\pm} x_{k,l}^{\pm}}{x_{i,k}^{\pm} x_{j,l}^{\pm}}, \tag{2.17}$$

where $x_{i,j}^{\pm} = x_i^{\pm} - x_j^{\pm}$, of which there are $N - 6$, since we have $2N$ coordinates x_i^{μ}, N relations $x_{i,i+1}^2 = 0$ and 6 generators of global conformal symmetry in two dimensions.

We now perform a change of variables[4]

$$\alpha(z, \bar{z}) = \log \partial\vec{X}.\bar{\partial}\vec{X}, \quad p^2(z) = \partial^2\vec{X}.\partial^2\vec{X}. \tag{2.18}$$

Using Eq.(2.16) it is easy to show that $p(z)$ is a holomorphic quantity, while $\alpha(z, \bar{z})$ satisfies a generalised Sinh-Gordon equation,

$$\partial\bar{\partial}\alpha - e^{\alpha} + p\bar{p}e^{-\alpha} = 0. \tag{2.19}$$

[4]Note that the function $p(z)$ is defined differently in [42], both definitions are, however, equivalent.

To get a feeling for the new variables, we can express the explicitly known four-cusp solution [27] in terms of these variables to find

$$p(z) = 1, \quad \alpha(z, \bar{z}) = 0. \tag{2.20}$$

Note that the four-cusp solution corresponds to the simplest possible case. For the case of $2n$ cusps, we generalise these observations by choosing $p(z)$ to be a polynomial of degree $n-2$,

$$p(z) = z^{n-2} + a_{n-4} z^{n-4} + \cdots + a_0, \tag{2.21}$$

since this choice is consistent with the four-cusp result Eq.(2.20) and it is the simplest possible choice which contains the same number of parameters as we have cross ratios, namely $n-3$ complex coefficients. In Eq.(2.21) we have used scaling and translation invariance to set the first and second parameter to 1 and 0, respectively.

This entails that $\alpha \to \frac{1}{2}\log p\bar{p}$ as $z \to \infty$ because this behaviour is both consistent with the 4-point result Eq.(2.20) and satisfies Eq.(2.19). Using the polynomial $p(z)$ we can furthermore define the variable w by the relation

$$dw = \sqrt{p(z)}dz. \tag{2.22}$$

The area we want to calculate is given in terms of these variables by

$$A = \int \frac{e^{\alpha}}{\sqrt{p\bar{p}}} d^2 w, \tag{2.23}$$

which is just the original action written in terms of the new coordinates. In fact, we know that this area will diverge as it approaches the boundary because the metric diverges. To define a regularised area, we simply subtract the boundary behaviour with $\alpha = \frac{1}{2}\log p\bar{p}$ and denote

$$A_{\text{reg}} = \int \left(\frac{e^{\alpha}}{\sqrt{p\bar{p}}} - 1 \right) d^2 w. \tag{2.24}$$

We focus on the regularised area in the following, the regularisation of the boundary behaviour is explained in [42]. The virtue of the new variables is that they allow us to introduce an integrable structure, i.e. a one-parameter family of flat connections, into the problem, as we shall see in the following. To begin, we write down two linear auxiliary problems, called left and right problem, for spinor fields on the world-sheet

$$(d + A^L)\psi^L_a = 0, \quad (d + A^R)\psi^R_{\dot{a}} = 0, \tag{2.25}$$

in which the new variables appear in the connections

$$A^L_z = \begin{pmatrix} \frac{1}{4}\partial\alpha & \frac{1}{\sqrt{2}} e^{\frac{1}{2}\alpha} \\ \frac{1}{\sqrt{2}} p e^{-\frac{1}{2}\alpha} & -\frac{1}{4}\partial\alpha \end{pmatrix}, \qquad A^L_{\bar{z}} = \begin{pmatrix} -\frac{1}{4}\bar{\partial}\alpha & \frac{1}{\sqrt{2}}\bar{p} e^{-\frac{1}{2}\alpha} \\ \frac{1}{\sqrt{2}} e^{\frac{1}{2}\alpha} & \frac{1}{4}\bar{\partial}\alpha \end{pmatrix}, \tag{2.26}$$

$$A^R_z = \begin{pmatrix} \frac{1}{4}\partial\alpha & -i\frac{1}{\sqrt{2}} e^{\frac{1}{2}\alpha} \\ -i\frac{1}{\sqrt{2}} p e^{-\frac{1}{2}\alpha} & -\frac{1}{4}\partial\alpha \end{pmatrix}, \quad A^R_{\bar{z}} = \begin{pmatrix} -\frac{1}{4}\bar{\partial}\alpha & i\frac{1}{\sqrt{2}}\bar{p} e^{-\frac{1}{2}\alpha} \\ i\frac{1}{\sqrt{2}} e^{\frac{1}{2}\alpha} & \frac{1}{4}\bar{\partial}\alpha \end{pmatrix}. \tag{2.27}$$

After finding a solution to these linear equations, we can reconstruct a solution to the original equations using

$$X_{a,\dot{a}} := \begin{pmatrix} X_{-1} + X_2 & X_1 - X_0 \\ X_1 + X_0 & X_{-1} + X_2 \end{pmatrix} = \psi^L_{\alpha,a} \delta^{\alpha\dot{\beta}} \psi^R_{\dot{\beta},\dot{a}}, \tag{2.28}$$

where indices $a, \dot{a}$ denote the two independent solutions to each of the auxiliary problems and α, β denote their components. Near the boundary, the connections simplify since $\alpha \sim \frac{1}{2} \log p\bar{p}$ and $p \sim z^{n-2}$. With these simplifications we can explicitly solve the linear problems for large z and schematically find

$$\psi_a^L \sim \lambda_a^+ \begin{pmatrix} 1 \\ 0 \end{pmatrix} e^{w+\bar{w}} + \lambda_a^- \begin{pmatrix} 0 \\ 1 \end{pmatrix} e^{-(w+\bar{w})}, \tag{2.29}$$

$$\psi_{\dot{a}}^R \sim \tilde{\lambda}_{\dot{a}}^+ \begin{pmatrix} 1 \\ 0 \end{pmatrix} e^{-i(w-\bar{w})} + \tilde{\lambda}_{\dot{a}}^- \begin{pmatrix} 0 \\ 1 \end{pmatrix} e^{i(w-\bar{w})}, \tag{2.30}$$

where $w \sim z^{\frac{n}{2}}$ at large z. The first solution to the left problem grows exponentially for $\mathrm{Re}(w) > 0$, while the second grows in the other half-plane. Similarly, each of the solutions of the right problem dominates in one of the half-planes $\mathrm{Im}(w) \lessgtr 0$. Put together, this shows that in each quadrant of the w-plane one solution of both ψ^L and ψ^R diverges as $z \to \infty$. Using Eq.(2.28) we see that this translates into the statement that for the first quadrant of the w-plane the space-time solution behaves like $X_{a,\dot{a}} \sim \lambda_a^+ \tilde{\lambda}_{\dot{a}}^+ e^{w+\bar{w}-i(w-\bar{w})}$ and diverges in the direction specified by the spinor product, i.e. it approaches a point at the boundary. As we change quadrants in the w-plane the dominant solution of either the left or the right problem changes, which means that the direction along which the space-time solution approaches the boundary changes. The fact that only one spinor changes when changing the quadrant can be related to the result that the space-time solution approaches a light-like curve at the boundary, as desired [42]. Since $w \sim z^{\frac{n}{2}}$ we encircle the w plane $\frac{n}{2}$ times during one rotation in the z-plane, giving rise to the $2n$ cusps of the boundary curve.

We have seen before that for each of the two linear problems the w-plane splits into two halves, leading to n such regions, as we have $\frac{n}{2}$ sheets for the w-plane. In each region we have one solution which grows and one which decays exponentially, called large and small solution, respectively. The small solution will play a key role in the following, because it is well-defined up to an overall factor, while the large solution can be contaminated with contributions from the small solution. We therefore define $s_i^{L/R}$ to be the solution to the linear problem indicated in the superscript with the fastest decay as $w \to \infty$ in region i. We then define the quantity

$$\psi_a^L \wedge \psi_b^L := \epsilon^{\alpha\beta} \psi_{\alpha,a}^L \psi_{\beta,b}^L \tag{2.31}$$

and similarly for the solutions of the right problem. Using the linear problem equations Eq.(2.25) it is easy to see that this product is independent of the location on the world-sheet and can be set to any value by normalising the solutions ψ accordingly. In particular, we can choose $\psi_a^L \wedge \psi_b^L = \epsilon_{ab}$. With this product we can project out the large component in a given region by

$$\psi_a^L \wedge s_i^L \sim \lambda_a^i, \tag{2.32}$$

where we neglected unimportant prefactors. This is a very useful identity, as it allows us to relate the space-time boundary polygon with the quantities appearing in the linear problems. To see this, let us introduce Poincaré coordinates on AdS_3, which are related to the embedding coordinates via

$$\frac{1}{r} = X_{-1} + X_2, \quad x^{\pm} = \frac{X_1 \pm X_0}{X_{-1} + X_2}. \tag{2.33}$$

Comparing with Eq.(2.28) we find that

$$x_i^+ = \frac{\lambda_2^i}{\lambda_1^i}, \quad x_i^- = \frac{\tilde{\lambda}_2^i}{\tilde{\lambda}_1^i}. \tag{2.34}$$

Using Eq.(2.34) and expanding out the inner products in the numerator, we see that

$$x_i^+ - x_j^+ = -\frac{s_i^L \wedge s_j^L}{\left(\psi_1^L \wedge s_i^L\right)\left(\psi_1^L \wedge s_j^L\right)}. \tag{2.35}$$

From several such differences we can reconstruct the conformal cross ratios Eq.(2.17) and obtain

$$\frac{x_{i,j}^+ x_{k,l}^+}{x_{i,k}^+ x_{j,l}^+} = \frac{\left(s_i^L \wedge s_j^L\right)\left(s_k^L \wedge s_l^L\right)}{\left(s_i^L \wedge s_k^L\right)\left(s_j^L \wedge s_l^L\right)}. \tag{2.36}$$

Note that in such an expression, the overall normalisation of the small solutions, as well as the denominator in Eq.(2.35), drop out. A similar relation with $+ \leftrightarrow -$ holds when we replace $L \leftrightarrow R$ in Eq.(2.36). This completes the dictionary between boundary objects and quantities of the linear problem.

A central insight is that we can introduce a spectral parameter ζ in the connection,

$$A_z(\zeta) = \frac{1}{4}\begin{pmatrix} \partial\alpha & 0 \\ 0 & -\partial\alpha \end{pmatrix} + \frac{1}{\zeta}\frac{1}{\sqrt{2}}\begin{pmatrix} 0 & e^{\frac{1}{2}\alpha} \\ pe^{-\frac{1}{2}\alpha} & 0 \end{pmatrix}, \tag{2.37}$$

$$A_{\bar{z}}(\zeta) = \frac{1}{4}\begin{pmatrix} -\bar{\partial}\alpha & 0 \\ 0 & \bar{\partial}\alpha \end{pmatrix} + \zeta\frac{1}{\sqrt{2}}\begin{pmatrix} 0 & \bar{p}e^{-\frac{1}{2}\alpha} \\ e^{\frac{1}{2}\alpha} & 0 \end{pmatrix}, \tag{2.38}$$

such that this one-parameter set of connections is flat for all values of ζ,

$$\partial A_{\bar{z}}(\zeta) - \bar{\partial} A_z(\zeta) + [A_z(\zeta), A_{\bar{z}}(\zeta)] = 0. \tag{2.39}$$

Note that the two connections introduced before are special cases of this deformed connection with $A^L = A(\zeta = 1)$, $A^R = A(\zeta = i)$. We hence drop the superscript from now on, as the left and right problem are just special cases of this more general problem.

This deformation allows us to study the linear problems with an additional dependence on the spectral parameter ζ,

$$\left(d + A(\zeta)\right) s_i(\zeta) = 0, \tag{2.40}$$

which also leads to a ζ-dependence of the cross ratios. Using the explicit form of the deformed connection Eqs.(2.37,2.38) it is easy to check that

$$A\left(e^{i\pi}\zeta\right) = \sigma_3 A(\zeta)\sigma_3, \tag{2.41}$$

with $\sigma_3 = \mathrm{diag}(1, -1)$. From Eq.(2.40) we immediately see that this entails $s_{i+1}(\zeta) = \sigma_3 s_i\left(e^{i\pi}\zeta\right)$, because a rotation by $i\pi$ shifts the region by one. More importantly, it follows that

$$\left(s_i \wedge s_j\right)\left(e^{i\pi}\zeta\right) = \left(s_{i+1} \wedge s_{j+1}\right)(\zeta), \tag{2.42}$$

relating inner products at different values of ζ. Normalising s_1 in such a way that $s_1 \wedge s_2 \equiv 1$, Eq.(2.42) leads to $s_i \wedge s_{i+1} = 1$. We can now write down a Schouten identity for a particular combination of small solutions,

$$(s_{k+1} \wedge s_{-k})(s_k \wedge s_{-k-1}) + (s_{k+1} \wedge s_{-k-1})(s_{-k} \wedge s_k) + (s_{k+1} \wedge s_k)(s_{-k-1} \wedge s_{-k}) = 0. \tag{2.43}$$

Introducing the objects $T_s := (s_0 \wedge s_{s+1}) \left(e^{-i(s+1)\frac{\pi}{2}}\zeta\right)$ for $s = 0, \ldots, n-2$ and the notation $T_s(\zeta)^{\pm} := T_s\left(e^{\pm i\frac{\pi}{2}}\zeta\right)$, as well as using our choice of normalisation we see that Eq.(2.43) leads to

$$T_s^+ T_s^- = T_{s+1}T_{s-1} + 1, \tag{2.44}$$

which are called Hirota equations. Going one step further, we define the quantities $\mathrm{Y}_s := T_{s-1}T_{s+1}$ with $s = 1, \ldots, n-3$, which, by their definition in terms of the small solutions, can be thought of as generalisations of the physical cross ratios to all values of ζ[5]. For these objects we obtain the equations

$$\mathrm{Y}_s^+ \mathrm{Y}_s^- = (1 + \mathrm{Y}_{s+1})(1 + \mathrm{Y}_{s-1}), \tag{2.45}$$

which relate Y-functions at different values of ζ through a functional relation. However, this relation was obtained from a Schouten identity, which follows from the rather trivial statement that in two dimensions at most two vectors can be linearly independent and therefore Eq.(2.45) cannot fully determine the Y-functions.

Instead, we consider the limits $\zeta \to 0, \infty$, in which the linear problem simplifies and can be analysed by means of a WKB approximation. Without going into details, it is shown in [42] that in these limits the Y-functions are well approximated by

$$\log \mathrm{Y}_s \cong -m_s \cosh\theta + \ldots, \tag{2.46}$$

where $\zeta =: e^{\theta}$, and furthermore that the combination

$$l_s := \log\left(\frac{\mathrm{Y}_s}{e^{-m_s\cosh\theta}}\right) \tag{2.47}$$

is analytic in the strip $|\mathrm{Im}\,\theta| \leq \frac{\pi}{2}$. The quantities m_s in Eq.(2.46) are in general $n-3$ complex parameters, matching the number of independent cross ratios. In Eqs.(2.46, 2.47) we choose them to be real for simplicity, the generalisation to the complex case will be discussed in the next section. Technically, the m_s arise as integrals of $\sqrt{p(z)}dz$ along certain cycles. In this way the information about the polygon which is stored in the polynomial $p(z)$ enters the Y-functions.

Taking the logarithm of the functional relation Eq.(2.45) and adding zero cleverly, we find that

$$l_s^+ + l_s^- = \log\left((1 + \mathrm{Y}_{s+1})(1 + \mathrm{Y}_{s-1})\right). \tag{2.48}$$

Convoluting the left-hand side with the kernel

$$K(\theta) = \frac{1}{2\pi}\frac{1}{\cosh\theta} \tag{2.49}$$

and choosing θ such that $|\mathrm{Im}\,\theta| < \frac{\pi}{2}$ we obtain

$$K \star (l_s^+ + l_s^-) := \int_{-\infty}^{+\infty} \frac{d\theta'}{2\pi} \frac{l_s\left(\theta' + i\frac{\pi}{2}\right) + l_s\left(\theta' - i\frac{\pi}{2}\right)}{\cosh(\theta - \theta')} = \oint_{\mathcal{C}} \frac{d\theta'}{2\pi i} \frac{l_s(\theta')}{\sinh(\theta - \theta')} = l_s(\theta), \tag{2.50}$$

[5] To see this, note that we have set some of the inner products of small solutions to one by our choice of normalisation.

where the contour $\mathcal{C}$ is the rectangle with the long sides $(-\infty - i\frac{\pi}{2}) \dots (+\infty - i\frac{\pi}{2})$ and $(\infty + i\frac{\pi}{2}) \dots (-\infty + i\frac{\pi}{2})$, and we have used that the l_s are analytic in that region in that we have only picked up the pole of the denominator. The small sides of the rectangle can be neglected since we know from Eq.(2.46) that $l_s \cong 0$ along these edges. Using Eq.(2.48) and Eq.(2.50), we have

$$\log \mathrm{Y}_s = -m_s \cosh\theta + K \star \log\left((1+\mathrm{Y}_{s+1})(1+\mathrm{Y}_{s-1})\right), \tag{2.51}$$

which is a set of coupled, non-linear integral equations, which determines the Y-functions and is therefore called the Y-system. It is easy to see that the expressions Eq.(2.51) satisfy the functional relations Eq.(2.45). These equations have the form of thermodynamic Bethe ansatz (TBA) equations which usually arise in quantum integrable models (for a review on T- and Y-systems in integrable models see [114]). The fact that such equations arise here shows that there is an auxiliary one-dimensional quantum integrable system which is designed exactly in such a way that its ground state energy Eq.(2.53) calculates the regulated area. The physical meaning of this auxiliary system is, however, unclear.

To find the value of the physical cross ratios for given values of the m_s we can evaluate the Y-functions at $\zeta = 1, i$. Typically, we would like to solve the inverse problem - prescribing values for the cross ratios and solve the Y-system at this kinematical point. This is more difficult and will be a key question in chapter 5, although it should be mentioned that there is a different version of the Y-system in which the physical cross ratios enter as parameters [57].

We still need to evaluate the area of the minimal surface. The area is independent of the spectral parameter ζ and again the problem simplifies when considering the limits $\zeta \to 0, \infty$. As is shown in [44], similar cycle integrals appear as in the definition of m_s. Therefore, the contributions can be extracted from a ζ-expansion of the integral equations Eq.(2.51), with the final result given by

$$\begin{aligned} A_{\text{reg}} =& A_{\text{per}} + A_{\text{free}} && (2.52)\\ =& A_{\text{per}}(m_s) + \sum_s \frac{m_s}{2\pi} \int d\theta \cosh\theta \log(1+\mathrm{Y}_s(\theta)), && (2.53) \end{aligned}$$

where A_{per} is a function of the m_s which we do not spell out explicitly. This determines the area in terms of the parameters m_s and the Y-functions and solves the problem of finding the area of the minimal surface. More details on the derivation can be found in the original papers [42–44]. Note that nowhere in this derivation the explicit form of the space-time solution entered. The integrability-based method computes the area without knowing the surface, just using the information on the boundary polygon.

2.3.3. General solution for AdS_5

The general solution for the AdS_5 case is more difficult to obtain because the number of parameters is larger and the shape of the boundary curve is more complicated, of course. The idea, however, still is to reformulate the problem using a linear auxiliary problem, introducing a spectral parameter which generates a symmetry of the problem and studying the behaviour of the small solutions of the linear problem as a function of the spectral parameter. In this way, one again obtains a set of Y-functions $\mathrm{Y}_{a,s}(\theta)$ which satisfy a

set of integral equation, which we describe in the following. A derivation can be found in [43, 44].

The general answer for the area of the minimal surface ending on an arbitrary light-like curve is given by several terms,

$$\text{Area} = A_{\text{div}} + A_{\text{BDS-like}} + A_{\text{per}} + A_{\text{free}}. \tag{2.54}$$

The first two terms encode the IR divergences. More specifically,

$$A_{\text{div}} = \frac{1}{8}\sum_{i=1}^{n} \log^2\left(\epsilon^2 x_{i,i+2}^2\right), \tag{2.55}$$

where ϵ is a small radial cutoff of AdS_5 and x_i are the dual variables defined by

$$p_i = x_{i-1} - x_i, \tag{2.56}$$

which we saw already in the construction of the boundary polygon in figure 2.2. Furthermore,

$$A_{\text{BDS-like}} = -c_n \sum_{i=1}^{n}\left(\log^2 x_{i,i+2}^2 + \sum_{k=0}^{2K}(-1)^{k+1}\log x_{i,i+2}^2 \log x_{i+2k+1,i+2k+3}^2\right), \tag{2.57}$$

where

$$c_n = \begin{cases} \frac{1}{8} & n = 4K+2 \\ \frac{1}{4} & n = 4K+2\pm 1 \end{cases} \tag{2.58}$$

We have neglected the case $n = 4K$ in the above formula, the reason being a complication due to a monodromy at infinity that shows up in the linear auxiliary problem. Since we will not consider the 8-gluon amplitude in this thesis, we will not go into any detail, the case is worked out in [115]. The BDS-like term is in fact a solution to the anomalous conformal Ward identity [28]. To compare strong coupling results with weak coupling field theory results, it is customary add and subtract the one-loop finite part of the BDS ansatz in Eq.(2.54), which introduces a new quantity

$$\Delta(u_i) := A_{\text{BDS-like}} - A_{\text{BDS}}. \tag{2.59}$$

As both $A_{\text{BDS-like}}$ and A_{BDS} satisfy the anomalous part of the conformal Ward identity, their difference can only be a function of the conformal cross ratios. We will spell out the explicit formulas when studying particular amplitudes in chapters 6 and 7.

We then turn to the most relevant piece for our studies, A_{free}. We begin by introducing $3n-15$ Y-functions $\mathrm{Y}_{a,s}(\theta)$ with $a = 1,2,3$ and $s = 1,\ldots,n-5$, which depend on a complex spectral parameter θ. These Y-functions have to satisfy a set of non-linear, coupled integral equations, the so-called Y-system, similar to Eq.(2.51),

$$\log \mathrm{Y}_{1,s} = -m_s \cosh\theta - C_s - \frac{1}{2}K_2 \star \beta_s - K_1 \star \alpha_s - \frac{1}{2}K_3 \star \gamma_s, \tag{2.60}$$

$$\log \mathrm{Y}_{2,s} = -\sqrt{2} m_s \cosh\theta - K_2 \star \alpha_s - K_1 \star \beta_s, \tag{2.61}$$

$$\log \mathrm{Y}_{3,s} = -m_s \cosh\theta + C_s - \frac{1}{2}K_2 \star \beta_s - K_1 \star \alpha_s + \frac{1}{2}K_3 \star \gamma_s, \tag{2.62}$$

where $3n-15$ auxiliary parameters appear, namely $n-5$ complex mass parameters m_s and $n-5$ chemical potentials C_s, which, in $(3,1)$-signature, are purely complex. For simplicity, we choose the parameters m_s to be real in Eqs.(2.60-2.62) and discuss the general case later on. Furthermore, we introduced the notation $K \star f$, which denotes the convolution integral

$$(K \star f)(\theta) := \int_{-\infty}^{\infty} d\theta' K(\theta-\theta') f(\theta'), \tag{2.63}$$

the kernel functions

$$K_1 = \frac{1}{2\pi}\frac{1}{\cosh\theta}, \quad K_2 = \frac{\sqrt{2}}{\pi}\frac{\cosh\theta}{\cosh 2\theta}, \quad K_3 = \frac{i}{\pi}\tanh 2\theta, \tag{2.64}$$

as well as certain combinations of Y-functions,

$$\alpha_s = \log\frac{(1+\mathrm{Y}_{1,s})(1+\mathrm{Y}_{3,s})}{(1+\mathrm{Y}_{2,s-1})(1+\mathrm{Y}_{2,s+1})}, \tag{2.65}$$

$$\beta_s = \log\frac{(1+\mathrm{Y}_{2,s})^2}{(1+\mathrm{Y}_{1,s-1})(1+\mathrm{Y}_{1,s+1})(1+\mathrm{Y}_{3,s-1})(1+\mathrm{Y}_{3,s+1})}, \tag{2.66}$$

$$\gamma_s = \log\frac{(1+\mathrm{Y}_{1,s-1})(1+\mathrm{Y}_{3,s+1})}{(1+\mathrm{Y}_{1,s+1})(1+\mathrm{Y}_{3,s-1})}. \tag{2.67}$$

The integral equations Eqs.(2.60-2.62) are only valid within the fundamental strip $|\mathrm{Im}\,\theta| \leq \frac{\pi}{4}$. Beyond those bounds, some of the kernels become singular along the line of integration and we have to pick up residue contributions of those poles. Instead of picking up the poles by hand, it is also possible to use functional relations similar to Eq.(2.45), which relate Y-functions with different imaginary parts:

$$\mathrm{Y}^{[r]}_{a,s} = \frac{\left(1+\mathrm{Y}^{[r+1]}_{a,s+1}\right)\left(1+\mathrm{Y}^{[r+1]}_{4-a,s-1}\right)}{\mathrm{Y}^{[r+2]}_{4-a,s}\left(1+\frac{1}{\mathrm{Y}^{[r+1]}_{a+1,s}}\right)\left(1+\frac{1}{\mathrm{Y}^{[r+1]}_{a-1,s}}\right)}, \tag{2.68}$$

where $\mathrm{Y}^{[r]}_{a,s}(\theta) = \mathrm{Y}_{a,s}\left(\theta + ir\frac{\pi}{4}\right)$ denotes a shift in θ by a multiple of $i\frac{\pi}{4}$. When using the recursion relations, it should be noted that we have boundary conditions $\mathrm{Y}_{0,s} = \mathrm{Y}_{4,s} = \infty$, as well as $\mathrm{Y}_{a,0} = \mathrm{Y}_{a,n-4} = 0$.

Once we allow the mass parameters to be complex, $m_s = |m_s|e^{i\phi_s}$, it is convenient to introduce shifted Y-functions $\tilde{\mathrm{Y}}_{a,s}(\theta) := \mathrm{Y}_{a,s}(\theta + i\phi_s)$. Using these functions, all changes in the Y-system can be accounted for by replacing

$$m_s \to |m_s|\,, \quad \mathrm{Y}_{a,s}(\theta) \to \tilde{\mathrm{Y}}_{a,s}(\theta), \quad K^{a,a'}_{s,s'}(\theta-\theta') \to K^{a,a'}_{s,s'}\left(\theta-\theta'+i(\phi_s-\phi_{s'})\right) \tag{2.69}$$

in Eqs.(2.60-2.62). A special case is the 6-point case, for which there is only one phase ϕ. In this case, there are no relative phases in the kernels of Eq.(2.69) and it is sometimes more convenient to work with the unshifted Y-functions $\mathrm{Y}(\theta)$ and to account for the

complex mass parameter by a shift in the driving term and a shifted integration contour, schematically

$$\log \mathrm{Y}_a(\theta) = -|m| \cosh(\theta - i\phi) + C + \sum_{a'} \int_{\mathbb{R}+i\phi} d\theta' K^{a,a'}\left(\theta - \theta'\right) \log\left(1 + \mathrm{Y}_{a'}(\theta')\right). \quad (2.70)$$

We see from Eq.(2.69) that the phases ϕ_s can also lead to a singular behaviour of the kernels. Again, we need to pick up the residues if the differences of the phases becomes too large. The pattern under which the Y-system changes is very interesting and has close connections to the wall crossing phenomenon of [116]. Picking up appropriate residue contributions will be of fundamental importance in chapter 4 and we will explain this procedure in detail there. As in the AdS_3 case, the cross ratios can be obtained from the Y-functions at special values of θ. We will spell out these relations when needed later on.

Once we have solved the Y-system, we can finally calculate the free energy contribution to the amplitude as

$$\mathrm{A}_{\text{free}} = \sum_s \frac{|m_s|}{2\pi} \int_{\mathbb{R}} d\theta \cosh\theta \left[\left(1 + \tilde{\mathrm{Y}}_{1,s}(\theta)\right)\left(1 + \tilde{\mathrm{Y}}_{3,s}(\theta)\right)\left(1 + \tilde{\mathrm{Y}}_{2,s}(\theta)\right)^{\sqrt{2}}\right]. \quad (2.71)$$

The last remaining piece of the amplitude, $A_{\text{per}}(m_s)$, is a function of the complex mass parameters introduced in the free energy part. General expressions are given in [44]. We refrain from spelling them out here and rather present the expressions for the necessary cases in later chapters.

Having assembled all pieces of the amplitude, we define the remainder function at strong coupling as

$$\text{Amp.} \sim e^{-\frac{\sqrt{\lambda}}{2\pi}(A_{\text{div}} + A_{\text{BDS}} + \Delta + A_{\text{per}} + A_{\text{free}})} =: e^{-\frac{\sqrt{\lambda}}{2\pi}(A_{\text{div}} + A_{\text{BDS}}) + R}. \quad (2.72)$$

This closes our general discussion of scattering amplitudes at strong coupling and we will start using the Y-system in chapter 4 after discussing the kinematics relevant to our studies.

3. The multi-Regge limit

As we have seen in the last chapter, the Y-system which describes scattering amplitudes at strong coupling is a rather complicated set of equations and it is not possible to find an analytic solution in general kinematics. We therefore specialise our choice of kinematics to the multi-Regge limit. So far, we have identified this somewhat sloppily with the high-energy regime. Since our special choice of kinematics will play a key role in this thesis, we will now present a proper definition of the limit, some kinematical considerations as well as a brief review of weak coupling results in the multi-Regge limit to which we want to compare our strong coupling results later on.

3.1. Definition

We are interested in $2 \to n-2$ production amplitudes of gluons, for which we have two incoming momenta $-p_1$, $-p_2$ and $n-2$ outgoing momenta $p_3, \ldots, p_n$, as shown in figure 3.1. For a n-particle amplitude there are $3n-10$ independent Mandelstam variables[1]. Since we will only be interested in $\mathcal{N}=4$ SYM, we describe the independent Mandelstam invariants in terms of *dual variables*,

$$p_i = x_{i-1} - x_i, \tag{3.1}$$

which are also indicated in figure 3.1. The dual variables are cyclic, $x_{i+n} = x_i$ and, defining the quantities $x_{i,j} := x_i - x_j$, we have the identity

$$x_{i,j}^2 = (p_{i+1} + \cdots + p_j)^2, \tag{3.2}$$

providing the connection between the dual variables and the Mandelstam invariants. Due to momentum conservation and cyclicity we also have that $x_{i,j}^2 = x_{j,i}^2$. These are of course the same variables used before in chapter 2. Furthermore, we have the constraints $x_{i,i+1}^2 = 0$ because of our light-like configuration. In terms of the dual variables, we define the following basis of Mandelstam invariants:

$$\begin{aligned} s_r &= x_{r+1,r+3}^2, \\ t_r &= x_{1,r+2}^2, \\ \eta_p &= \frac{x_{p-2,p}^2 x_{p-1,p+1}^2}{x_{p-2,p+1}^2}, \end{aligned} \tag{3.3}$$

where $r = 1, \ldots, n-3$ labels the t-channels and $p = 4, \ldots, n-1$ labels the produced particles. As we discussed before, the remainder function of $\mathcal{N}=4$ SYM is invariant under dual conformal symmetry, i.e. conformal symmetry acting on the dual variables x_i.

[1] We have $4n$ momentum components, subject to n relations $p_i^2 = 0$ and we have 10 symmetry generators of the Poincaré group. Note that momentum conservation is accounted for by the generators of translation.

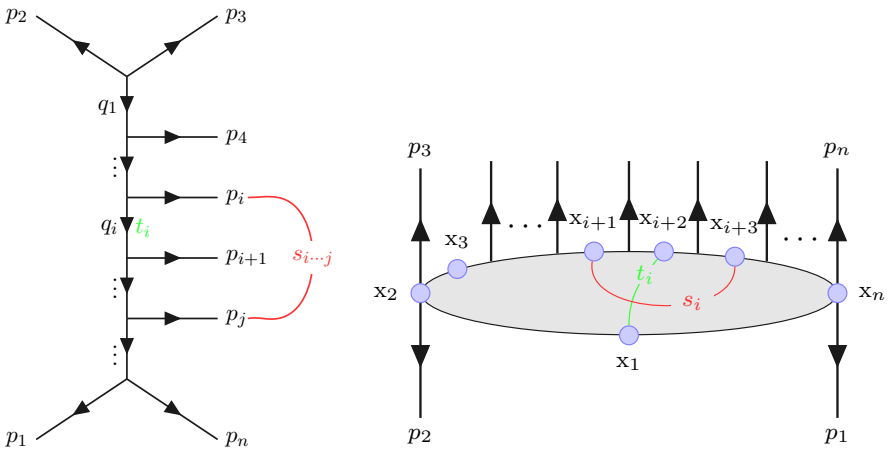

Figure 3.1.: Left: standard parametrisation of a $2 \to n-2$ scattering process, together with the location of Mandelstam invariants $t_i (= q_i^2)$ and the multi-indexed $s_{i\cdots j} = (p_i + \cdots + p_j)^2$. Right: parametrisation in terms of the dual variables x_i, together with the location of the Mandelstam invariants we use, cf. Eq.(3.3).

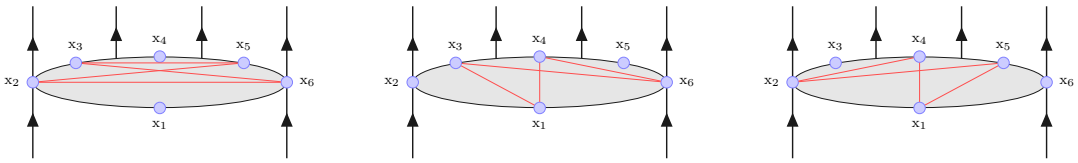

Figure 3.2.: Graphical representation of the conformal cross ratios Eq.(3.4) for the 6-point case.

Therefore, our set of variables Eq.(3.3) is actually too large and we just need $3n-15$ conformal cross ratios[2]. For these, we choose the following basis:

$$\begin{aligned} u_{1\sigma} &= \frac{x^2_{\sigma+1,\sigma+5} x^2_{\sigma+2,\sigma+4}}{x^2_{\sigma+2,\sigma+5} x^2_{\sigma+1,\sigma+4}}, \\ u_{2\sigma} &= \frac{x^2_{1,\sigma+2} x^2_{n,\sigma+3}}{x^2_{n,\sigma+2} x^2_{1,\sigma+3}}, \\ u_{3\sigma} &= \frac{x^2_{2,\sigma+3} x^2_{1,\sigma+4}}{x^2_{1,\sigma+3} x^2_{2,\sigma+4}}, \end{aligned} \tag{3.4}$$

where $\sigma = 1, \ldots, n-5$. A convenient representation of the cross ratios is depicted in figure 3.2. An important symmetry used later on is target-projectile symmetry, which, as the name suggests, reflects the fact that the amplitude should be invariant when the two incoming particles are swapped. In terms of the graphical representation in figure 3.2 this symmetry amounts to a reflection on the central vertical axis of each blob. It is easy to

[2]The counting is: $4n$ coordinates for the x_i, subject to n constraints $x^2_{i,i+1} = 0$ and we have 15 symmetry generators of the dual conformal group in four dimensions.

verify that under this symmetry the cross ratios are interchanged as

$$u_{1\sigma} \leftrightarrow u_{1n-4-\sigma},\ u_{2\sigma} \leftrightarrow u_{3n-4-\sigma}. \tag{3.5}$$

The primary goal of section 3.3 is to understand the behaviour of this choice of cross ratios in the multi-Regge limit, but first let us properly define this limit. To do so, we define the subenergies

$$s_{i\cdots j} := (p_i + \cdots + p_j)^2 = x^2_{i-1,\,j}. \tag{3.6}$$

Note that this definition includes the total energy $s = s_{3\cdots n}$, as well as our basis elements $s_r = s_{r+2\,r+3}$, which are just two-particle subenergies. In terms of these variables we define the multi-Regge limit to be the kinematical regime in which the t_i remain fixed and negative, while all subenergies go to infinity with the hierarchy

$$s \gg s_{3\cdots n-1}, s_{4\cdots n} \gg s_{3\cdots n-2}, \ldots, s_{5\cdots n} \gg \cdots \gg s_{34}, \ldots, s_{n\,n-1} \gg -t_1, \ldots, -t_{n-3}. \tag{3.7}$$

A formally more precise definition is that in the multi-Regge limit the rapidities of the produced particles are strongly ordered with their transverse momenta being of the same order. However, in terms of Mandelstam invariants this just entails our definition Eq.(3.7), see [117] for details. In this sense, the multi-Regge limit is the generalisation of the more familiar Regge limit $s \gg -t$ for $2 \to 2$ scattering. In terms of our basis Eq.(3.3), the multi-Regge limit corresponds to sending all s_r to infinity, while keeping both the t_r and η_p fixed.

3.2. Kinematical identities

As a preparation for the analysis of the cross ratios in the multi-Regge limit, we need some kinematical identities, which we obtain in the centre-of-mass system of the two incoming particles. We introduce two light-like reference vectors $\hat{p}_1 = -p_1$, $\hat{p}_2 = -p_2$, for which $2\hat{p}_1\hat{p}_2 = s$ holds, and use them to parametrise the transferred momenta (cf. figure 3.1) as

$$q_r = \delta_r \hat{p}_1 + \gamma_r \hat{p}_2 + q_{r\perp}, \tag{3.8}$$

where $q_\perp$ is a vector pointing in the plane perpendicular to the two reference vectors. Therefore $\hat{p}_1 q_{r\perp} = \hat{p}_2 q_{r\perp} = 0$. This is called *Sudakov parametrisation*. It should be noted that by our definition of the t_r in Eq.(3.3), $t_r = q_r^2$. Using momentum conservation, the subenergies can be rewritten as[3]

$$s_{3\cdots r+2} = (p_3 + \cdots + p_{r+2})^2 = (-p_2 - q_1 + \cdots + q_{r-1} - q_r)^2 = (p_2 + q_r)^2\,, \tag{3.9}$$

$$s_{r+3\cdots n} = (p_{r+3} + \cdots + p_n)^2 = (q_r - q_{r+1} + \cdots + q_{n-3} - p_1)^2 = (p_1 - q_r)^2\,, \tag{3.10}$$

which we can use to determine the Sudakov parameters,

$$s_{3\cdots r+2} = 2q_r p_2 + t_r = -\delta_r s + t_r \quad \Rightarrow \quad \delta_r = \frac{t_r - s_{3\cdots r+2}}{s}, \tag{3.11}$$

and

$$s_{r+3\cdots n} = t_r - 2q_r p_1 \quad \Rightarrow \quad \gamma_r = \frac{s_{r+3\cdots n} - t_r}{s}. \tag{3.12}$$

[3]Note that the first definition uses $s_{3\cdots 3} = (p_3)^2 = 0$ for $r = 1$.

We now use the strong ordering of the subenergies Eq.(3.7) and see that this, together with the expressions Eqs.(3.11,3.12) implies a strong ordering of the Sudakov parameters

$$1 \gg \gamma_1 \gg \gamma_2 \gg \cdots \gg \gamma_{n-3} \tag{3.13}$$

and

$$1 \gg -\delta_{n-3} \gg -\delta_{n-4} \gg \cdots \gg -\delta_1. \tag{3.14}$$

The above expressions also imply that in the multi-Regge limit

$$t_r = q_r^2 = s\gamma_r\delta_r + q_{r\perp}^2 \cong -\frac{s_{3\cdots r+2}s_{r+3\cdots n}}{s} + q_{r\perp}^2 \cong q_{r\perp}^2, \tag{3.15}$$

where '$\cong$' will always denote identities that hold strictly only in the multi-Regge limit. This means that the transverse components of q_r stay finite in the multi-Regge limit and, because of the relation $p_{r+3} = q_r - q_{r+1}$, so do the transverse components of the momenta of the produced particles p_{r+3}, where $r = 1, \ldots, n-4$. To calculate the magnitude of the transverse momentum, we make use of the on-shell condition for the produced gluons,

$$0 = p_r^2 = (q_{r-3} - q_{r-2})^2 \cong -s\gamma_{r-3}\delta_{r-2} + p_{r\perp}^2 \cong \frac{s_{3\cdots r}s_{r\cdots n}}{s} + p_{r\perp}^2, \tag{3.16}$$

where we used the strong ordering of the Sudakov parameters in the first step. From this identity we conclude that

$$\frac{s_{3\cdots r}s_{r\cdots n}}{s} \cong -p_{r\perp}^2 = \vec{p}_{r\perp}^{\,2}, \tag{3.17}$$

where we introduced the two-dimensional transverse vector $\vec{p}_{r\perp}$. Similarly to Eq.(3.16) we can now calculate the leading behaviour of the subenergies. Explicitly, we obtain

$$\begin{aligned} s_r = (q_{r-1} - q_{r+1})^2 &\cong -s\gamma_{r-1}\delta_{r+1} + (p_{r+2} + p_{r+3})_\perp^2 \\ &\cong \frac{s_{3\cdots r+3}s_{r+2\cdots n}}{s} + (p_{r+2} + p_{r+3})_\perp^2 , \end{aligned} \tag{3.18}$$

where $r = 2, \ldots, n-4$, and

$$\begin{aligned} s_{p-1\,p\,p+1} = (q_{p-4} - q_{p-1})^2 &\cong -s\gamma_{p-4}\delta_{p-1} + (p_{p-1} + p_p + p_{p+1})_\perp^2 \\ &\cong \frac{s_{3\cdots p+1}s_{p-1\cdots n}}{s} + (p_{p-1} + p_p + p_{p+1})_\perp^2 \end{aligned} \tag{3.19}$$

for the three-particle subenergies with $p = 5, \ldots, n-2$. Looking back at our basis of Mandelstam invariants Eq.(3.3), we see that this is all we need to determine the η_p in the multi-Regge limit. By plugging in the leading behaviour of the subenergies and using relation Eq.(3.17) we find that

$$\eta_p = \frac{s_{p-3}s_{p-2}}{s_{p-1\,p\,p+1}} \cong -p_{p\perp}^2 = \vec{p}_{p\perp}^{\,2}, \tag{3.20}$$

which is indeed a finite quantity in the multi-Regge limit. We can lift our analysis to subenergies involving more particles and obtain

$$\begin{aligned} s_{r+2\cdots r'+3} = (p_{r+2} + \cdots + p_{r'+3})^2 &\cong \frac{s_{r+2\cdots n}s_{3\cdots r'+3}}{s} + (p_{r+2} + \cdots + p_{r'+3})_\perp^2 \\ &\cong \frac{s_r \cdots s_{r'}}{\eta_{r+3} \cdots \eta_{r'+2}}, \end{aligned} \tag{3.21}$$

where the last step follows by using the leading terms of Eqs.(3.18,3.19) repeatedly. Eq.(3.21) is one of the main results of this section and will be crucial for the determination of the behaviour of the cross ratios in the multi-Regge limit.

We need one last ingredient from the kinematical analysis which is the angle between different vectors $\vec{q}_{i\perp}$, which we obtain from the relation

$$\vec{p}^{\,2}_{r+3\perp} = (\vec{q}_{r\perp} - \vec{q}_{r+1\perp})^2 = |t_r| + |t_{r+1}| - 2\sqrt{|t_r||t_{r+1}|}\cos\theta_{r,r+1}, \tag{3.22}$$

where $r = 1, \ldots, n-4$. From Eq.(3.20), we see that the left-hand side of Eq.(3.22) is just equal to η_{r+3} and find

$$\cos\theta_{r,r+1} \cong \frac{|t_r| + |t_{r+1}| - \eta_{r+3}}{2\sqrt{|t_r||t_{r+1}|}}. \tag{3.23}$$

Since we will need it in the following, we spell out the sine of this angle, which is given by

$$\sin\theta_{r,r+1} = \sqrt{1 - \cos^2\theta_{r,r+1}} \cong \frac{\lambda(|t_r|, |t_{r+1}|, \eta_{r+3})}{2\sqrt{|t_r||t_{r+1}|}}, \tag{3.24}$$

where we defined

$$\lambda^2(|t_r|, |t_{r+1}|, \eta_{r+3}) = 2|t_r||t_{r+1}| + 2\eta_{r+3}|t_r| + 2\eta_{r+3}|t_{r+1}| - |t_r|^2 - |t_{r+1}|^2 - \eta^2_{r+3}. \tag{3.25}$$

From the expressions Eqs.(3.23,3.24) we can obtain the angle between any two $\vec{q}_{i\perp}$ because these are two-dimensional vectors and therefore angles are additive.

3.3. Cross ratios in the multi-Regge limit

We now have all the information we need to determine the behaviour of our basis of cross ratios Eq.(3.4) in the multi-Regge limit. Using Eq.(3.21) and our definition of the Mandelstam variables Eq.(3.3) we find that

$$u_{2\sigma} = \frac{t_\sigma}{t_{\sigma+1}} \frac{x^2_{\sigma+3,n}}{x^2_{\sigma+2,n}} \cong \frac{t_\sigma}{t_{\sigma+1}} \frac{\eta_{\sigma+4}}{s_{\sigma+1}}, \tag{3.26}$$

$$u_{3\sigma} = \frac{t_{\sigma+2}}{t_{\sigma+1}} \frac{x^2_{2,\sigma+3}}{x^2_{2,\sigma+4}} \cong \frac{t_{\sigma+2}}{t_{\sigma+1}} \frac{\eta_{\sigma+3}}{s_{\sigma+1}}. \tag{3.27}$$

We see that both sets of cross ratios vanish in the multi-Regge limit. However, the ratios

$$\frac{u_{2\sigma}}{u_{3\sigma}} \cong \frac{t_\sigma}{t_{\sigma+2}} \frac{\eta_{\sigma+4}}{\eta_{\sigma+3}} \tag{3.28}$$

are a function of quantities which remain finite in the multi-Regge limit. This leaves us with the $u_{1\sigma}$, whose definition Eq.(3.4) we can write in terms of Mandelstam variables as

$$u_{1\sigma} = \frac{s_{\sigma+2\cdots\sigma+5} s_{\sigma+3\,\sigma+4}}{s_{\sigma+3\cdots\sigma+5} s_{\sigma+2\cdots\sigma+4}}. \tag{3.29}$$

Plugging in Eq.(3.21), we see that all factors cancel and we get $u_{1\sigma} \cong 1$. However, to compare the behaviour of the $u_{1\sigma}$ with the other cross ratios, we want the first subleading term, as well, which requires more work. To determine the subleading piece, we write

down the analogue of Eq.(3.18) for the subenergy $s_{\sigma+3\,\sigma+4}$ and expand by subenergies to obtain

$$\begin{aligned}1 =&\frac{s_{\sigma+2\cdots\sigma+4}s_{\sigma+3\cdots\sigma+5}}{s_{\sigma+3\,\sigma+4}s_{\sigma+2\cdots\sigma+5}}\left(\frac{1}{s_{\sigma+3\cdots\sigma+5}}\frac{s_{3\cdots\sigma+5}s_{\sigma+3\cdots n}}{s}\right)\left(\frac{1}{s_{\sigma+2\cdots\sigma+4}}\frac{s_{3\cdots\sigma+4}s_{\sigma+2\cdots n}}{s}\right)\\ &\times\left(\frac{s}{s_{3\cdots\sigma+5}s_{\sigma+2\cdots n}}s_{\sigma+2\cdots\sigma+5}\right)+\frac{(p_{\sigma+3}+p_{\sigma+4})_\perp^2}{s_{\sigma+3\,\sigma+4}}.\end{aligned} \tag{3.30}$$

Note that the first factor on the right-hand side is just $u_{1\sigma}^{-1}$. Inserting the leading behaviour for the three factors multiplying $u_{1\sigma}^{-1}$, we see that they are all equal to one, with corrections of the order of the first factor in each parentheses. These are all much smaller than the last term in Eq.(3.30) in the multi-Regge regime, because they involve subenergies with more particles. Therefore, we can consistently replace all factors multiplying $u_{1\sigma}^{-1}$ with one and only keep the last term to get the subleading piece. Solving for $u_{1\sigma}$ we find

$$u_{1\sigma} = 1 + \frac{(p_{\sigma+3}+p_{\sigma+4})_\perp^2}{s_{\sigma+3\,\sigma+4}}. \tag{3.31}$$

To write the numerator of Eq.(3.31) in terms of our basis of Mandelstam variables, we use our result from the last section that angles in the two-dimensional transverse space are additive to write

$$\begin{aligned}\rho_\sigma :&= (\vec{p}_{\sigma+3}+\vec{p}_{\sigma+4})^2 = (\vec{q}_\sigma-\vec{q}_{\sigma+2})^2\\ &= |t_\sigma|+|t_{\sigma+2}|-2\sqrt{|t_\sigma||t_{\sigma+2}|}\cos\left(\theta_{\sigma,\sigma+1}+\theta_{\sigma+1,\sigma+2}\right).\end{aligned} \tag{3.32}$$

This can be rewritten with the help of Eqs.(3.23,3.24) to find the lengthy expression

$$\begin{aligned}\rho_\sigma(t,\eta) =&|t_\sigma|+|t_{\sigma+2}|-2\sqrt{|t_\sigma||t_{\sigma+2}|}\left(\frac{|t_\sigma|+|t_{\sigma+1}|-\eta_{\sigma+3}}{2\sqrt{|t_\sigma||t_{\sigma+1}|}}\frac{|t_{\sigma+1}|+|t_{\sigma+2}|-\eta_{\sigma+4}}{2\sqrt{|t_{\sigma+1}||t_{\sigma+2}|}}\right.\\ &\left.-\frac{\lambda(|t_\sigma|,|t_{\sigma+1}|,\eta_{\sigma+3})}{2\sqrt{|t_\sigma||t_{\sigma+1}|}}\frac{\lambda(|t_{\sigma+1}|,|t_{\sigma+2}|,\eta_{\sigma+4})}{2\sqrt{|t_{\sigma+1}||t_{\sigma+2}|}}\right).\end{aligned} \tag{3.33}$$

This finishes our kinematical analysis. In the multi-Regge limit, our basis of cross ratios naturally splits into triplets. Within each triplet, the cross ratios $u_{2\sigma}$ and $u_{3\sigma}$ go to zero, while $u_{1\sigma}$ goes to one in such a way that the reduced cross ratios

$$\tilde{u}_{2\sigma} = \frac{u_{2\sigma}}{1-u_{1\sigma}}, \quad \tilde{u}_{3\sigma} = \frac{u_{3\sigma}}{1-u_{1\sigma}} \tag{3.34}$$

remain finite.

3.4. Weak coupling results

Until now we have treated the multi-Regge limit simply as given by the definition Eq.(3.7). In this section, we want to highlight why the multi-Regge limit is a very interesting kinematical regime and briefly review some weak coupling results. We will concentrate on those facts relevant for our studies at strong coupling and do so mostly following references [25, 75, 118]. Other general introductions of (multi-)Regge theory include [117, 119, 120].

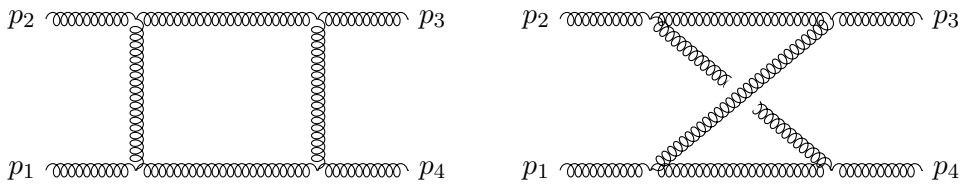

Figure 3.3.: Dominant one-loop diagrams in the Regge limit $s \to \infty$ for $2 \to 2$ gluon scattering in $SU(N_c)$ gauge theory.

Let us begin our survey of the multi-Regge limit at weak coupling with a simple problem, the calculation of the $2 \to 2$ gluon amplitude at one-loop level in $SU(N_c)$ gauge theory. In the Regge limit we are only interested in the dominant pieces as the Mandelstam variable $s \to \infty$. As is shown in [117], the leading virtual corrections in this limit are given by the two diagrams shown in figure 3.3[4], which give rise to the amplitude

$$iA_{h_i}^{a_i} \cong iA_{h_i}^{a_i,\text{tree}} \log\left(\frac{s}{-t}\right) \alpha(t) \tag{3.35}$$

where

$$\alpha(t) \cong -\frac{\alpha_s N_c}{4\pi} \log\left(\frac{-t}{\mu^2}\right) \tag{3.36}$$

for an IR-cutoff μ. Furthermore,

$$iA_{h_i}^{a_i,\text{tree}} \cong -8\pi i\alpha_s \frac{s}{t} f^{a_2 a_3 c} f^{a_1 a_4 c} g_{\mu_2\mu_3} g_{\mu_1\mu_4} \epsilon_{h_1}^{\mu_1}(p_1) \epsilon_{h_2}^{\mu_2}(p_2) \epsilon_{h_3}^{\mu_3}(p_3) \epsilon_{h_4}^{\mu_4}(p_4) \tag{3.37}$$

is the tree level amplitude with a_i and h_i being the colour indices and helicities of the scattered gluons, respectively. Note that the suppression of the one-loop amplitude relative to the tree level result comes with a factor $\alpha_s \log s$. While α_s will be small in a perturbative expansion, we are interested in the regime $s \to \infty$, in which the large logarithm can compensate the smallness of the coupling constant such that $\alpha_s \log s \sim \mathcal{O}(1)$. Then, however, we cannot stop at one-loop level. In fact, we know that the leading contribution to the n-loop amplitude will be $\sim \alpha_s^n \log^n s$, which means that we have to identify the relevant subset of diagrams contributing to this leading behaviour and then resum those. This expansion is known as the leading logarithmic approximation (abbreviated LLA). Subleading terms $\sim \alpha_s^n \log^{n-1} s$ are collected in the next-to-leading logarithmic approximation (NLLA), with an obvious generalisation to N^{k}LLA. Note that every logarithmic order contains information from all loop orders in the coupling constant α_s.

It turns out that the relevant diagrams are given by a specific set of ladder diagrams, which, once resummed, give the following form for the scattering amplitude of two particles with colour indices a_1, a_2 and helicities h_1, h_2 in $SU(N_c)$ Yang-Mills theory in dimensional regularisation,

$$A_{2\to 2} = -2g_s \delta_{h_2,h_3} T^c_{a_2 a_3} \frac{s^{1+\omega(t)}}{-t} T^c_{a_1 a_4} g_s \delta_{h_1,h_4}, \tag{3.38}$$

[4]To be more precise, one should note that neglecting self-energy graphs and vertex corrections only gives the correct leading contributions when working in a physical gauge.

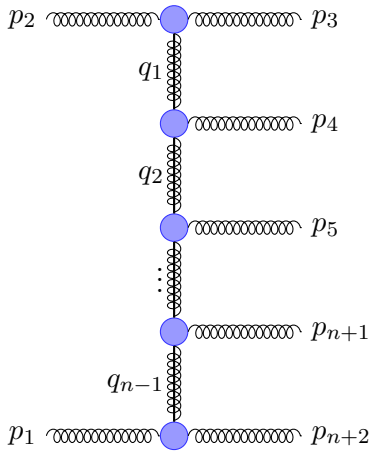

Figure 3.4.: $2 \to n$ production amplitudes in the multi-Regge limit. The blobs represent Lipatov vertices and the decorated propagators in the t-channels are propagators for the reggeised gluons.

where $g_s^2 = 4\pi\alpha_s$, T^c_{ab} are the generators of the gauge group $SU(N_c)$ and

$$\omega(t) = -\frac{\alpha_s N_c}{4\pi^2}(2\pi\mu)^{2\epsilon}\int d^{2-2\epsilon}k\frac{\vec{q}^2}{\vec{k}^2(\vec{q}-\vec{k})^2} \cong -\frac{\alpha_s N_c}{2\pi}\left(4\pi e^{-\gamma}\right)^{\epsilon}\left(\log\frac{-t}{\mu^2}-\frac{1}{\epsilon}\right) \tag{3.39}$$

is the called the gluon Regge trajectory. In writing Eq.(3.39) we used that $t = -\vec{q}^2$ and introduced μ to be the renormalisation scale of the 't Hooft coupling constant $\lambda = \frac{\alpha_s N_c}{2\pi}(4\pi e^{-\gamma})^{\epsilon}$. This is a remarkable result, as it shows that the resummation of an infinite number of diagrams combines in such a way that it mimics the exchange of a particle with t-dependent spin, called a Reggeon. This process is also called reggeisation of the gluon. One way of showing the above result Eq.(3.38) uses unitarity in the form of the Cutkosky rules, which relate the imaginary part of the desired amplitude with products of lower loop amplitudes (see [121]). From the imaginary part, the amplitude can then be reconstructed using a dispersion relation. The building blocks from which the LLA of the desired amplitude can be constructed are given by production amplitudes in the multi-Regge limit shown in figure 3.4, which take the factorised form

$$A_{2\to n} = -2sg_s\delta_{h_1,h_4}T^{c_1}_{a_1a_4}\frac{s_1^{\omega(t_1)}}{(-t_1)}g_sC(q_1,q_2,k_1)T^{d_1}_{c_1c_2}\frac{s_2^{\omega(t_2)}}{(-t_2)}\cdots\frac{s_n^{\omega(t_n)}}{(-t_n)}g_s\delta_{h_2,h_3}T^{c_n}_{a_2a_3}, \tag{3.40}$$

where the propagators are those for reggeised gluons and the vertices $C(q_i, q_{i+1}, k_i)$ are effective vertices describing the coupling of two Reggeons to a normal gluon, see [122]. These production amplitudes will be explored from the strong coupling perspective in later chapters. Note that both the gluon Regge trajectory $\omega(t_i)$ and the so-called Lipatov vertices $C(q_i, q_{i+1}, k_i)$ are universal quantities. Once calculated for amplitudes with a small number of gluons as e.g. $2 \to 2$ and $2 \to 3$ gluon scattering, they can be used to build up the $2 \to n$ gluon amplitude as in Eq.(3.40).

As mentioned before, the MRL production amplitudes can be used to build up the $2 \to 2$ amplitude Eq.(3.38), with the Reggeon being a composite state of reggeised gluons.

If the Reggeon carries vacuum quantum numbers, it is called a Pomeron. The evolution of the Pomeron in transverse space is governed by the BFKL equation [121,123,124], which is a Schrödinger-like equation for the Pomeron wave function whose ground state determines the intercept of the Pomeron $\Delta = \omega_P(0)$, which in LLA is given by $\Delta = \frac{4}{\pi}\alpha_s N_c \log 2$. The intercept in turn determines the total cross section $\sigma_{\text{tot}} \sim s^{\Delta}$. Since this quantity in LLA is positive, the cross section violates the Froissart bound $\sigma < \log^2 s$, which signals a violation of unitarity. To restore unitarity, multi-Reggeon exchanges have to be taken into account. This modifies the BFKL equation to the BKP equation, which governs the evolution of a colourless n-Reggeon state [125,126]. Remarkably, in the limit $N_c \to \infty$, the BKP Hamiltonian is that of a spin chain and is therefore integrable [67–69]. Historically, this was one of the first instances that spin chain integrability entered high-energy physics.

Having at our disposal an exact expression for the $2 \to 2$ and $2 \to 3$ amplitude in $\mathcal{N} = 4$ SYM through the BDS ansatz, it is a natural question to ask how the BDS ansatz behaves in the multi-Regge regime and whether it is compatible with the factorised form Eq.(3.40). Indeed, as is shown in [25], the $2 \to 2$ BDS amplitude in dimensional regularisation can be written as[5]

$$M_{2\to 2} = \Gamma(t) \left(\frac{-s}{\mu^2}\right)^{\omega(t)} \Gamma(t), \tag{3.41}$$

up to higher corrections in ϵ, from which the gluon Regge trajectory $\omega(t)$ and the vertices $\Gamma(t)$ can be extracted to all-loop order in the 't Hooft coupling λ. These formulas, however, are lengthy and we refrain from spelling them out. They are given in [25]. As before, μ^2 is the renormalisation point for λ.

Going from the elastic amplitude to the first production amplitude, [25] show that the $2 \to 3$ BDS amplitude can be written as

$$M_{2\to 3} = \Gamma(t_1) \left(\frac{-s_1}{\mu^2}\right)^{\omega(t_1)} \Gamma(t_1, t_2, \eta_4) \left(\frac{-s_2}{\mu^2}\right)^{\omega(t_2)} \Gamma(t_2). \tag{3.42}$$

As explained before, the quantities $\Gamma(t)$ and $\omega(t)$ are universal and are therefore the same as in Eq.(3.41). The new ingredient in Eq.(3.42) is the Reggeon-Reggeon-gluon vertex $\Gamma(t_1, t_2, \eta_4)$ which again can be extracted to all-loop order from the general BDS ansatz. Both Eq.(3.41) and Eq.(3.42) are originally derived for the kinematical region in which all invariants s_i, t_i are negative, called the Euclidean region. This is a nice kinematical regime as all singularities in the s_i-planes are on the right-hand side. Therefore the amplitude is real and it factorises nicely as in the above equations. From Eq.(3.42) it is then possible to study expressions in other kinematical regions where some of the Mandelstam invariants s_i are positive. These so-called Regge regions will be investigated in more detail in chapter 5. To study the other kinematical regions, we analytically continue in the s_i to reach regions where all or some of the s_i are positive. For such a continuation, one starts in the Euclidean regime with phases $s_i = e^{i\pi}|s_i|$ and then continues the phase from π to ε to end up above the cut on the right-hand side. As it turns out, the production amplitude $M_{2\to 3}$ can, in all kinematical regimes, be written as

$$\frac{M_{2\to 3}}{\Gamma(t_1)\Gamma(t_2)} = c_1 \left(\frac{-s_1}{\mu^2}\right)^{\omega(t_1)-\omega(t_2)} \left(\frac{-s\eta_4}{\mu^4}\right)^{\omega(t_2)} + c_2 \left(\frac{-s_2}{\mu^2}\right)^{\omega(t_2)-\omega(t_1)} \left(\frac{-s\eta_4}{\mu^4}\right)^{\omega(t_1)} \tag{3.43}$$

[5] Recall from Eq.(1.2) that M_n corresponds to the amplitude divided by the tree level expression.

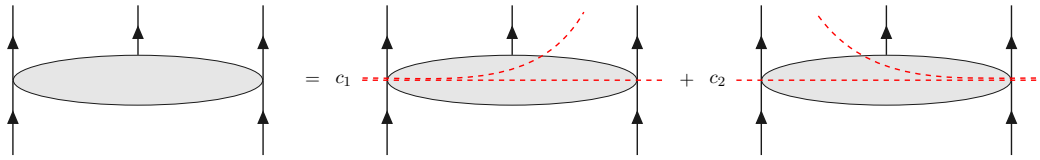

Figure 3.5.: Graphical representation of the analytic representation of the $2 \to 3$ amplitude in the multi-Regge limit, Eq.(3.43). In every kinematical regime, the amplitude can be written as a sum of two terms which make the discontinuities in the s-variables manifest. Note that lines indicating the s-variables which appear in a given term are not allowed to cross as explained in the main text.

with certain coefficients c_i. These coefficients can be fixed by making an ansatz as in Eq.(3.43) and then comparing to the BDS ansatz in the given kinematical regime. The form of the amplitude Eq.(3.43) can be represented graphically as in figure 3.5. This is called an *analytic representation* of the amplitude in [25], because the discontinuities of the amplitude in the s-variables can be easily read off from Eq.(3.43). Eq.(3.43) is an example of a much more general principle, namely that an amplitude in the multi-Regge limit can only display discontinuities in non-overlapping channels. As is shown in [127, 128], this has connections with the so-called Steinmann relations [129]. Physically, this is the statement that a produced gluon cannot be in a bound state with two different particles simultaneously.

We now move on the $2 \to 4$ amplitude. Assuming for now that the BDS ansatz gives the full answer, the amplitude in the Euclidean region reads

$$M_{2\to4} = \Gamma(t_1)\left(\frac{-s_1}{\mu^2}\right)^{\omega(t_1)}\Gamma(t_1,t_2,\eta_4)\left(\frac{-s_2}{\mu^2}\right)^{\omega(t_2)}\Gamma(t_2,t_3,\eta_5)\left(\frac{-s_3}{\mu^2}\right)^{\omega(t_3)}\Gamma(t_3). \quad (3.44)$$

One can then write down an ansatz for an analytic representation of the $2 \to 4$ amplitude, similar to Eq.(3.43). The number of terms that have to be included in such an ansatz for the $2 \to n-2$ MHV gluon amplitude quickly grows with n and is given by the Catalan number C_n since we are counting non-overlapping subsets. The ansatz for the $2 \to 4$ amplitude is then given by

$$\begin{aligned}
\frac{M_{2\to4}}{\Gamma(t_1)\Gamma(t_3)} = {} & d_1\left(\frac{-s_1}{\mu^2}\right)^{\omega(t_1)-\omega(t_2)}\left(\frac{-s_{345}\eta_4}{\mu^4}\right)^{\omega(t_2)-\omega(t_3)}\left(\frac{-s\eta_4\eta_5}{\mu^6}\right)^{\omega(t_3)} \\
& + d_2\left(\frac{-s_3}{\mu^2}\right)^{\omega(t_3)-\omega(t_2)}\left(\frac{-s_{456}\eta_5}{\mu^4}\right)^{\omega(t_2)-\omega(t_1)}\left(\frac{-s\eta_4\eta_5}{\mu^6}\right)^{\omega(t_1)} \\
& + d_3\left(\frac{-s_2}{\mu^2}\right)^{\omega(t_2)-\omega(t_1)}\left(\frac{-s_{345}\eta_4}{\mu^4}\right)^{\omega(t_1)-\omega(t_3)}\left(\frac{-s\eta_4\eta_5}{\mu^6}\right)^{\omega(t_3)} \\
& + d_4\left(\frac{-s_2}{\mu^2}\right)^{\omega(t_2)-\omega(t_3)}\left(\frac{-s_{456}\eta_5}{\mu^4}\right)^{\omega(t_3)-\omega(t_1)}\left(\frac{-s\eta_4\eta_5}{\mu^6}\right)^{\omega(t_1)} \\
& + d_5\left(\frac{-s_3}{\mu^2}\right)^{\omega(t_3)-\omega(t_2)}\left(\frac{-s_1}{\mu^2}\right)^{\omega(t_1)-\omega(t_2)}\left(\frac{-s\eta_4\eta_5}{\mu^6}\right)^{\omega(t_2)}. \quad (3.45)
\end{aligned}$$

This ansatz should be valid in all kinematical regimes. However, comparing this ansatz to the BDS expression once we go to the mixed region in which

$$s, s_2 > 0, \quad s_1, s_3, s_{345}, s_{456} < 0, \tag{3.46}$$

there is no solution for the parameters d_i as is shown in [25]. This means that the BDS ansatz in this kinematical region is not compatible with Regge factorisation. In fact, in this region the BDS ansatz has the asymptotic form

$$\frac{M_{2\to4}}{\Gamma(t_1)\Gamma(t_3)} = C\left(\frac{-s_1}{\mu^2}\right)^{\omega(t_1)}\Gamma(t_1,t_2,\eta_4)\left(\frac{-s_2}{\mu^2}\right)^{\omega(t_2)}\Gamma(t_2,t_3,\eta_5)\left(\frac{-s_3}{\mu^2}\right)^{\omega(t_3)}, \tag{3.47}$$

with an additional phase C, which reads

$$C = e^{i\frac{\pi}{4}\gamma_K(\lambda)\left(\log\left(\frac{\vec{q}_1^{\,2}\vec{q}_3^{\,2}}{(\vec{q}_1-\vec{q}_3)^2\mu^2}\right)-\frac{1}{\epsilon}\right)}. \tag{3.48}$$

The appearance of this phase explains the wrong analytic structure of the BDS ansatz. As explained in [25], this phase is the one-loop approximation of a Regge cut contribution, which appears because the BDS ansatz is one-loop exact. However, an explicit calculation in [75] shows that starting from two loops this Regge cut piece is not contained in the BDS ansatz. We now know that this failure starting from two loops is due to the appearance of the remainder function, which then accounts for the Regge cut. Physically, the BDS ansatz accounts correctly for the Regge poles. However, starting from the $2 \to 4$ amplitude, two Reggeons can form a bound state in the s_2-channel which then gives rise to a Regge cut contribution.

A precise study of the Regge cut piece is carried out in [75, 76] and amounts to finding a solution to the BFKL equation in the colour octet channel, with the result that the remainder function in the mixed region Eq.(3.46) for the $2 \to 4$ amplitude can be written as

$$e^{R+i\delta}\Big|_{\text{MRL}} = \tag{3.49}$$
$$\cos\pi\omega_{ab} + i\frac{\lambda}{2}\sum_n(-1)^n\left(\frac{r}{r^*}\right)^{\frac{n}{2}}\int\frac{d\nu}{\nu^2+\frac{n^2}{4}}\,|r|^{2i\nu}\,\Phi_{\text{Reg}}(\nu,n)\left(-(1-u_1)\sqrt{\tilde{u}_2\tilde{u}_3}\right)^{-\omega(\nu,n)},$$

where

$$\delta = \gamma_K(\lambda)\frac{\pi}{4}\log\left(\sqrt{\tilde{u}_2\tilde{u}_3}\right) \tag{3.50}$$

is a phase and

$$\omega_{ab} = \frac{1}{8}\gamma_K(\lambda)\log\frac{\tilde{u}_3}{\tilde{u}_2} \tag{3.51}$$

is the Regge pole contribution, which both include the cusp anomalous dimension γ_K. Furthermore, we have introduced the complex quantity r which, for the n-point amplitude, is defined as[6]

$$\frac{u_{2\sigma}}{1-u_{1\sigma}} =: \frac{1}{|1+r_\sigma|^2}, \quad \frac{u_{3\sigma}}{1-u_{1\sigma}} =: \frac{|r_\sigma|^2}{|1+r_\sigma|^2}, \tag{3.52}$$

[6] Note that in the weak coupling literature this quantity is usually called w_σ, cf. [130]. We choose a different letter here to avoid confusion with the strong coupling variable w_σ which we introduce in the next chapter, as they are not equivalent.

where $\sigma = 1, \ldots, n-5$ and we omit the index in Eq.(3.49) since $\sigma = 1$ is the only possibility. The universal quantities that feed into Eq.(3.49) are the BFKL eigenvalue $\omega(\nu, n)$ and the regularised impact factor $\Phi_{\text{reg}}(\nu, n)$, which allow a perturbative expansion,

$$\omega(\nu, n) = -\lambda(E_{\nu,n} + \lambda E^{(1)}_{\nu,n} + \mathcal{O}(\lambda^2)), \tag{3.53}$$

$$\Phi_{\text{Reg}}(\nu, n) = 1 + \lambda \Phi^{(1)}_{\text{Reg}}(\nu, n) + \mathcal{O}(\lambda^2). \tag{3.54}$$

Note that the regularised impact factor $\Phi_{\text{reg}}(\nu, n)$ is in fact an effective quantity, being the product of two impact factors,

$$\frac{\Phi_{\text{reg}}(\nu, n)}{\nu^2 + \frac{n^2}{4}} = \Phi^*(\nu, n)\Phi(\nu, n), \tag{3.55}$$

see [75, 76]. To show the class of functions that appear, we write out their explicit form to NLLA accuracy [75, 76, 130]:

$$E_{\nu,n} = -\frac{1}{2}\frac{|n|}{\nu^2 + \frac{n^2}{4}} + \psi\left(1 + i\nu + \frac{|n|}{2}\right) + \psi\left(1 - i\nu + \frac{|n|}{2}\right) - 2\psi(1), \tag{3.56}$$

$$\begin{aligned} E^{(1)}_{\nu,n} = &-\frac{1}{4}\Bigg(\psi''\left(1 + i\nu + \frac{|n|}{2}\right) + \psi''\left(1 - i\nu + \frac{|n|}{2}\right) \\ &-\frac{2i\nu}{\nu^2 + \frac{n^2}{4}}\left(\psi'\left(1 + i\nu + \frac{|n|}{2}\right) - \psi'\left(1 - i\nu + \frac{|n|}{2}\right)\right)\Bigg) \\ &- \zeta_2 E_{\nu,n} - 3\zeta_3 - \frac{|n|}{4}\frac{(\nu^2 - \frac{n^2}{4})}{\left(\nu^2 + \frac{n^2}{4}\right)^3} \end{aligned} \tag{3.57}$$

and

$$\Phi^{(1)}_{\text{Reg}}(\nu, n) = -\frac{1}{2}E^2_{\nu,n} - \frac{3}{8}\frac{n^2}{\left(\nu^2 + \frac{n^2}{4}\right)^2} - \zeta_2, \tag{3.58}$$

with the digamma function $\psi(z) = \frac{\Gamma'(z)}{\Gamma(z)}$ and the zeta values $\zeta_n = \zeta(n)$. By now, the BFKL eigenvalue is known to N^{2}LLA accuracy, while the impact factor is known to N^{3}LLA accuracy [31]. Furthermore, there is a proposal for all-loop expressions [131] for both quantities from an ansatz built on the similarity of Eq.(3.49) with the OPE-expansion of [61]. Eq.(3.49) is the form of the remainder function for which we want to find an analogue at strong coupling.

4. The Y-system in the multi-Regge limit

We now combine the two preceding chapters by studying how the Y-system behaves in the multi-Regge limit. We will find that there is a specific choice of the Y-system parameters which represents the multi-Regge limit. Finding the values of the Y-system parameters requires a careful analysis of the Y-system equations and possible modifications which arise from residue contributions. However, our result will be worth the effort, as the Y-system is shown to simplify drastically in this special kinematical limit.

4.1. Cross ratios and Y-functions

To begin, we need to be more explicit about the relation between our basis of cross ratios Eq.(3.4) and the Y-functions evaluated at special values of θ. This relation is worked out in [44] and can be easily stated by introducing the functions

$$U_s^{[r]} := 1 + \frac{1}{Y_{2,s}^{[r]}} := 1 + \frac{1}{\mathrm{Y}_{2,s}}\bigg|_{\theta=i\pi r/4} = 1 + \frac{1}{\mathrm{Y}_{2,s}^{[r]}}\bigg|_{\theta=0}, \tag{4.1}$$

where we introduced the italic $Y_{2,s}^{[r]}$ to denote the Y-functions evaluated at a multiple of $i\frac{\pi}{4}$. The cross ratios of pairs of adjacent points in dual space are then given by

$$U_{2k-2}^{[2p]} = \frac{x^2_{-k+p,k+p}x^2_{-k+p-1,k+p-1}}{x^2_{-k+p-1,k+p}x^2_{-k+p,k+p-1}} \tag{4.2}$$

if the number of cusps $2k-2$ between x_{-k+p} and x_{k+p-1} is even and

$$U_{2k-1}^{[2p+1]} = \frac{x^2_{-k+p,k+p+1}x^2_{-k+p-1,k+p}}{x^2_{-k+p-1,k+p+1}x^2_{-k+p,k+p}} \tag{4.3}$$

if the number of cusps $2k-1$ between x_{-k+p} and x_{k+p} is odd. Since our basis of cross ratios only connects pairs of points with adjacent indices, we can immediately write down the relations with the Y-functions, which read

$$u_{1\sigma} = \frac{x^2_{\sigma+1,\sigma+5}x^2_{\sigma+2,\sigma+4}}{x^2_{\sigma+2,\sigma+5}x^2_{\sigma+1,\sigma+4}} = \left(U_1^{[2\sigma+7]}\right)^{-1} = \frac{Y_{2,1}^{[2\sigma+7]}}{1+Y_{2,1}^{[2\sigma+7]}}, \tag{4.4}$$

$$u_{2\sigma} = \frac{x^2_{\sigma+3,n}x^2_{1,\sigma+2}}{x^2_{\sigma+2,n}x^2_{1,\sigma+3}} = \left(U_\sigma^{[\sigma+4]}\right)^{-1} = \frac{Y_{2,\sigma}^{[\sigma+4]}}{1+Y_{2,\sigma}^{[\sigma+4]}}, \tag{4.5}$$

$$u_{3\sigma} = \frac{x^2_{2,\sigma+3}x^2_{1,\sigma+4}}{x^2_{1,\sigma+3}x^2_{2,\sigma+4}} = \left(U_\sigma^{[\sigma+6]}\right)^{-1} = \frac{Y_{2,\sigma}^{[\sigma+6]}}{1+Y_{2,\sigma}^{[\sigma+6]}}. \tag{4.6}$$

The idea of our following analysis is simple. The right-hand side of the equations (4.4-4.6) depends on the Y-system parameters $|m_s|$, C_s and ϕ_s. If we demand that the cross ratios on the left-hand side of Eqs.(4.4-4.6) show multi-Regge behaviour, i.e. the behaviour worked out in section 3.3, this will give rise to constraints on the values the Y-system parameters can take. We will see that these constraints are indeed powerful enough to fix $2n-10$ of the Y-system parameters.

For a large number of gluons, the upper indices in Eqs.(4.4-4.6) will also become large. Fortunately, we can make use of the symmetry

$$U_s^{[l]} = U_{n-4-s}^{[l\pm n]} \tag{4.7}$$

which originates in the $\mathbb{Z}_4$ symmetry of the Hitchin system underlying the Y-system. Using this symmetry we can always decrease the absolute value of the upper index to be smaller than or equal to $\lfloor \frac{n}{2} \rfloor$. From there, we can use the recursion relations Eq.(2.68) to express the cross ratios in terms of Y-functions in the fundamental strip $|\mathrm{Im}\,\theta| < \frac{\pi}{4}$. Applying the symmetry twice, we find that

$$U_s^{[l]} = U_s^{[l\pm 2n]}. \tag{4.8}$$

This relation is in fact necessary to be consistent with the cyclicity of the dual variables $x_i = x_{i+n}$.

4.2. The multi-Regge limit of the Y-system

4.2.1. The 6-point case

We will begin with the simplest case of six gluons, which was first analysed in [78]. We review the results here to spell out some quantities which we will try to generalise in the following. Note that in the 6-point case, the index s of the Y-functions is fixed to one and will be dropped in the following. The three cross ratios and their associated Y-functions are

$$u_1 = \frac{x_{3,5}^2 x_{2,6}^2}{x_{3,6}^2 x_{2,5}^2} = \frac{Y_2^{[-3]}}{1+Y_2^{[-3]}},\ u_2 = \frac{x_{1,3}^2 x_{4,6}^2}{x_{1,4}^2 x_{3,6}^2} = \frac{Y_2^{[-1]}}{1+Y_2^{[-1]}},\ u_3 = \frac{x_{1,5}^2 x_{2,4}^2}{x_{1,4}^2 x_{2,5}^2} = \frac{Y_2^{[1]}}{1+Y_2^{[1]}}. \tag{4.9}$$

We know from our kinematical analysis that u_1 has to go to one, while the other two cross ratios have to approach zero. From Eqs.(4.4-4.6) it is clear that if a cross ratio vanishes, the associated Y-function has to go to zero, as well, while a cross ratio going to one forces the corresponding Y-function to go to infinity. Writing out schematically the equation governing $Y_2^{[1]}$,

$$\log \mathrm{Y}_2\left(i\frac{\pi}{4}\right) = -\sqrt{2}|m|\cos\left(\frac{\pi}{4}-\phi\right) + \sum_{a'} K^{2,a'} \star \log\left(1+\mathrm{Y}_{a'}\right), \tag{4.10}$$

we see that $\log Y_2^{[1]}$ has to be large and negative to make u_3 small. This can certainly be achieved if we take $|m| \to \infty$, as long as $\phi \in \left(-3\frac{\pi}{4}, \frac{\pi}{4}\right)$. This limit has the further virtue that the leading contribution of the integral terms will schematically be given by

$$\int_{-\infty}^{\infty} d\theta' K(\theta-\theta')\log\left(1+\mathrm{Y}(\theta')\right) \cong \int_{-\infty}^{\infty} d\theta' K(\theta-\theta')\log\left(1+e^{-|m|\cosh(\theta'-i\phi)}\right) \to 0, \tag{4.11}$$

which is negligible compared to the term $\sim |m|$ in Eq.(4.10) in the large $|m|$ limit. Indeed, in [78] it is shown that the parameter choice

$$|m| \to \infty, \quad \phi \to 0, \quad C = \text{const.} \tag{4.12}$$

reproduces the multi-Regge limit. Since we can neglect the integrals in the Y-system equations in the fundamental strip $|\mathrm{Im}\,\theta| < \frac{\pi}{4}$ as we saw in Eq.(4.11) above, the Y-functions simplify drastically and read

$$\mathrm{Y}_1(\theta) \cong e^{-|m|\cosh(\theta - i\phi) - C}, \ \mathrm{Y}_2(\theta) \cong e^{-\sqrt{2}|m|\cosh(\theta - i\phi)}, \ \mathrm{Y}_3(\theta) \cong e^{-|m|\cosh(\theta - i\phi) + C}. \tag{4.13}$$

Using these expressions and the recursion relation Eq.(2.68), we can determine the cross ratios and find

$$u_1 = 1 - \left(w + \frac{1}{w} + 2\cosh C\right)\varepsilon + \mathcal{O}(\varepsilon^2), \ u_2 = w\varepsilon + \mathcal{O}(\varepsilon^2), \ u_3 = \frac{\varepsilon}{w} + \mathcal{O}(\varepsilon^2), \tag{4.14}$$

where we have introduced the quantities

$$\varepsilon = e^{-|m|\cos\phi}, \quad w = e^{|m|\sin\phi}, \tag{4.15}$$

which have the limits $\varepsilon \to 0$ and $w \to$ const. in the multi-Regge limit. Eq.(4.14) shows exactly the behaviour we have found from a purely kinematical analysis in section 3.3. We now turn to the 7-point case to see how this result extends to more gluons.

4.2.2. The 7-point case

In the 7-point case, we now have six cross ratios given by

$$\begin{aligned}
u_{11} &= \frac{x_{2,6}^2 x_{3,5}^2}{x_{3,6}^2 x_{2,5}^2} = \frac{Y_{2,2}^{[2]}}{1 + Y_{2,2}^{[2]}}, \quad u_{21} = \frac{x_{4,7}^2 x_{1,3}^2}{x_{3,7}^2 x_{1,4}^2} = \frac{Y_{2,2}^{[-2]}}{1 + Y_{2,2}^{[-2]}}, u_{31} = \frac{x_{2,4}^2 x_{1,5}^2}{x_{1,4}^2 x_{2,5}^2} = \frac{Y_{2,2}^{[0]}}{1 + Y_{2,2}^{[0]}}, \\
u_{12} &= \frac{x_{3,7}^2 x_{4,6}^2}{x_{4,7}^2 x_{3,6}^2} = \frac{Y_{2,1}^{[-3]}}{1 + Y_{2,1}^{[-3]}}, u_{22} = \frac{x_{5,7}^2 x_{1,4}^2}{x_{4,7}^2 x_{1,5}^2} = \frac{Y_{2,1}^{[-1]}}{1 + Y_{2,1}^{[-1]}}, u_{32} = \frac{x_{2,5}^2 x_{1,6}^2}{x_{1,5}^2 x_{2,6}^2} = \frac{Y_{2,1}^{[1]}}{1 + Y_{2,1}^{[1]}},
\end{aligned} \tag{4.16}$$

It is to be expected that the multi-Regge limit for the 7-point case still connected with the large $|m_s|$-regime[1]. For the moment, let us assume that we can still neglect the integrals in the fundamental strip as described in Eq.(4.11). We will justify this once we have determined all parameters.

To determine the correct limit, let us start by analysing the cross ratio u_{11} which approaches one in the multi-Regge limit. Using the recursion relation Eq.(2.68) for the associated Y-function, we find that

$$Y_{2,2}^{[2]} \cong \frac{1 + e^{-\sqrt{2}|m_1|\cos\left(\frac{\pi}{4} - \phi_1\right)}}{e^{-\sqrt{2}|m_2|\cos\phi_2}\left(1 + e^{|m_2|\cos\left(\frac{\pi}{4} - \phi_2\right) - C_2}\right)\left(1 + e^{|m_2|\cos\left(\frac{\pi}{4} - \phi_2\right) + C_2}\right)} \to \infty. \tag{4.17}$$

[1] For example, we can return to the 6-point case by taking a collinear limit.

This Y-function can only diverge if every term in the denominator vanishes. Expanding the denominator as

$$e^{-\sqrt{2}|m_2|\cos\phi_2} + e^{\sqrt{2}|m_2|\sin\phi_2} + 2\cosh C_2 e^{-|m_2|\cos\left(\frac{\pi}{4}+\phi_2\right)}, \tag{4.18}$$

this forces ϕ_2 to lie in the interval

$$\phi_2 \in \left(-\frac{\pi}{2},\frac{\pi}{2}\right) \cap (-\pi,0) \cap \left(-\frac{3\pi}{4},\frac{\pi}{4}\right) = \left(-\frac{\pi}{2},0\right). \tag{4.19}$$

In writing the intersection, we have assumed that ϕ_2 stays at least in the range $-\pi \leq \phi_2 \leq \pi$. To determine the exact value of ϕ_2 we analyse the fraction $\frac{u_{21}}{u_{31}}$, which we know stays finite in the multi-Regge limit. Since both cross ratios go to zero individually, we see that the leading term for this fraction in terms of the Y-functions is given by

$$\frac{u_{21}}{u_{31}} \cong \frac{Y_{2,2}^{[-2]}}{Y_{2,2}^{[0]}} \cong \frac{1+e^{-\sqrt{2}|m_1|\cos\left(\frac{\pi}{4}+\phi\right)}}{e^{-2\sqrt{2}|m_2|\cos\phi_2}\left(1+e^{|m_2|\cos\left(\frac{\pi}{4}+\phi_2\right)-C_2}\right)\left(1+e^{|m_2|\cos\left(\frac{\pi}{4}+\phi_2\right)+C_2}\right)} \to \text{const.} \tag{4.20}$$

As before, we can expand the denominator. If this expression shall converge to a constant, at least one of the terms in the denominator has to remain finite, with all other terms going to zero. This allows the two choices $\phi_2 \to -\frac{\pi}{4}$ or $\phi_2 \to \frac{\pi}{2}$, of which the latter is excluded by Eq.(4.19). A similar analysis determines ϕ_1. Instead of presenting all equations and the constraints we derive from them, it is an easier task to just show that the parameter choice

$$\begin{aligned} &|m_s| \to \infty, \quad C_s = \text{const.}, \\ &\phi_1 \to 0, \qquad \phi_2 \to -\frac{\pi}{4} \end{aligned} \tag{4.21}$$

leads to the correct behaviour for the cross ratios. For completeness, we spell out the remaining constraint equations in appendix B.

To check that Eq.(4.21) is indeed the correct choice of parameters, we start by defining

$$\begin{aligned} \varepsilon_1 &= e^{-|m_1|\cos\phi_1}, & w_1 &= e^{|m_1|\sin\phi_1}, \\ \varepsilon_2 &= e^{-|m_2|\cos\left(\frac{\pi}{4}+\phi_2\right)}, & w_2 &= e^{|m_2|\sin\left(\frac{\pi}{4}+\phi_2\right)}, \end{aligned} \tag{4.22}$$

which have the limits $\varepsilon_s \to 0$ and $w_s \to$ const. in the multi-Regge limit. From the Y-functions in the fundamental strip we obtain the relations

$$u_{32} = \frac{Y_{2,1}^{[1]}}{1+Y_{2,1}^{[1]}} \cong \frac{e^{-\sqrt{2}|m_1|\cos\left(\frac{\pi}{4}-\phi_1\right)}}{1+e^{-\sqrt{2}|m_1|\cos\left(\frac{\pi}{4}-\phi_1\right)}} = \frac{\frac{\varepsilon_1}{w_1}}{1+\frac{\varepsilon_1}{w_1}} = \frac{\varepsilon_1}{w_1} + \mathcal{O}(\varepsilon^2), \tag{4.23}$$

$$u_{22} = \frac{Y_{2,1}^{[-1]}}{1+Y_{2,1}^{[-1]}} \cong \frac{e^{-\sqrt{2}|m_1|\cos\left(\frac{\pi}{4}+\phi_1\right)}}{1+e^{-\sqrt{2}|m_1|\cos\left(\frac{\pi}{4}+\phi_1\right)}} = \frac{\varepsilon_1 w_1}{1+\varepsilon_1 w_1} = \varepsilon_1 w_1 + \mathcal{O}(\varepsilon^2), \tag{4.24}$$

$$u_{31} = \frac{Y_{2,2}^{[0]}}{1+Y_{2,2}^{[0]}} \cong \frac{e^{-\sqrt{2}|m_2|\cos\phi_2}}{1+e^{-\sqrt{2}|m_2|\cos\phi_2}} = \frac{\frac{\varepsilon_2}{w_2}}{1+\frac{\varepsilon_2}{w_2}} = \frac{\varepsilon_2}{w_2} + \mathcal{O}(\varepsilon^2). \tag{4.25}$$

To obtain the other cross ratios we have to employ the recursion relation Eq.(2.68) and find

$$Y_{2,2}^{[-2]} = \frac{1+Y_{2,1}^{[-1]}}{Y_{2,2}^{[0]}\left(1+\frac{1}{Y_{3,2}^{[-1]}}\right)\left(1+\frac{1}{Y_{1,2}^{[-1]}}\right)} \cong \frac{1+\varepsilon_1 w_1}{\frac{\varepsilon_2}{w_2}(1+\frac{e^{-C_2}}{\varepsilon_2})(1+\frac{e^{C_2}}{\varepsilon_2})} = \varepsilon_2 w_2 + \mathcal{O}(\varepsilon^2), \quad (4.26)$$

from which we conclude that

$$u_{21} = \frac{Y_{2,2}^{[-2]}}{1+Y_{2,2}^{[-2]}} \cong \frac{\varepsilon_2 w_2}{1+\varepsilon_2 w_2} = \varepsilon_2 w_2 + \mathcal{O}(\varepsilon^2). \quad (4.27)$$

Similarly, we get

$$Y_{2,2}^{[2]} \cong \frac{1+\frac{\varepsilon_1}{w_1}}{\frac{\varepsilon_2}{w_2}\left(1+w_2 e^{-C_2}\right)\left(1+w_2 e^{C_2}\right)}, \quad (4.28)$$

which leads to

$$u_{11} = \frac{Y_{2,2}^{[2]}}{1+Y_{2,2}^{[2]}} \cong 1 - \left(w_2 + \frac{1}{w_2} + 2\cosh C_2\right)\varepsilon_2 + \mathcal{O}(\varepsilon^2). \quad (4.29)$$

For the last cross ratio, u_{11}, we have to use the recursion relation Eq.(2.68) several times and find after a straightforward calculation that

$$\begin{aligned} Y_{2,1}^{[-3]} &= \frac{1+Y_{2,2}^{[-2]}}{Y_{2,1}^{[-1]}\left(1+\frac{1}{Y_{3,1}^{[-2]}}\right)\left(1+\frac{1}{Y_{1,1}^{[-2]}}\right)} \\ &\cong \frac{(1+\varepsilon_2 w_2)}{\varepsilon_1 w_1\left(1+\frac{e^{-C_1}\varepsilon_1\left(1+\frac{1}{\varepsilon_1 w_1}\right)}{1+e^{C_2}\varepsilon_2}\right)\left(1+\frac{e^{C_1}\varepsilon_1\left(1+\frac{1}{\varepsilon_1 w_1}\right)}{1+e^{-C_2}\varepsilon_2}\right)}, \end{aligned} \quad (4.30)$$

from which we calculate the cross ratio to be given by

$$u_{12} = \frac{Y_{2,1}^{[-3]}}{1+Y_{2,1}^{[-3]}} \cong 1 - \left(w_1 + \frac{1}{w_1} + 2\cosh C_1\right)\varepsilon_1 + \mathcal{O}(\varepsilon^2). \quad (4.31)$$

We see that we can again find the correct values of the Y-system parameters for the multi-Regge limit. Making this parameter choice, the cross ratios split into two triplets, which resemble a 'double copy' of the 6-point case. To obtain this result, it is essential that ϕ_2 is non-zero, as one can nicely see from Eq.(4.25). Pushing on to more gluons, again assuming that all integrals can just naively be neglected, we see hints that in general $\phi_s = (1-s)\frac{\pi}{4}$ seem to be the values for the phases in the multi-Regge limit. However, as was explained in section 2.3.3, the Y-system has to be modified once large phases enter the game. We will therefore analyse when residue contributions from the kernels have to be picked up before we can prove our suspicion for the values of ϕ_s.

4.3. Large phases and residue contributions

In this section, we will make the following ansatz for the Y-system parameters:

$$|m_s| \to \infty,\ C_s = \text{const.},\ \phi_s \to (1-s)\frac{\pi}{4}. \tag{4.32}$$

Furthermore, we introduce parameters

$$\varepsilon_s := e^{-|m_s|\cos\left((s-1)\frac{\pi}{4}+\phi_s\right)},\ w_s := e^{|m_s|\sin\left((s-1)\frac{\pi}{4}+\phi_s\right)}, \tag{4.33}$$

where $s = 1, \ldots, n-5$ and as before we have that $\varepsilon_s \to 0$ and $w_s \to$ const. in the multi-Regge limit. Our goal is to show that for this choice of parameters we indeed find the correct behaviour of the cross ratios. As mentioned before, the reason this is non-trivial is that large phases appear in our ansatz Eq.(4.32). Let us therefore begin by spelling out the relevant Y-system formula for complex mass parameters again:

$$\log\tilde{\mathrm{Y}}_{2,s}(\theta) = -\sqrt{2}|m_s|\cosh\theta + \sum_{a',s'}\int_{\mathbb{R}} d\theta' K^{2,a'}_{s,s'}(\theta-\theta'+i\phi_s-i\phi_{s'})\log(1+\tilde{\mathrm{Y}}_{a',s'}(\theta')), \tag{4.34}$$

where, as before, $\tilde{\mathrm{Y}}_{2,s}(\theta) = \mathrm{Y}_{2,s}(\theta+i\phi_s)$. The kernels that appear in Eq.(4.34) have simple poles along the lines $\mathrm{Im}\,(\theta + i\phi_s - i\phi_{s'}) = ik\frac{\pi}{4}$, where $k = 2(2n+1)$ for K_1 and $k = 2n+1$ for K_2, K_3 for $n \in \mathbb{Z}$. Whenever we cross such a line, we have to pick up a residue contribution. However, note that the line actually has to be crossed, for $\theta = ik\frac{\pi}{4}$ we can still use an $i\varepsilon$-prescription to avoid the singularities (for more details see [44] and section 5.3). Once we have accounted for all crossed poles, our Y-system equations schematically read

$$\begin{aligned}\log\tilde{\mathrm{Y}}_{2,s}(\theta) = &-\sqrt{2}|m_s|\cosh\theta + \sum_{a',s'}\int_{\mathbb{R}} d\theta' K^{2,a'}_{s,s'}(\theta-\theta'+i\phi_s-i\phi_{s'})\log(1+\tilde{\mathrm{Y}}_{a',s'}(\theta')) \\ &+ \sum_{\nu} n_\nu \log\left(1+\tilde{\mathrm{Y}}_{a_\nu,s_\nu}\left(\theta+i\phi_s-i\phi_{s_\nu}-ik_\nu\frac{\pi}{4}\right)\right),\end{aligned} \tag{4.35}$$

where we have introduced an index ν that counts all crossed poles. The coefficient n_ν allows for a sign factor which depends on which kernel the crossed pole belongs to and where it was crossed.

Since we integrate along the real axis, the Y-functions which appear in the integrand of Eq.(4.34) are always evaluated at real values of θ'. Note that due to the structure of the Y-system Eqs.(2.60-2.62) kernels are only non-zero if $s' = s \pm 1$ or $s' = s$. However, for those values of s' the phase difference is always equal to $\pm i\frac{\pi}{4}$ or zero due to our ansatz Eq.(4.32). For those imaginary parts in the kernels we can still use an $i\varepsilon$-prescription, which in turn implies that for real values of θ we never have to pick up residue contributions and can keep on using the standard form Eq.(4.34). This means that as we go to the region of large mass parameters, we can always use the asymptotic form

$$\tilde{\mathrm{Y}}_{1,s}(\theta) \cong e^{-|m_s|\cosh\theta - C_s},\ \tilde{\mathrm{Y}}_{2,s}(\theta) \cong e^{-\sqrt{2}|m_s|\cosh\theta},\ \tilde{\mathrm{Y}}_{3,s}(\theta) \cong e^{-|m_s|\cosh\theta + C_s}, \tag{4.36}$$

without any additional residue contributions, allowing us to use the argument spelled out in Eq.(4.11) to conclude that the integral contributions can always be neglected in the large

mass limit. Still, the integrals can leave their imprint on the Y-functions for arguments with a non-vanishing imaginary part through the residue terms, which we have to pick up before neglecting the integrals.

As the cross ratios are given in terms of the $\mathrm{Y}_{2,s}$-functions and not the $\tilde{\mathrm{Y}}_{2,s}$-functions, we shift the argument in Eq.(4.35) and find

$$\log \mathrm{Y}_{2,s}(\theta) = -\sqrt{2}|m_s| \cosh\left(\theta - i\phi_s\right) + \sum_{\nu} n_\nu \log\left(1 + \mathrm{Y}_{a_\nu,s_\nu}\left(\theta - ik_\nu \frac{\pi}{4}\right)\right), \tag{4.37}$$

where we already dropped the integral contributions. Our main task is now to figure out which $\mathrm{Y}_{2,s}$-functions are modified by residue terms and how the cross ratios are affected by this.

4.3.1. The 8-point case

To fill the formulas presented in the last section with some life, let us analyse the 8-point amplitude. As a specific example, let us study $Y_{2,2}^{[-2]}$, which is connected with the cross ratio u_{22}. Note that due to our choice of phases, this is equivalent to calculating $\tilde{Y}_{2,2}^{[-1]}$. To find the residue contributions, imagine starting from $\theta = 0$ where Eq.(4.34) holds without residue terms because $\theta = 0$ is a real value (cf. the discussion around Eq.(4.36)) and then moving $\theta \to -i\frac{\pi}{4}$. Looking at the kernels $K_{2,s'}^{2,a'}(\theta - \theta' + i\phi_2 - i\phi_{s'})$, we see that only for $s' = 1$ do we cross $\mathrm{Im}(\theta + i\phi_2 - i\phi_{s'}) = -i\frac{\pi}{4}$. The only kernel with both a singularity at $-i\frac{\pi}{4}$ and a coefficient with $s' = 1$ is $K_{2,1}^{2,2}$. Therefore we need to pick up a residue and get a contribution $\sim \log\left(1 + \tilde{\mathrm{Y}}_{2,1}\left(-i\frac{\pi}{4}\right)\right)$, which, after shifting back to the Y-functions, leads to

$$Y_{2,2}^{[-2]} = e^{-\sqrt{2}|m_2|\cos\left(\frac{\pi}{2}+\phi_2\right)}\left(1 + Y_{2,1}^{[-1]}\right) = \varepsilon_2 w_2 \left(1 + Y_{2,1}^{[-1]}\right). \tag{4.38}$$

Note that for this specific example, the residue contribution is negligible since $Y_{2,1}^{[-1]} \cong \varepsilon_1 w_1$. However, it serves to show how residue contributions can affect our equations and that we have to be careful in taking them into account.

In the same way we analyse the remaining Y-functions relevant for the evaluation of the cross ratios and present a graphical representation of our results in figure 4.1. Every node in figure 4.1 corresponds to the three possible values $Y_{a,s}^{[k]}$ with s and k fixed. Encircled nodes correspond to Y-functions which receive no residue contributions. Arrows point to nodes in which a given Y-function shows up as a residue contribution. Y-functions not indicated above have a more complicated residue structure and should be evaluated using the recursion relation Eq.(2.68). However, since we need it later, we explain how to read off the residue contribution for those functions in appendix C.

Now that we have understood the residue structure, we can go ahead and calculate the cross ratios. The quickest way to do this is to note from figure 4.1 that all $Y_{a,s}^{[-1]}$ do not receive any corrections from residues and that with their help we can determine the $Y_{a,s}^{[0]}$. We then use the recursion relation to express all cross ratios through these six Y-functions.

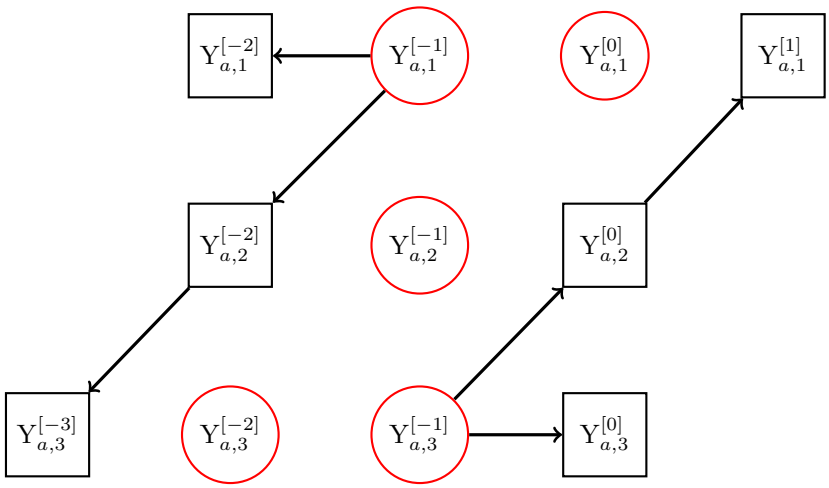

Figure 4.1.: Structure of residue contributions for the 8-point case. Every node corresponds to the 3 values $Y_{a,s}^{[k]}$ with s and k fixed. Encircled nodes correspond to Y-functions which receive no residue contributions. Arrows point to nodes in which a given Y-function appears as a residue contribution. Y-functions not indicated above have a more complicated residue structure.

After a quick calculation, we find that the cross ratios are given by

$$\begin{aligned} u_{1\sigma} &= 1 - \left(w_{n-4-\sigma} + \frac{1}{w_{n-4-\sigma}} + 2\cosh C_{n-4-\sigma} \right) \varepsilon_{n-4-\sigma} + \mathcal{O}(\varepsilon^2), \\ u_{2\sigma} &= \varepsilon_{n-4-\sigma} w_{n-4-\sigma} + \mathcal{O}(\varepsilon^2), \\ u_{3\sigma} &= \frac{\varepsilon_{n-4-\sigma}}{w_{n-4-\sigma}} + \mathcal{O}(\varepsilon^2), \end{aligned} \tag{4.39}$$

and nicely show the expected behaviour (cf. section 3.3). Note that target-projectile symmetry Eq.(3.5) interchanges the parameters above as

$$\varepsilon_\sigma \leftrightarrow \varepsilon_{n-4-\sigma},\ w_\sigma \leftrightarrow \frac{1}{w_{n-4-\sigma}},\ \cosh C_\sigma \leftrightarrow \cosh C_{n-4-\sigma}, \tag{4.40}$$

and this prescription will turn out to carry over to higher-point cases, as well.

4.3.2. The n-point case

After all the preparatory work, we are now able to tackle the general n-gluon case. As stated before, we want to show that the cross ratios have multi-Regge behaviour if we assume that $\phi_s = (1-s)\frac{\pi}{4}$. We use the fact that kernels in the Y-system are only non-vanishing if $s' = s \pm 1$ or $s' = s$, which means that the imaginary parts in the arguments of the kernels due to phase differences are always given by $\pm i\frac{\pi}{4}$ or zero. This allows us to lift the analysis of the residues of the 8-point case to the general case, with results shown in figure 4.2. Figure 4.2 looks similar to figure 4.1 with some changes. Grey boxes, just like Y-functions not shown in the figure, have a more complicated residue structure, as explained in appendix C. If a cross ratio is determined by a given function $Y_{2,s}^{[k]}$ we have

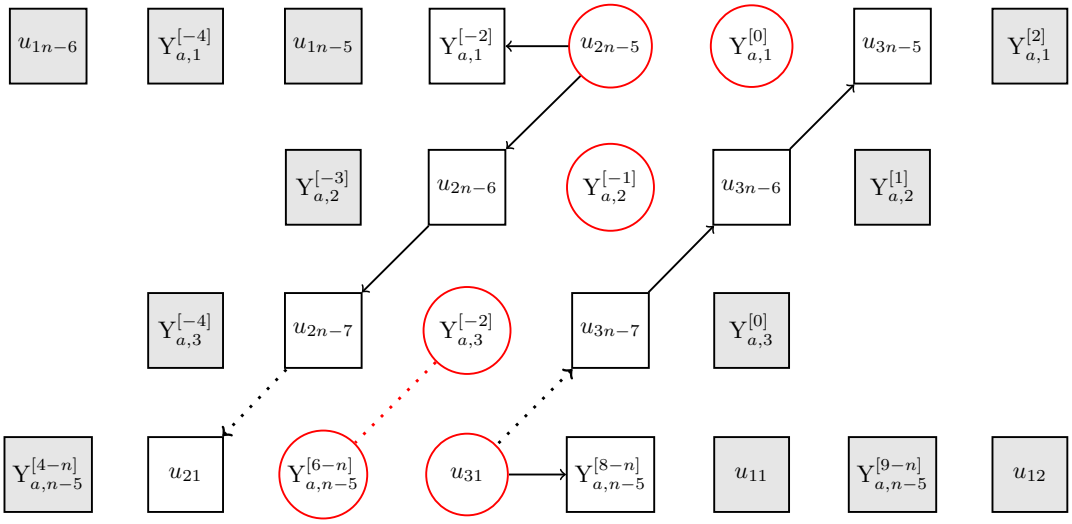

Figure 4.2.: Structure of residue contributions for the n-point case. Every node corresponds to the three values $Y^{[k]}_{a,s}$ with s and k fixed. Encircled nodes correspond to Y-functions which receive no residue contributions. Arrows point to nodes in which a given Y-function shows up as a residue contribution. Grey boxes and Y-functions not indicated above have a more complicated residue structure. If a cross ratios is determined by a given function $Y^{[k]}_{2,s}$ we have indicated this by putting the cross ratio in the box instead of the Y-function.

indicated this by putting the cross ratio in the box instead of the Y-function. Note that we have employed the shift symmetry Eqs.(4.7, 4.8) to have the cross ratios $u_{1\sigma}$ in the first row at negative values of θ.

In the central region of figure 4.2 something remarkable happens. Along the diagonals on which all cross ratios $u_{2\sigma}$ and $u_{3\sigma}$ lie the 'residue flow' is very simple. First of all, there are two functions which do not receive any residue corrections and can be evaluated immediately. From our general formulas

$$u_{2\sigma} = \frac{Y^{[-(n-4-\sigma)]}_{2,n-4-\sigma}}{1+Y^{[-(n-4-\sigma)]}_{2,n-4-\sigma}}, \qquad u_{3\sigma} = \frac{Y^{[-(n-6-\sigma)]}_{2,n-4-\sigma}}{1+Y^{[-(n-6-\sigma)]}_{2,n-4-\sigma}} \tag{4.41}$$

we find that

$$u_{31} = \frac{\varepsilon_{n-5}}{w_{n-5}}, \qquad u_{2\,n-5} = \varepsilon_1 w_1. \tag{4.42}$$

Furthermore, every $Y^{[k]}_{2,s}$-function (except for the two functions discussed above) along those diagonals gets a correction by only one residue term involving $Y^{[k\pm1]}_{2,s\mp1}$ and the Y-function itself appears as a residue correction for the function $Y^{[k\mp1]}_{2,s\pm1}$, where the upper sign is valid for the $u_{2\sigma}$-diagonal and the lower sign is valid for the $u_{3\sigma}$-diagonal. This allows an iterative determination of the cross ratios. Ignoring the residue contributions for a moment, we see that the Y-functions along the $u_{2\sigma}$-diagonal are given by

$$Y^{[-s]}_{2,s} = e^{-\sqrt{2}|m_s|\cos\left(\frac{\pi}{4}+(s-1)\frac{\pi}{4}+\phi_s\right)} \cdot (\text{Residue Terms}) = \varepsilon_s w_s \cdot (\text{Residue Terms}), \tag{4.43}$$

and similarly

$$Y_{2,s}^{[-s+2]} = e^{-\sqrt{2}|m_s|\cos\left(-\frac{\pi}{4}+(s-1)\frac{\pi}{4}+\phi_s\right)} \cdot (\text{Residue Terms}) = \frac{\varepsilon_s}{w_s} \cdot (\text{Residue Terms}) \,. \quad (4.44)$$

This allows us to obtain the first non-trivial element along the $u_{2\sigma}$-diagonal. We find

$$Y_{2,2}^{[-2]} = \varepsilon_2 w_2 \cdot \left(1 + Y_{2,1}^{[-1]}\right) = \varepsilon_2 w_2 \cdot (1 + \varepsilon_1 w_1) = \varepsilon_2 w_2 + \mathcal{O}\left(\varepsilon^2\right). \quad (4.45)$$

Due to the simple residue structure along the two diagonals, this structure repeats itself and we can conclude that

$$u_{2\sigma} = \varepsilon_{n-4-\sigma} w_{n-4-\sigma}, \quad u_{3\sigma} = \frac{\varepsilon_{n-4-\sigma}}{w_{n-4-\sigma}}. \quad (4.46)$$

We are left with the large cross ratios $u_{1\sigma}$ which lie along the first row and therefore have a more complicated residue structure. To determine those, consider adding another gluon to a n-point amplitude. This introduces another triplet of Y-functions. Furthermore, all cross ratios $u_{1\sigma}$ in the first row are shifted to the left by two boxes and a new cross ratio $u_{1\,(n+1)-5}$ appears which is connected to $Y_{2,1}^{[-3]}$. However, in the multi-Regge limit where all integral contributions are negligible, the only way the new functions can influence the values of the n-point Y-functions is through residue contributions. If a given n-point Y-function is not affected by residues of the three new Y-functions, it will keep its old value. Since the functions that appear in a residue term could, of course, also be affected by the new Y-functions, the question which Y-functions keep their value is a bit subtle. Following our analysis of the grey boxes in appendix C it turns out that a Y-function keeps its value if it lies in or on the triangle spanned by the $u_{2\sigma}$ diagonal and the diagonal starting from u_{22} going to the upper left in the $(n+1)$-point analogue of figure 4.2. This diagonal intersects the first row at the node $Y_{a,1}^{[13-2n]}$, which, comparing with Eq.(4.4), means that the last $u_{1\sigma}$ which is not affected by the new Y-functions is u_{13}. In turn, this means that all cross ratios $u_{1\sigma}$ with $\sigma \geq 3$ take the values of the n-point cross ratios $u_{1\kappa}$ with shifted indices. The two remaining undetermined cross ratios u_{11}, u_{12} can be fixed using target-projectile symmetry Eq.(3.5), which relates them with $u_{1\,(n+1)-5}$ and $u_{1\,(n+1)-4}$, respectively. This fixes all cross ratios. Since we have shown explicitly for the 7- and 8-point amplitude that the cross ratios show multi-Regge behaviour, we can now conclude that this is true for an arbitrary number of gluons. Explicitly, the cross ratios $u_{1\sigma}$ are given by

$$u_{1\sigma} = 1 - \left(w_{n-4-\sigma} + \frac{1}{w_{n-4-\sigma}} + 2\cosh C_{n-4-\sigma}\right)\varepsilon_{n-4-\sigma}. \quad (4.47)$$

Comparing the results Eqs.(4.46, 4.47) with the definition of the weak coupling parameter r_σ, Eq.(3.52), we find the relation

$$r_\sigma = \frac{1}{w_{n-4-\sigma}} e^{iC_{n-4-\sigma}}. \quad (4.48)$$

between the various parameters.

Summing up, we showed that there is a particular choice of the Y-system parameters which leads to the behaviour expected from multi-Regge kinematics. Furthermore, we see that the n-point multi-Regge limit is given by a $(n-5)$-fold copy of the 6-point case.

Before we close this chapter, let us mention a point that we skimmed over before. In section 4.2.2 we analysed the 7-point case and just assumed we could neglect the integrals without considering any residue terms. Looking at figure 4.2, we see that we were indeed justified in doing so, as the Y-functions at $\theta = -i\frac{\pi}{4}$ and $\theta = 0$ for the 7-point case do not receive residue contributions for our choice of phases and all other Y-functions were obtained using the recursion relation Eq.(2.68).

5. Calculating amplitudes in the multi-Regge limit

In the last chapter, we have seen that the Y-system simplifies drastically in multi-Regge kinematics. However, this simplification was only analysed on the level of the Y-system equations and not on the level of the amplitude. In this chapter we will therefore outline our method for the computation of the amplitudes and comment on the numerical algorithms used before applying our programme to the 6- and 7-point amplitude in the following chapters.

5.1. Excited states and Bethe ansatz

In this section, we will study the Y-system and the free energy contribution to the amplitude more carefully. The other contributions are rather simple and will be discussed once we do actual calculations.

We start from the schematic form of the Y-system equations

$$\log \tilde{\mathrm{Y}}_{a,s}(\theta) = -p_{a,s}(\theta) + \sum_{a',s'} \int_{\mathbb{R}} d\theta' K^{a,a'}_{s,s'}(\theta,\theta') \log(1+\tilde{\mathrm{Y}}_{a',s'}(\theta')), \tag{5.1}$$

where we have allowed for a general dependence of the kernels on the variables θ, θ' for reasons which become clear in section 5.2. $p_{a,s}(\theta)$ will be called *driving term* in the following. Once we have solved the Y-system equations, we get the free energy contribution to the amplitude by calculating

$$A_{\text{free}} = \sum_s \frac{|m_s|}{2\pi} \int_{\mathbb{R}} d\theta \cosh\theta \log\left((1+\tilde{\mathrm{Y}}_{1,s}(\theta))(1+\tilde{\mathrm{Y}}_{3,s}(\theta))(1+\tilde{\mathrm{Y}}_{2,s}(\theta))^{\sqrt{2}}\right). \tag{5.2}$$

As we showed in chapter 4, in the multi-Regge limit the Y-functions simplify and are well approximated by

$$\log \tilde{\mathrm{Y}}_{a,s}(\theta) \cong -p_{a,s}(\theta), \tag{5.3}$$

at least in the vicinity of the real axis. In principle, we could use this form of the Y-functions to calculate the free energy contribution and we will do so in section 6.2 for the 6-point case. However, in this setup the free energy will be zero in the multi-Regge limit. We therefore need to be more general. In particular, we want to be able to incorporate the idea of changing the kinematical regions as discussed in section 3.4 into our calculations. As we explained there, changing the so-called Regge region amounts to changing the sign of some of the Mandelstam invariants. We achieve these sign changes by an analytic continuation in the Mandelstam invariants or, in $\mathcal{N}=4$ SYM, an analytic continuation in the cross ratios. To map this onto the strong coupling formulation recall that the kinematical configuration of our scattering problem is parametrised by the Y-system parameters. Therefore, an

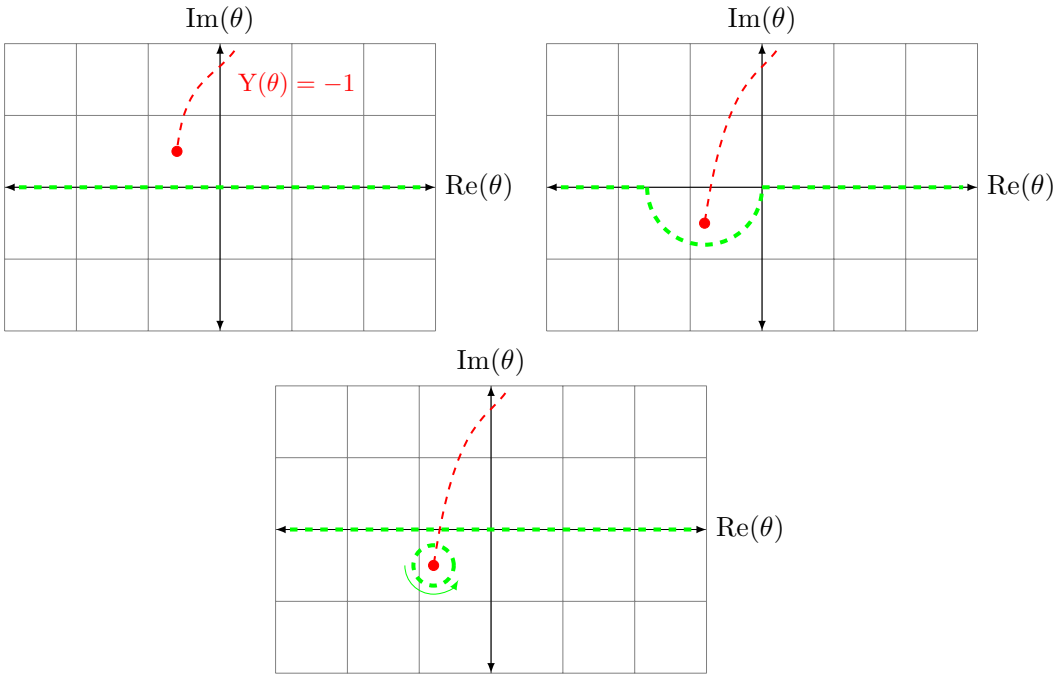

Figure 5.1.: A solution of $Y(\theta) = -1$ (red dashed line) approaches the integration contour (green dashed line). Right before a solution crosses the real axis, we can deform the integration contour to keep the functional form of the Y-system fixed with a more complicated integration contour. However, once we rewrite the Y-system in standard form with integration along $\mathbb{R}$, we have to pick up a residue contribution as displayed above.

analytic continuation in the cross ratios will correspond to an analytic continuation in the parameters $|m_s|$, ϕ_s and C_s.

For a given Y-function $\tilde{Y}_{a,s}(\theta)$ there are positions θ_0 where

$$\tilde{Y}_{a,s}(\theta_0) = -1. \tag{5.4}$$

The location of these solutions of course depends on the values of the Y-system parameters. Therefore, the points θ_0 where Eq.(5.4) is satisfied will move in the θ-plane as we analytically continue the Y-system parameters. It can happen that the position of such a solution comes close to the integration contour in Eq.(5.1). Of course, at a point where Eq.(5.4) holds the integrand of Eq.(5.1) has a pole. Hence, if such a solution crosses the integration contour we have to pick up the residue of the pole as depicted in figure 5.1. A nice way to parametrise these residues is obtained by introducing objects

$$-2\pi i K_{s,s'}^{a,a'}(\theta,\theta') =: \partial_{\theta'} \log S_{s,s'}^{a,a'}(\theta,\theta'), \tag{5.5}$$

which we call S-matrices, for reasons that will become clear later. For example, the S-matrices for the kernels Eq.(2.64), which depend only on one variable, are given by

$$S_1(\theta) = i\frac{1-ie^{\theta}}{1+ie^{\theta}}, \quad S_2(\theta) = \frac{2i\sinh\theta - \sqrt{2}}{2i\sinh\theta + \sqrt{2}}, \quad S_3(\theta) = \cosh 2\theta. \tag{5.6}$$

We list the S-matrices for the various Y-systems we use in appendix D. Every time such a crossing occurs, we have to modify the Y-system equations. Integrating by parts a schematic integral contribution we find

$$\begin{aligned}\int d\theta' K(\theta,\theta')\log(1+\tilde{\mathrm{Y}}(\theta')) &= -\frac{1}{2\pi i}\int d\theta' \partial_{\theta'}\log S(\theta,\theta')\log(1+\tilde{\mathrm{Y}}(\theta')) \\ &= +\frac{1}{2\pi i}\int d\theta' \log S(\theta,\theta')\frac{\partial_{\theta'}\tilde{\mathrm{Y}}(\theta')}{1+\tilde{\mathrm{Y}}(\theta')},\end{aligned} \tag{5.7}$$

where we neglected the boundary terms since we know that the $\tilde{\mathrm{Y}}$-functions decay exponentially as $\theta' \to \pm\infty$, cf. Eq.(2.46). From the result of Eq.(5.7) it is clear that a solution of $\tilde{\mathrm{Y}}(\theta_0) = -1$ on the integration contour is a simple pole with residue

$$\operatorname*{Res}_{\theta'=\theta_0}\left(\frac{\partial_{\theta'}\tilde{\mathrm{Y}}(\theta')}{1+\tilde{\mathrm{Y}}(\theta')}\right) = 1. \tag{5.8}$$

Picking up such a pole in Eq.(5.7) will therefore lead to residue contributions

$$\pm \log S(\theta-\theta_0). \tag{5.9}$$

Going back to the full Y-system, we can enumerate the positions of the crossed solutions by $\theta_{0,\nu}$ and write the modified Y-system as

$$\begin{aligned}\log \tilde{\mathrm{Y}}'_{a,s}(\theta) = &- p'_{a,s}(\theta) + \sum_{a',s'}\int_{\mathbb{R}} d\theta' K^{a,a'}_{s,s'}(\theta,\theta')\log(1+\tilde{\mathrm{Y}}'_{a',s'}(\theta')) \\ &+ \sum_{\nu}(-\mathrm{sgn}(\mathrm{Im}(\theta_{0,\nu})))\log S^{a,a_\nu}_{s,s_\nu}(\theta,\theta_{0,\nu}),\end{aligned} \tag{5.10}$$

where the prime just indicates that the equations we consider have changed due to the crossing. It should be noted that the location of a crossed solution $\theta_{0,\nu}$ of course still changes after crossing the real axis until it reaches its endpoint at the end of the analytic continuation. Furthermore, note that the sign of the contribution depends on whether a solution crosses into the positive or negative half-plane, as should be clear from figure 5.1. Since the same kind of integrand appears in the free energy Eq.(5.2), it undergoes similar modifications,

$$\begin{aligned}A'_{\text{free}} = &\sum_s \frac{|m_s|'}{2\pi}\int_{\mathbb{R}} d\theta \cosh\theta \log\left((1+\tilde{\mathrm{Y}}'_{1,s}(\theta))(1+\tilde{\mathrm{Y}}'_{3,s}(\theta))(1+\tilde{\mathrm{Y}}'_{2,s}(\theta))^{\sqrt{2}}\right) \\ &+ \sum_\nu \mathrm{sgn}(\mathrm{Im}(\theta_{0,\nu}))i|m_s|'\sinh\theta_{0,\nu}.\end{aligned} \tag{5.11}$$

Note that after analytic continuation the quantities $|m_s|'$ are no longer necessarily real. As mentioned before, the free energy contribution in Eq.(5.2) calculates the *ground state* energy of the auxiliary one-dimensional quantum integrable system. We see from Eq.(5.11) that the free energy has changed and now receives contributions of *excited states* of the auxiliary system[1]. This idea is formulated in the context of integrable models in [133,134].

[1] The idea that the contributions come from excited states is, roughly speaking, that the functional form of the eigenvalue problem we solve for the 1D-auxiliary quantum integrable system does not change if we follow a closed path in the space of the system parameters. If we then find an eigenstate of the system at the end of the continuation and the energy has changed, it must correspond to an excited state of the original theory, cf. [132].

At the endpoint of our continuation we always want to go back to the multi-Regge regime, where the integrals can be dropped and the equations simplify to

$$\log \tilde{\mathrm{Y}}'_{a,s}(\theta) = -p'_{a,s}(\theta) + \sum_{\nu}(-\mathrm{sgn}(\mathrm{Im}(\theta_{0,\nu}))) \log S^{a,a_\nu}_{s,s_\nu}(\theta,\theta_{0,\nu}). \tag{5.12}$$

We see that changing the Regge region can leave a clear signature in the equations through the contributions of the S-matrices. In fact, in the multi-Regge limit the free energy is dominated by the contributions of the excited states,

$$A'_{\mathrm{free}} = \sum_{\nu} \mathrm{sgn}(\mathrm{Im}(\theta_{0,\nu}))i|m_s|' \sinh\theta_{0,\nu}, \tag{5.13}$$

as we show in detail in chapter 6. We still have to determine the endpoints of the crossed solutions, which explicitly enter Eqs.(5.12,5.13). To do so, we evaluate the Y-system equations for which a solution has crossed at $\theta_{0,i}$ and use that, by definition, $\tilde{\mathrm{Y}}'_{a_i,s_i}(\theta_{0,i}) = -1$:

$$i\pi = \log\left(\tilde{\mathrm{Y}}'_{a_i,s_i}(\theta_{0,i})\right) = -p'_{a_i,s_i}(\theta_{0,i}) + \sum_{\nu}(-\mathrm{sgn}(\mathrm{Im}(\theta_{0,\nu}))) \log S^{a_i,a_\nu}_{s_i,s_\nu}(\theta_{0,i},\theta_{0,\nu}). \tag{5.14}$$

Exponentiating and rearranging these equations a bit we find

$$-e^{p'_{a_i,s_i}(\theta_{0,i})} = \prod_{\nu} S^{a_i,a_\nu}_{s_i,s_\nu}(\theta_{0,i},\theta_{0,\nu})^{-\mathrm{sgn}(\mathrm{Im}(\theta_{0,\nu}))}, \tag{5.15}$$

which is a set of Bethe ansatz equations. For this reason, the $\theta_{0,i}$ will also be called Bethe roots. In its original context, the Bethe ansatz enforces single-valuedness of the wave function of a magnon propagating on a spin-chain. The driving term represents the momentum of the magnon, while the S-matrix factors represent the scattering of the magnon with the particles on the spin-chain sites, thus explaining the name. The set of equations (5.15) are called *endpoint conditions* in the following. Since we always end up in a regime where the driving terms p'_{a_i,s_i} have a large absolute value, we already see from Eq.(5.15) that the endpoints $\theta_{0,i}$ need to approach zeros or poles of the S-matrices to show the same behaviour as the driving term.

We conclude that for the scattering amplitudes we are after, there exists a set of Bethe ansatz equations which encodes essential information for the calculation of the remainder function. Finding the correct Bethe ansatz equations for a given amplitude will be the crucial aspect of our programme. We will provide explicit examples in later chapters.

5.2. An alternative Y-system

In the last section, we have explained that the central part of our calculations will be the determination of the solutions of the equations $\tilde{\mathrm{Y}}_{a,s}(\theta) = -1$ which cross the integration contour. Following these solutions through the θ-plane will be done numerically, using the algorithm described in section 5.3. In this subsection, we prepare this discussion by presenting an alternative form of the Y-system which is better suited for the numerical evaluation.

A major problem in performing the analytic continuation of the Y-system is that the paths of the Y-system parameters $|m_s|$, ϕ_s, C_s are a priori unknown. We will therefore

rewrite the Y-system in such a way that only quantities related to the cross ratios enter, as was first proposed in [57]. To begin, note that the Y-functions related our choice of cross ratios can always be expressed through the functions

$$\hat{\mathrm{Y}}_{a,s}(0) := \begin{cases} \mathrm{Y}_{a,s}(0) & a+s \quad \text{even} \\ \mathrm{Y}_{a,s}\left(-i\frac{\pi}{4}\right) & a+s \quad \text{odd} \end{cases} \tag{5.16}$$

using the recursion relation Eq.(2.68). We can now evaluate the Y-system equations at the points $\hat{\mathrm{Y}}(0)$ and solve for the original parameters. For simplicity, we will keep the phase parameters ϕ_s fixed to their limiting values in the multi-Regge limit (cf. Eq.(4.32)). We will relax this condition in the 6-point case later. This leaves us with $2n-10$ parameters to solve for. Solving the $\tilde{\mathrm{Y}}$-functions at the points Eq.(5.16) for the auxiliary parameters we find

$$\begin{aligned} C_s =& \frac{1}{2}\log\left(\frac{\tilde{\mathrm{Y}}_{3,s}(0)}{\tilde{\mathrm{Y}}_{1,s}(0)}\right) - \frac{1}{2}K_3 \star \gamma_s\big|_{\theta=0}, \\ |m_s| =& -\frac{1}{2}\log\left(\tilde{\mathrm{Y}}_{1,s}(0)\tilde{\mathrm{Y}}_{3,s}(0)\right) - \frac{1}{2}K_2 \star \beta_s\big|_{\theta=0} - K_1 \star \alpha_s\big|_{\theta=0}. \end{aligned} \tag{5.17}$$

These expressions can now be plugged into the original Y-system equations and we end up with expressions for the Y-functions whose driving terms are functions of the cross ratios only:

$$\begin{aligned} \log\tilde{\mathrm{Y}}_{1,s}(\theta) =& \frac{1}{2}\log\left(\tilde{\mathrm{Y}}_{1,s}(0)\tilde{\mathrm{Y}}_{3,s}(0)\right)\cosh\theta - \frac{1}{2}\log\left(\frac{\tilde{\mathrm{Y}}_{3,s}(0)}{\tilde{\mathrm{Y}}_{1,s}(0)}\right) \\ &+ \sum_{a',s'}\int d\theta' \mathcal{K}^{1,a'}_{s,s'}(\theta,\theta')\log\left(1+\tilde{\mathrm{Y}}_{a',s'}(\theta')\right), \end{aligned} \tag{5.18}$$

$$\begin{aligned} \log\tilde{\mathrm{Y}}_{2,s}(\theta) =& \frac{1}{\sqrt{2}}\log\left(\tilde{\mathrm{Y}}_{1,s}(0)\tilde{\mathrm{Y}}_{3,s}(0)\right)\cosh\theta \\ &+ \sum_{a',s'}\int d\theta' \mathcal{K}^{2,a'}_{s,s'}(\theta,\theta')\log\left(1+\tilde{\mathrm{Y}}_{a',s'}(\theta')\right), \end{aligned} \tag{5.19}$$

$$\begin{aligned} \log\tilde{\mathrm{Y}}_{3,s}(\theta) =& \frac{1}{2}\log\left(\tilde{\mathrm{Y}}_{1,s}(0)\tilde{\mathrm{Y}}_{3,s}(0)\right)\cosh\theta + \frac{1}{2}\log\left(\frac{\tilde{\mathrm{Y}}_{3,s}(0)}{\tilde{\mathrm{Y}}_{1,s}(0)}\right) \\ &+ \sum_{a',s'}\int d\theta' \mathcal{K}^{3,a'}_{s,s'}(\theta,\theta')\log\left(1+\tilde{\mathrm{Y}}_{a',s'}(\theta')\right). \end{aligned} \tag{5.20}$$

Note that it was necessary to introduce the functions $\hat{\mathrm{Y}}(0)$ to ensure that the new driving terms can be expressed through our choice of cross ratios. The relations between our cross ratios and the $\hat{\mathrm{Y}}(0)$ will typically be solved numerically, analytic expressions are only available in special cases. In fact, note that the relevant quantities in Eq.(5.17) are $\tilde{\mathrm{Y}}_{1,s}(0)$ and $\tilde{\mathrm{Y}}_{3,s}(0)$. Starting from 8 gluons, the functions $\tilde{\mathrm{Y}}_{1/3,3}(0)$ will not be part of the set $\hat{\mathrm{Y}}_{a,s}(0)$ because of our choice of phases. This, however, is not an in principle obstruction to the construction above, as we can always determine the $\tilde{\mathrm{Y}}_{1/3,s}(0) = \mathrm{Y}_{1/3,s}(i\phi_s)$ numerically from the $\hat{\mathrm{Y}}(0)$.

What we have gained is that we can easily prescribe the behaviour of the driving terms during the analytic continuation. The price to pay is that the kernels $\mathcal{K}_{s,s'}^{a,a'}$ appearing in Eqs.(5.18-5.20) and the corresponding S-matrices are more complicated than those in the original Y-system. They are spelled out for the special case of seven gluons in appendix D. Note that, in contrast to appendix F of [57], we do not rewrite the full Y-system in terms of the functions $\hat{\mathrm{Y}}$, because the free energy is given by a simple integral over the $\tilde{\mathrm{Y}}$-functions and not the $\hat{\mathrm{Y}}$-functions. We therefore stick to the former in our description of the Y-system.

5.3. Numerical evaluation of the Y-functions

To solve the Y-system numerically, we employ an algorithm similar to the one proposed in [44]. We start by setting the Y-function equal to its driving terms only,

$$\tilde{\mathrm{Y}}_{a,s}^{(0)}(\theta) = e^{-p_{a,s}(\theta)}, \tag{5.21}$$

and then iterate the integral equations by plugging the solution above in the integrand:

$$\log \tilde{\mathrm{Y}}_{a,s}^{(k)}(\theta) = -p_{a,s}(\theta) + \sum_{a',s'} \int_{\mathbb{R}} d\theta' K_{s,s'}^{a,a'}(\theta,\theta') \log\left(1 + \tilde{\mathrm{Y}}_{a',s'}^{(k-1)}(\theta)\right). \tag{5.22}$$

We iterate this process until the Y-function has converged. This determines the $\tilde{\mathrm{Y}}$-functions along the integration contour. Once the $\tilde{\mathrm{Y}}$-functions have converged we can determine the function values for any θ in the fundamental strip, again using Eq.(5.22) with the converged function on the right-hand side. For very large values of $|\mathrm{Im}\,\theta|$ we employ the recursion relation Eq.(2.68). The driving terms which feed into Eqs.(5.21, 5.22) are also determined numerically by solving the recursion relations for the functions $\hat{\mathrm{Y}}(0)$ introduced earlier in terms of the cross ratios. For the multi-Regge limit, where the driving terms are large, this convergence is rather fast. In fact, for the paths we studied so far, the driving terms alone give the correct crossing picture, although higher iterations are needed to produce continuous Y-functions at the points where solutions cross. Note that some of the kernels of our rewritten Y-system Eqs.(5.18-5.20) spelled out in appendix D have poles along the integration contour. We handle those by performing a principal value integration and add the appropriate residue contribution of the kernel.

At every point of the continuation, we determine the position of the solutions $\tilde{\mathrm{Y}}_{a,s}(\theta) = -1$ by a standard root-finding algorithm. Whenever a solution crosses the real axis, we have to modify our equations as described in section 5.1. Since the position of a crossed solution explicitly enters the Y-functions through the S-matrices (cf. Eq.(5.10)), we have to solve the Bethe ansatz at each point during the continuation after a solution has crossed. We do so using the zeroth iteration, i.e.

$$\tilde{\mathrm{Y}}_{a_0,s_0}^{\prime(0)}(\theta_0) = -1, \tag{5.23}$$

which, depending on how many solutions have crossed, can be either a single equation or a set of coupled equations. Towards the end of the continuation where the integrals can be neglected, Eq.(5.23) will already give us the correct positions θ_0. However, during the continuation when the integrals still give non-negligible contributions, the position of the

crossed solution as determined by Eq.(5.23) will receive corrections through the integral contributions, as well. We determine those corrections by an analogous iteration procedure as in Eq.(5.22). In chapter 7 we will find an example in which poles cross the real axis at different times during the continuation. In such a case, it turns out to be simpler to deform the integration contour such that no poles cross the contour rather than modifying the integral equations several times. Once all poles have crossed the real axis, we pull the integration contour back and pick up the appropriate residues.

In Eq.(5.10) we have shown that the contribution of the crossing solution consists of residue contributions by partial integration. However, the locations $\tilde{Y}(\theta) = -1$ are not just simple poles, they are branch points and we choose the branch cuts to point away from the real axis. This means that once solutions have crossed the real axis and we pull back the integration contour, the integrand in Eq.(5.10) crosses the branch cuts and we have to keep it continuous by adding the appropriate cut contributions. This gives the same result as deforming the integration contour such that no poles cross, as is easily shown. These remarks become especially important when using our rewritten Y-system Eqs.(5.18-5.20), because, as mentioned above, the kernels for this Y-system have poles on the integration contour and we have to pick up residue contributions. When pulling back the contour, one has to be careful on which sheet these residues are picked up and add compensating factors. Again, the comparison with the deformed contour will always lead to the correct result. All numerical calculations in this thesis were performed using *Mathematica*.

5.4. Regge regions

In section 5.1 we have discussed an algorithm to find the valid equations for the Y-system during a given analytic continuation of the cross ratios. Let us now discuss briefly how we identify the correct prescriptions for the analytic continuation of the cross ratios. We start from the amplitude in the physical region where all energies s_i are positive[2]. In this region all produced particles are outgoing and the energy component of the momentum of those particles is positive. For each produced particle we can then analytically continue into regions where the energy component of the momentum of the produced particle is negative, i.e. we choose the particle to be incoming. Hence, we consider 2^{n-4} so-called Regge regions for a $2 \to n-2$ amplitude. A graphical representation of a Regge region is shown in figure 5.2.

Since the amplitude is a function of the Mandelstam invariants and not the momenta, the continuation between different Regge regions must be defined in terms of Mandelstam variables. Two-particle invariants of massless particles are simply inner products of momenta $s_{ii+1} \sim p_i \cdot p_{i+1}$. In the centre-of-mass system of particles i and $i+1$, a sign change in the energy component of particle i will hence translate into a sign change of the Mandelstam variable s_{ii+1}. The simplest continuation for a two-particle invariant is therefore along a path $s_{ii+1} \to s_{ii+1}e^{i\varphi}$ from $\varphi = 0 \dots \pi$. For Mandelstam invariants including more particles, we can use that in the multi-Regge limit those invariants are products of two-particle invariants, cf. Eq.(3.21). If the numerator for a given subenergy

[2]Note that the Y-system is originally derived in the Euclidean regime where all energies are negative. However, as we will see in the next chapter, none of the cross ratios change as we perform the analytic continuation from the Euclidean to the physical region with all energies being positive and we can use the Y-system without modifications also in this physical region.

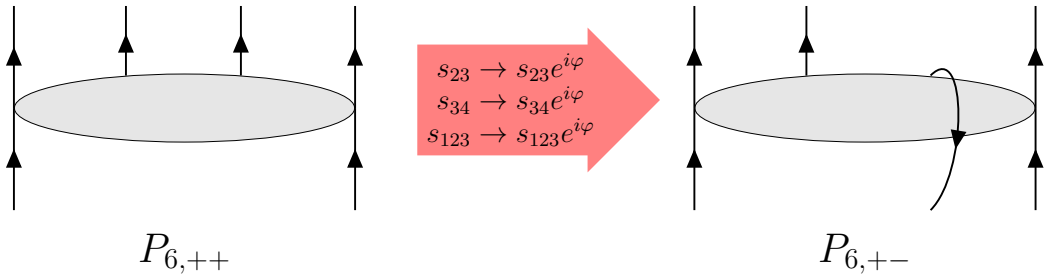

Figure 5.2.: Graphical representation for the continuation from the physical regime with all energies being positive to a Regge region in which some energies are negative. Effectively, this corresponds to choosing one of the particles to be incoming. The transition between the two regions is carried out by continuing the s-variables indicated in the arrow as $se^{i\varphi}$ from $\varphi = 0 \dots \pi$. We denote the Regge region by $P_{6,+-}$, where we indicate for each produced particle whether it is incoming $(-)$ or outgoing $(+)$.

$s_{i\dots j}$ in Eq.(3.21) contains an odd number of two-particle invariants which are continued, it will be continued as $s_{i\dots j} \to s_{i\dots j}e^{i\varphi}$, as well, otherwise we keep it fixed. The t-variables are kept fixed during the continuation. In the graphical representation in figure 5.2 one can read off which subenergies are analytically continued by the following mnemonic: If the two particles spanning the subenergy lie on different sides of the central blob, the subenergy is continued. If they lie on the same side, the subenergy is kept fixed.

Once we have figured out which Mandelstam variables we need to continue, we can feed this information into the definition of the cross ratios Eq.(3.4) to see how the cross ratios should be analytically continued. For the example shown in figure 5.2 we find that

$$u_1 \to u_1, \quad u_2 \to u_2 e^{i\varphi}, \quad u_3 \to u_3 e^{-i\varphi}. \tag{5.24}$$

Note that the choice to continue along a half-circle is made because it is the simplest possible path which changes the sign of the energy variables. The Regge regions are only defined by the signs of the Mandelstam invariants and the path between two regions is somewhat ambiguous. In fact, we will see in chapter 7 that it is not always possible to stick to this choice. We will comment on these subtleties once they become relevant.

6. The 6-point amplitude

In this chapter, we perform our first computation of the remainder function for the 6-gluon amplitude. Remember that the 4- and 5-point amplitude are completely captured by the BDS ansatz and that the 6-point amplitude is the first non-trivial case where deviations from the BDS ansatz are obtained, because it is the lowest number of gluons for which we can build conformal cross ratios out of the $x_{i,j}^2$. After describing the equations governing the 6-point case, we show that the remainder function vanishes in the Euclidean regime. We then describe different Regge regions and the corresponding analytic continuations and go on to show that we indeed find a non-trivial remainder function in a particular Regge region. This calculation was first carried out in [78]. However, in [79] we reconsider the problem and identify some mistakes made in the original publication.

6.1. Equations for the 6-point case

We already discussed the general formulas and kinematics for the n-point case in chapters 3 and 4. However, since this is our first proper calculation of an amplitude, let us restate the relevant quantities for convenience. In the 6-point case we have three independent cross ratios which read

$$u_1 = \frac{x_{2,6}^2 x_{3,5}^2}{x_{3,6}^2 x_{2,5}^2} = \frac{Y_{2,1}^{[-3]}}{1+Y_{2,1}^{[-3]}},\ u_2 = \frac{x_{4,6}^2 x_{3,1}^2}{x_{3,6}^2 x_{4,1}^2} = \frac{Y_{2,1}^{[-1]}}{1+Y_{2,1}^{[-1]}},\ u_3 = \frac{x_{2,4}^2 x_{1,5}^2}{x_{1,4}^2 x_{2,5}^2} = \frac{Y_{2,1}^{[1]}}{1+Y_{2,1}^{[1]}}. \quad (6.1)$$

We also have three Y-functions $\mathrm{Y}_{a,1}(\theta)$ and the corresponding Y-system parameters have to attain the values

$$|m| \to \infty,\ \phi \to 0 \text{ and } C = \text{const.} \quad (6.2)$$

in the multi-Regge limit. Then the cross ratios can be parametrised using the quantities ε and w (cf. Eq.(4.15)) as

$$u_1 = 1 - \varepsilon\left(w + \frac{1}{w} + 2\cosh C\right),\ u_2 = \varepsilon w,\ u_3 = \frac{\varepsilon}{w}. \quad (6.3)$$

As there is only one triplet of Y-functions for the 6-point case, we will suppress the second index in the following. The connection between the cross ratios and the Y-functions has already been spelled out in Eq.(6.1). For the case at hand, we can actually use these equations and solve the recursion relations Eq.(2.68) for the driving terms of our modified Y-system Eqs.(5.18-5.20) in terms of the cross ratios analytically. We obtain

$$\mathrm{Y}_1(0) = \frac{1}{2u_1}\left(1-u_1-u_2-u_3-\sqrt{-4u_1u_2u_3+(1-u_1-u_2-u_3)^2}\right), \quad (6.4)$$

$$\mathrm{Y}_2\left(-i\frac{\pi}{4}\right) = \frac{u_2}{1-u_2}, \quad (6.5)$$

$$\mathrm{Y}_3(0) = \frac{1}{2u_1}\left(1-u_1-u_2-u_3+\sqrt{-4u_1u_2u_3+(1-u_1-u_2-u_3)^2}\right), \quad (6.6)$$

which we can use to prescribe the behaviour of the driving terms during the continuation to different Regge regions.

The two different sets of Y-system equations we are going to use have already been presented in sections 2.3.3 and 5.2, respectively. We will use Eqs.(5.18-5.20) for the numerical evaluation during the continuation and Eqs.(2.60-2.62) at the starting point and the endpoint of the continuation. Once we have solved for the Y-functions, we calculate the remainder function using the contributions

$$R_6 = -\frac{\sqrt{\lambda}}{2\pi}\left(A_{\text{free}} + A_{\text{per}} + \Delta\right), \tag{6.7}$$

where

$$A_{\text{free}} = \frac{|m|}{2\pi}\int d\theta \cosh\theta \log\left[(1+\tilde{\text{Y}}_1(\theta))(1+\tilde{\text{Y}}_3(\theta))(1+\tilde{\text{Y}}_2(\theta))^{\sqrt{2}}\right], \tag{6.8}$$

$$A_{\text{per}} = \frac{1}{4}|m|^2 \quad \text{and} \tag{6.9}$$

$$\Delta = -\sum_{i=1}^{3}\left(\frac{1}{8}\log^2 u_i + \frac{1}{4}\text{Li}_2(1-u_i)\right). \tag{6.10}$$

In the form written out above, the equations are valid in the Euclidean regime, where all Mandelstam invariants are negative, as well as in the physical regime, where all s-like variables are positive, while t-like variables are negative. The change between these two regions is an analytic continuation in all s-like variables. However, since the cross ratios always involve an even number of s-variables, the change does not affect the Y-system or the remainder function.

6.2. The remainder function R_6 in the Euclidean regime

Let us first study the remainder function in the Euclidean regime. To do so, we use the original Y-system Eqs.(2.60-2.62), as we do not need to perform any analytic continuation. We start with the free energy contribution,

$$A_{\text{free}} = \frac{|m|}{2\pi}\int d\theta \cosh\theta \log\left[(1+\tilde{\text{Y}}_1(\theta))(1+\tilde{\text{Y}}_3(\theta))(1+\tilde{\text{Y}}_2(\theta))^{\sqrt{2}}\right]. \tag{6.11}$$

For a single Y-function, we can use that in the multi-Regge limit $\log(1+\tilde{\text{Y}}_a(\theta')) \cong \tilde{\text{Y}}_a(\theta')$ and find that schematically (i.e. neglecting possible factors of $e^{\pm C}$ or factors of $\sqrt{2}$)

$$\begin{aligned}\frac{|m|}{2\pi}\int d\theta \cosh\theta \log\left(1+\tilde{\text{Y}}_a(\theta)\right) &\cong \frac{|m|}{2\pi}\int d\theta \cosh\theta e^{-|m|\cosh\theta} \\ &= \frac{|m|}{2\pi}K_1(|m|),\end{aligned} \tag{6.12}$$

where $K_\alpha(x)$ is the modified Bessel function of second kind (cf. [135]). Using its large x behaviour,

$$K_1(x) \sim \sqrt{\frac{\pi}{2x}}e^{-x} \text{ for } x \to \infty, \tag{6.13}$$

we see that the contribution of a given Y-function to the A_{free}-part of the amplitude is given by

$$\frac{|m|}{2\pi}\int d\theta \cosh\theta \log\left(1+\tilde{\mathrm{Y}}_a(\theta')\right) \cong \frac{1}{2}\sqrt{\frac{|m|}{\pi}}e^{-|m|} \tag{6.14}$$

and is therefore negligible in the multi-Regge limit $|m| \to \infty$.

The periods part A_{per} can be rewritten using the definitions Eq.(4.15) as

$$A_{\text{per}} = \frac{1}{4}|m|^2 = \frac{1}{4}\left(\log^2\varepsilon + \log^2 w\right) \tag{6.15}$$

in the multi-Regge limit. This leaves us with Δ, which was spelled out in Eq.(6.10). To compare it with the A_{per}-contribution, we use the multi-Regge form of the cross ratios Eq.(6.3) and expand around $\varepsilon = 0$ to find

$$\Delta = -\frac{1}{4}\log^2\varepsilon - \frac{1}{4}\log^2 w + \text{const.} + \mathcal{O}(\varepsilon). \tag{6.16}$$

We can now assemble all pieces of the amplitude and find that

$$A_{\text{free}} + A_{\text{per}} + \Delta = \text{const.} + \mathcal{O}(\varepsilon), \tag{6.17}$$

i.e. the remainder function is constant. In fact, the constant from the Δ-part comes from the series expansion of the Li_2-functions and therefore cancels against a term with opposite sign in the A_{BDS}-part. Therefore, we indeed confirm the weak coupling prediction that the remainder function is trivial in the Euclidean regime of the multi-Regge limit [25].

6.3. Regge regions

In chapter 5 we described the general algorithm for the computation of the remainder function in different Regge regions. Before we delve into any concrete calculation, let us try to gain some intuition about the necessary conditions for a crossing solution to occur. In the following, we prefer to work with the unshifted Y-functions, see the discussion around Eq.(2.70).

If a solution $\mathrm{Y}_a(\theta) = -1$ crosses the real axis, the corresponding Y-function has to become of $\mathcal{O}(1)$ along the real axis. This, however, means that the approximation

$$\mathrm{Y}_a(\theta) \cong e^{-|m|'\cosh(\theta - i\phi') \pm C'} \tag{6.18}$$

has to fail and corrections from the integrals can no longer be neglected. From the arguments given in chapter 4 it is clear that this is only possible if the driving term becomes small, which in turn implies that C has to become of $\mathcal{O}(|m|)$ during the continuation, otherwise there will be no crossing solution[1].

For the special case of the 6-gluon amplitude we can be more specific because of the exact relation

$$\cosh C = \frac{-1+u_1+u_2+u_3}{2\sqrt{u_1u_2u_3}}, \tag{6.19}$$

[1] One might argue that alternatively $|m|$ could become small. However, from Eqs.(5.17, 6.4-6.6) one can see that the leading contribution to the mass parameter is $\sim \log(u_2u_3)$ which stays large throughout all continuations studied here.

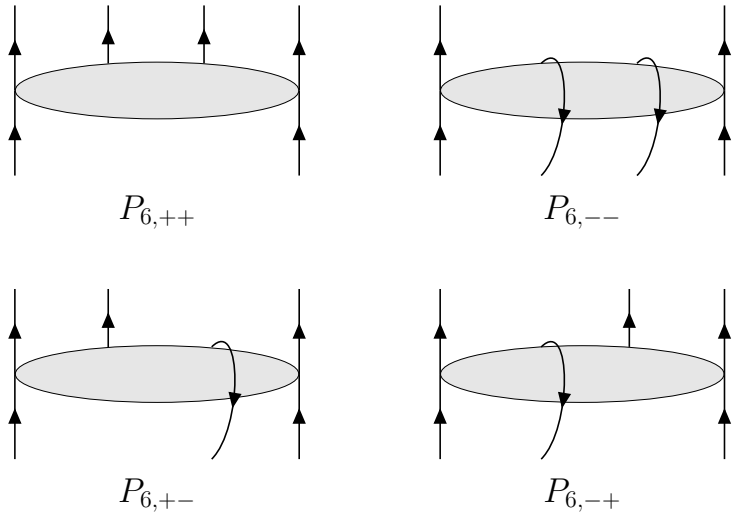

Figure 6.1.: Graphical representation of the Regge regions for the 6-point amplitude.

which we obtain by using the relation

$$\frac{\mathrm{Y}_3(\theta)}{\mathrm{Y}_1(\theta)} = \frac{\mathrm{Y}_3(0)}{\mathrm{Y}_1(0)} = e^{2C} \tag{6.20}$$

and Eqs.(6.4-6.6). Relation Eq.(6.20) does not hold for more external gluons because of the appearance of the kernel K_3 starting from the 7-point amplitude (cf. Eqs.(2.60)-(2.62)). We can now plug the behaviour of the cross ratios during a given continuation in Eq.(6.19) and see whether C becomes large or not. If it does not, there will be no crossing solutions and the remainder function will be trivial.

For the 6-point amplitude we have the following Regge regions with the corresponding continuation from the physical region with all energies being positive indicated:

$$P_{6,+-}: \quad u_1 \to u_1, \qquad u_2 \to e^{i\varphi}u_2, \qquad u_3 \to e^{-i\varphi}u_3 \tag{6.21}$$

$$P_{6,-+}: \quad u_1 \to u_1, \qquad u_2 \to e^{-i\varphi}u_2, \qquad u_3 \to e^{i\varphi}u_3 \tag{6.22}$$

$$P_{6,--}: \quad u_1 \to e^{-2i\varphi}u_1, \quad u_2 \to u_2, \qquad u_3 \to u_3. \tag{6.23}$$

The graphical representation of these regions is shown in figure 6.1. The first two paths do not involve a rotation of the large cross ratio u_1 and indeed it is easy to check that for these paths C does not become large and hence there is no crossing solution. Therefore, in these regions the remainder function is trivial, in agreement with the weak coupling computation of [25]. This leaves us with P_{--}. Indeed, by plugging the paths of the cross ratios into Eq.(6.19), we see that C becomes large around $\varphi \sim \frac{\pi}{2}$ and crossing can potentially occur. We study this path in detail in the next section.

6.4. The remainder function $R_{6,--}$

After having specified the behaviour of the cross ratios during the continuation, we have all the information we need to determine the remainder function $R_{6,--}$. For this path,

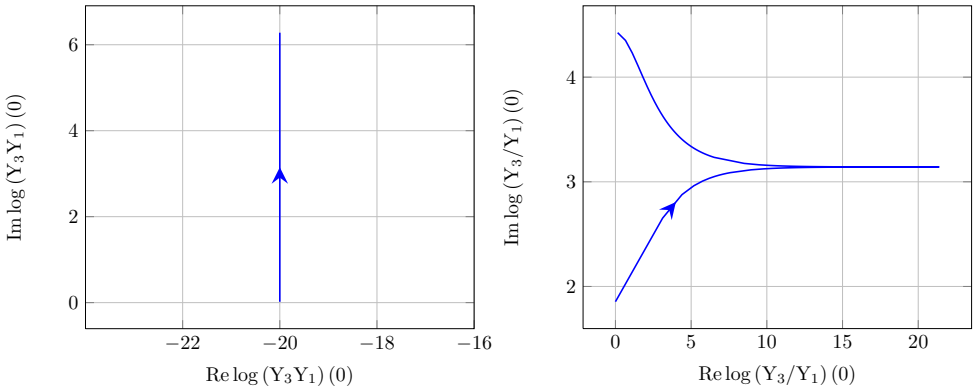

Figure 6.2.: Paths of the driving terms for the path Eq.(6.23). The direction of growing φ is indicated by an arrow. The plots are produced for the specific starting values $|m| = 10$, $C = \operatorname{arccosh}\left(\frac{3}{5}\right)$, $\phi = 0$.

the driving terms can be inferred from Eqs.(6.4-6.6) and the behaviour we specify for the cross ratios, Eq.(6.23). The paths of the driving terms during the continuation are shown in figure 6.2.

6.4.1. Crossing solutions

We begin by checking whether crossing solutions exists for this path. We do so numerically, employing the algorithm described in section 5.3. Note again that we study paths with ϕ fixed throughout the continuation for simplicity, we will release this restriction later on. In figures 6.3, 6.4 we present the results of our numerical investigations. Indeed, we see that a pair of solutions of $\mathrm{Y}_3(\theta) = -1$ crosses the real axis[2]. As described before, at this point we have to modify our equations by picking up the appropriate residues. Furthermore, a pair of solutions $\mathrm{Y}_2(\theta)$ approaches the origin at the end of the continuation.

Let us remark that we can calculate the paths of the original Y-system parameters using Eq.(5.17). For the path under investigation, the results are shown in figure 6.5. We see that we nicely reproduce the results of [78], who use the original Y-system equations and a different numerical method to find the path of continuation for the original Y-system parameters. While this was to be expected because the two Y-systems are equivalent, it is of course nice to see agreement in the different approaches. Note that during the continuation C reaches values $\sim \mathcal{O}(|m|)$. As remarked in section 6.3, this is a necessary condition for crossing solutions.

6.4.2. Symmetries of the Y-system and endpoint conditions

We now need to determine the endpoints of the solutions that have crossed the real axis. To do so, it makes sense to relax the condition $\phi \equiv 0$ and allow for a small deviation. For small ϕ this does not spoil the picture of the crossing solutions as numerical studies confirm, while allowing a more general statement about the endpoint positions. In the

[2]The reason the crossing appears in Y_3 is the starting value we choose for C. Choosing $-C$ would lead to crossing solutions of Y_1.

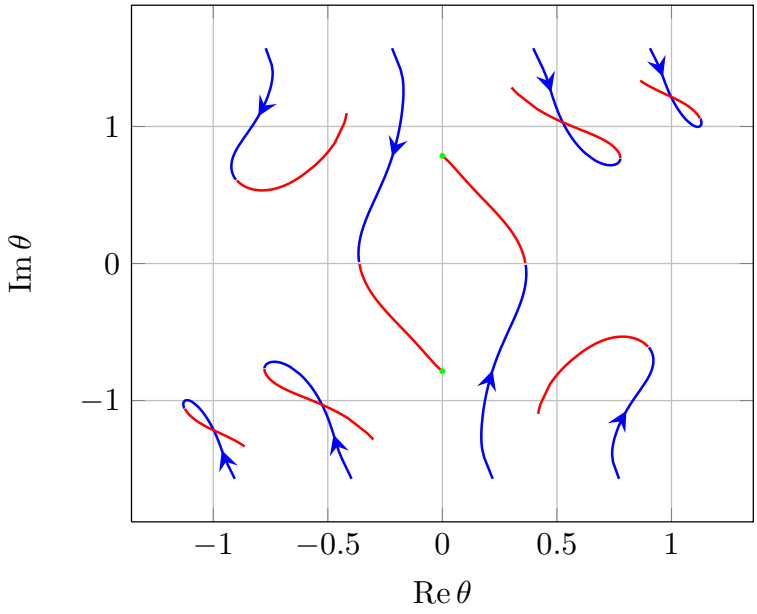

Figure 6.3.: Movement of the solutions of $\mathrm{Y}_3(\theta) = -1$ as we vary φ. The direction of growing φ is indicated by the arrows. We switch the colour of the plot at the point where the first solution crosses the real axis. The green dots show the endpoints that enter in the calculation of the remainder function. The crossing is plotted for the specific initial values $|m| = 10$, $C = \operatorname{arccosh}\left(\frac{3}{5}\right)$ and $\phi = 0$.

case of non-zero ϕ, the Y-system equations before any continuation read

$$\log \mathrm{Y}_a(\theta) = -|m_a| \cosh\left(\theta - i\phi\right) + C_a + \sum_{a'} \int_{\mathbb{R}+i\phi} d\theta' K^{aa'}\left(\theta - \theta'\right) \log\left(1 + \mathrm{Y}_{a'}(\theta')\right), \quad (6.24)$$

cf. Eq.(2.70), where we introduced the collective parameters

$$|m_a| = \begin{cases} |m| & a = 1 \\ \sqrt{2}|m| & a = 2 \\ |m| & a = 3 \end{cases} \quad \text{and} \quad C_a = \begin{cases} -C & a = 1 \\ 0 & a = 2 \\ C & a = 3 \end{cases}. \quad (6.25)$$

These equations have a simple mirror symmetry

$$\mathrm{Y}_a(\theta + i\phi) = \mathrm{Y}_a(-\theta + i\phi). \quad (6.26)$$

To prove the above symmetry we mimic the way we solve the Y-system equations numerically and write

$$\log \mathrm{Y}_a^{(k)}(\theta) = -|m_a| \cosh\left(\theta - i\phi\right) + C_a + \sum_{a'} \int_{\mathbb{R}+i\phi} d\theta' K^{aa'}\left(\theta - \theta'\right) \log\left(1 + \mathrm{Y}_{a'}^{(k-1)}(\theta')\right) \quad (6.27)$$

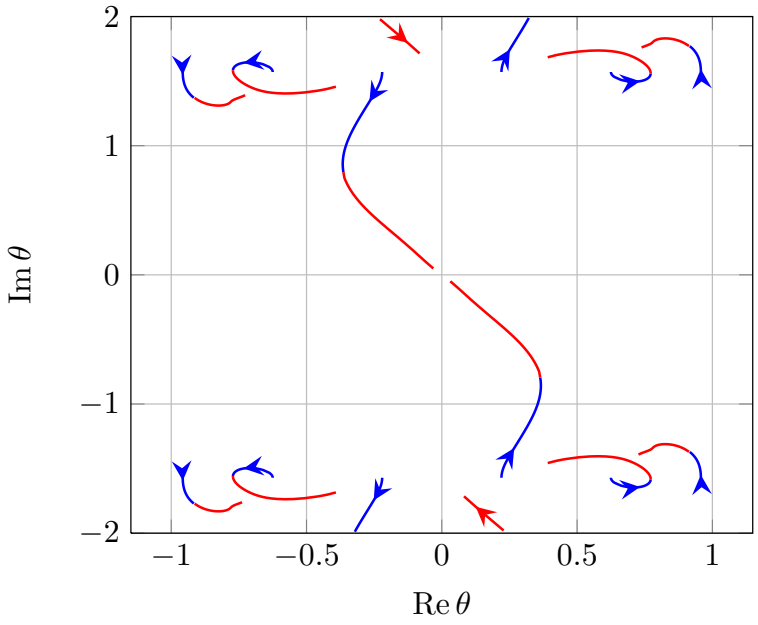

Figure 6.4.: Movement of the solutions of $\mathrm{Y}_2(\theta) = -1$ as we vary φ. The direction of growing φ is indicated by the arrows. We switch the colour of the plot at the point where the first solution of $\mathrm{Y}_3(\theta) = -1$ crosses the real axis. The crossing is plotted for the specific initial values $|m| = 10$, $C = \operatorname{arccosh}\left(\frac{3}{5}\right)$ and $\phi = 0$.

for the k-th iteration, where

$$\log \mathrm{Y}_a^{(0)} = -|m_a| \cosh(\theta - i\phi) + C_a \tag{6.28}$$

is just the driving term without integral contributions. To start, it is obvious that the driving terms satisfy the symmetry. If we then assume that the k-th iteration satisfies the mirror symmetry, we can write the integral contribution at $\theta + i\phi$ to the $k+1$-th iteration as

$$\begin{aligned}
&\int\limits_{\mathbb{R}+i\phi} d\theta' K\left(\theta + i\phi - \theta'\right) \log\left(1 + \mathrm{Y}^{(k)}(\theta')\right) = \int\limits_{\mathbb{R}} dx K\left(\theta + x\right) \log\left(1 + \mathrm{Y}^{(k)}(-x + i\phi)\right) \\
&= \int\limits_{\mathbb{R}} dx K\left(-\theta - x\right) \log\left(1 + \mathrm{Y}^{(k)}(x + i\phi)\right) = \int\limits_{\mathbb{R}+i\phi} d\theta' K\left(-\theta + i\phi - \theta'\right) \log\left(1 + \mathrm{Y}^{(k)}(\theta')\right),
\end{aligned} \tag{6.29}$$

where we suppressed all indices for simplicity. In the second step, we used that $K(-x) = K(x)$, which only holds for the kernels in the 6-gluon case, as well as our assumption that $\mathrm{Y}^{(k)}(\theta + i\phi) = \mathrm{Y}^{(k)}(-\theta + i\phi)$. We see that the result of Eq.(6.29) is just the integral contribution for $-\theta + i\phi$. Therefore, each iteration obeys the symmetry Eq.(6.26) and so does the converged solution. Again, this symmetry is special to the 6-point case because the Y-system for more gluons contains integration kernels with shifted arguments.

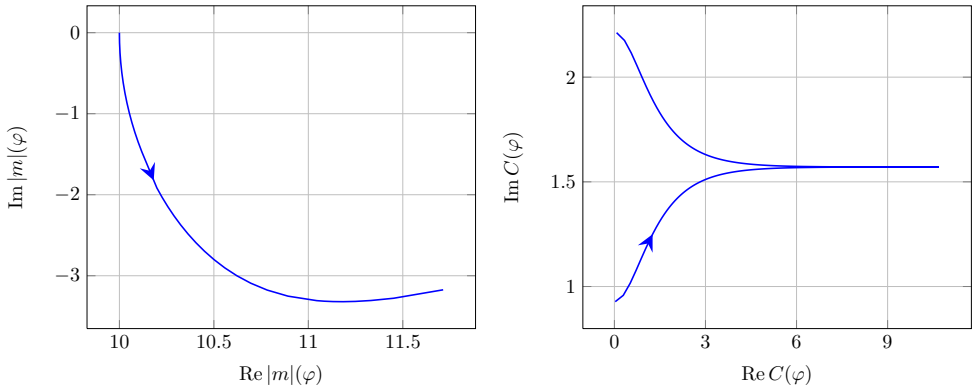

Figure 6.5.: Paths of the original Y-system parameters during the continuation as calculated from Eq.(5.17). The direction of increasing φ is indicated by the arrows. The starting values for the parameters in this plot are $|m| = 10$, $C = \operatorname{arccosh}\left(\frac{3}{5}\right)$ and $\phi = 0$. Note that the results nicely match those obtained in [78]. Furthermore, note that while $|m|(\varphi)$ is a real quantity at the starting point, it becomes complex during the analytic continuation.

We can use this symmetry to determine the endpoints of the crossed solutions. In the following we will denote the endpoint of the crossed solution of $\mathrm{Y}_3(\theta) = -1$ with positive (negative) imaginary part with θ_+ (θ_-). As we end up in a regime where the integral contributions can be neglected, the equation for $\mathrm{Y}_3'(\theta)$ is given by

$$\log \mathrm{Y}_3'(\theta) = -|m|' \cosh\left(\theta - i\phi'\right) + C' + \log\left(\frac{S_1(\theta-\theta_-)}{S_1(\theta-\theta_+)}\right), \tag{6.30}$$

where a prime always indicates a quantity at the endpoint of the continuation. Evaluating Eq.(6.30) at the endpoint of the crossed Bethe root, we obtain the endpoint condition (cf. Eq.(5.15))

$$-1 = \mathrm{Y}_3'(\theta_+) = e^{-|m|' \cosh(\theta_+ - i\phi') + C'}\left(\frac{S_1(\theta_+-\theta_-)}{S_1(0)}\right). \tag{6.31}$$

As explained in general in section 5.1, the two factors on the right-hand side have to combine into a finite product. Since we send $|m|' \to \infty$, this means that the Bethe roots have to approach a pole of the S-matrix factors to compensate the exponentially decreasing driving term. Specifically, we read off from Eq.(6.31) and the definition of $S_1(x)$, Eq.(5.6), that

$$\theta_+ - \theta_- = i\frac{\pi}{2}. \tag{6.32}$$

Since there are only two Bethe roots in the vicinity of the real axis and ϕ is small throughout the continuation, we can use the symmetry Eq.(6.26) to conclude that

$$\theta_- = -\theta_+ + 2i\phi', \tag{6.33}$$

which, together with Eq.(6.32), implies

$$\theta_\pm = \pm i\frac{\pi}{4} + i\phi'. \tag{6.34}$$

It is conceivable that the solutions $\theta_\pm$ leave the fundamental strip $|\mathrm{Im}(\theta - i\phi')| < \frac{\pi}{4}$, in which case we would have to pick up residue terms of the form $\sim \left(1 + \mathrm{Y}_{2,1}\left(\theta \pm i\frac{\pi}{4}\right)\right)$ in Eq.(6.30), which in principle could also compensate the divergence of the driving term in Eq.(6.31). However, assuming that $\mathrm{Im}(\theta_+ - i\phi') > \frac{\pi}{4}$, we immediately see that

$$\mathrm{Im}(\theta_- - i\phi') = \mathrm{Im}(-\theta_+ + i\phi') = -\mathrm{Im}(\theta_+ - i\phi') < -\frac{\pi}{4}, \tag{6.35}$$

from which we conclude that Eq.(6.30) holds as it stands for θ_-. An analogous statement is true for the case $\mathrm{Im}(\theta_- - i\phi') < -\frac{\pi}{4}$. Therefore, Eq.(6.30) is always the correct equation for at least one of the Bethe roots, which suffices to conclude that the endpoints must attain the values Eq.(6.34).

Let us now turn to the two solutions of $\mathrm{Y}_2(\theta)$ which approach each other towards the end of the continuation. After neglecting the integrals, the equation governing $\mathrm{Y}_2'(\theta)$ reads

$$\log \mathrm{Y}_2'(\theta) = -\sqrt{2}|m|' \cosh\left(\theta - i\phi'\right) + \log\left(\frac{S_2(\theta - \theta_-)}{S_2(\theta - \theta_+)}\right). \tag{6.36}$$

After inserting the values Eq.(6.34), we can use the same argument as before to conclude that the Bethe roots of Y_2 have to approach a pole of the function

$$\frac{S_2\left(\theta + i\frac{\pi}{4} - i\phi'\right)}{S_2\left(\theta - i\frac{\pi}{4} - i\phi'\right)} = \coth\left(\frac{1}{2}(\theta - i\phi')\right)^2, \tag{6.37}$$

which leads to the conclusion that both solutions have to end at the point $\theta_2 = i\phi'$. This, however, is the imaginary part of the integration contour, so that the Bethe roots pinch the contour, but never cross. Therefore, they do not give rise to additional contributions in the Y-system or the free energy. Note that this conclusion differs from [78], where a contribution of one of the Bethe roots of $\mathrm{Y}_2(\theta)$ to the free energy was considered.

6.4.3. Calculation of the amplitude

Now that we have understood the crossing pattern and the endpoints of the crossed solutions, we can finally calculate the amplitude. As a first step, we use Eqs.(6.36,2.68) to calculate the cross ratios at the endpoint of the continuation and obtain

$$u_1 = \frac{\mathrm{Y}_2'^{[-3]}}{1 + \mathrm{Y}_2'^{[-3]}} = 1 - \varepsilon'\gamma\left(w' + \frac{1}{w'} - 2\cosh C'\right) + \mathcal{O}\left(\varepsilon'^2\right), \tag{6.38}$$

$$u_2 = \frac{\mathrm{Y}_2'^{[-1]}}{1 + \mathrm{Y}_2'^{[-1]}} = \gamma\varepsilon' w' + \mathcal{O}\left(\varepsilon'^2\right), \tag{6.39}$$

$$u_3 = \frac{\mathrm{Y}_2'^{[1]}}{1 + \mathrm{Y}_2'^{[1]}} = \gamma\frac{\varepsilon'}{w'} + \mathcal{O}\left(\varepsilon'^2\right), \tag{6.40}$$

where $\gamma = -3 - 2\sqrt{2}$, $\varepsilon' := e^{-|m|'\cos\phi'}$ and $w' := e^{|m|'\sin\phi'}$. By definition of our path Eq.(6.23), the cross ratios come back to themselves at the endpoint of the continuation. We therefore identify $u_a' = u_a$ and use this identification to express the new parameters through the old ones. We find

$$\varepsilon' = \gamma^{-1}\varepsilon + \mathcal{O}\left(\varepsilon^2\right), \quad w' = w + \mathcal{O}\left(\varepsilon^2\right), \quad \cosh C' = -\cosh C + \mathcal{O}\left(\varepsilon^2\right), \tag{6.41}$$

where the last equation simply follows from our analytic formula for C, Eq.(6.19). Note that these equations can also be used to calculate the original Y-system parameters at the end of the calculation. For example, for the case $|m| = 10$, $\phi = \phi' = 0$ we find from Eq.(6.41)

$$|m|' = \log\gamma + |m| \approx 11.76 - i\pi, \tag{6.42}$$

nicely matching our numerical result shown in figure 6.5. Since we will need it in the following, let us remark that Eq.(6.42) can be turned around and, together with the numerical result Fig.6.5 used to determine the ambiguity in the imaginary part of $\log\gamma$. For example, in this case we find

$$\log\gamma = -i\pi + \log(3 + 2\sqrt{2}). \tag{6.43}$$

The free energy part of the amplitude receives contributions from the two crossing solutions,

$$\begin{aligned} A'_{\text{free}} =& \frac{|m|'}{2\pi} \int\limits_{\mathbb{R}+i\phi'} d\theta \cosh(\theta - i\phi') \log\left[(1+\mathrm{Y}'_1(\theta))(1+\mathrm{Y}'_3(\theta))(1+\mathrm{Y}'_2(\theta))^{\sqrt{2}}\right] \\ &+ |m|' i\sinh(\theta_+ - i\phi') - |m|' i\sinh(\theta_- - i\phi'). \end{aligned} \tag{6.44}$$

As we end up in a regime where the integrals can be neglected, the integral contributions drop out and after inserting the endpoint positions Eq.(6.34) we end up with

$$\begin{aligned} A'_{\text{free}} &\cong -\sqrt{2}|m|' \cong \sqrt{2}\log\varepsilon' \\ &= \sqrt{2}\log\varepsilon - \sqrt{2}\log\gamma. \end{aligned} \tag{6.45}$$

In Eq.(6.45) we used the relation $|m|' = \sqrt{\log^2\varepsilon' + \log^2 w'} \cong -\log\varepsilon'$. The periods part at the endpoint can be evaluated easily,

$$\begin{aligned} A'_{\text{per}} &= \frac{1}{4}|m|'^2 = \frac{1}{4}|m|'^2 - \frac{1}{4}|m|^2 + A_{\text{per}} \\ &\cong -\frac{1}{2}\log\gamma\log\varepsilon + \frac{1}{4}\log^2\gamma + A_{\text{per}} \end{aligned} \tag{6.46}$$

and the Δ-contribution is given by

$$\begin{aligned} \Delta' &= \Delta + i\frac{\pi}{2}\left(\log u_1 - \log(1-u_1)\right) + \frac{\pi^2}{2} \\ &\cong -i\frac{\pi}{2}\log\varepsilon - \frac{\pi}{2}i\log\left(2\cosh C + w + \frac{1}{w}\right) + \frac{\pi^2}{2} + \Delta, \end{aligned} \tag{6.47}$$

where in the first step we have inserted the phase from the path of continuation Eq.(6.23) and in the second step inserted the multi-Regge behaviour Eq.(6.3). Note that since the Δ-contribution is given directly in terms of the cross ratios, the unprimed quantities appear in Eq.(6.47). For Δ and A_{per} we have added and subtracted the respective contribution before the continuation because we know that the original contributions cancel in the full amplitude. The parts in the above expressions other than the original piece are therefore the contribution due to the continuation of the cross ratios. Assembling all pieces, we find for the pieces of the remainder function

$$A'_{\text{free}} + A'_{\text{per}} + \Delta' + i\delta' \cong -e_2\log\varepsilon - i\pi e_2 + \text{const.}, \tag{6.48}$$

where $e_2 = -\sqrt{2} + \frac{1}{2}\log\left(3+2\sqrt{2}\right) \sim -0.533$ and $\delta' = \frac{\pi}{2}\log\left(2\cosh C + w + \frac{1}{w}\right)$ is a phase that comes from the expansion of the Li_2-functions appearing in the Δ-contribution. Since the Li_2-functions only appear in the A_{BDS}-part of Δ (cf. Eq.(2.59)), this phase cancels with a corresponding term in the BDS ansatz and does not appear in the full amplitude. Using the relation

$$\varepsilon = (1-u_1)\sqrt{\tilde{u}_2\tilde{u}_3} \tag{6.49}$$

we can write the remainder function in terms of the cross ratios and find our final result

$$e^{R_{6,--}+i\delta_{6,--}}\Big|_{\mathrm{MRL}} \sim \left(-(1-u_1)\sqrt{\tilde{u}_2\tilde{u}_3}\right)^{\frac{\sqrt{\lambda}}{2\pi}e_2}. \tag{6.50}$$

In Eq.(6.50) the phase on the left-hand side is given by

$$\delta_{6,--} = \frac{1}{4}\sqrt{\lambda}\log\sqrt{\tilde{u}_2\tilde{u}_3} = \frac{\pi}{4}\gamma_K\log\sqrt{\tilde{u}_2\tilde{u}_3}, \tag{6.51}$$

where in the last step we used the strong coupling expansion of the cusp anomalous dimension $\gamma_K = \frac{\sqrt{\lambda}}{\pi} + \dots$ [85]. We see that the remainder function in the region $P_{6,--}$ is indeed non-vanishing and shows nice Regge-like power-law behaviour $R_{6,--} \sim (1-u_1)^{\omega}$.

It should be noted that our result does not vanish in the collinear limits $\tilde{u}_s \to 0$. This is in contrast to the general argument that in the collinear limit the 6-point function reduces to a 5-point amplitude and therefore the remainder function must vanish. One might argue that after analytic continuation we have ended up on a different sheet where this is no longer true. However, all expressions given in [70] from a weak coupling expansion vanish in the collinear limit even after the analytic continuation. We are probably facing an order of limits issue here. As our numerical studies have to be performed for a generic value of w, we should not make any statement about the collinear limits $w \to 0$ or $w \to \infty$. We have checked that our result persists in the range $10^{-1} \leq w \leq 10$. A more detailed study on the collinear limit in the Regge region $P_{6,--}$ is in progress.

6.4.4. Comparison with weak coupling

Let us take a moment to compare our result Eq.(6.50) with the weak coupling dispersion relation Eq.(3.49)

$$e^{R_{6,--}+i\delta_{6,--}}\Big|_{\mathrm{MRL}} = \tag{6.52}$$
$$\cos\pi\omega_{ab} + i\frac{\lambda}{2}\sum_{n=-\infty}^{\infty}(-1)^n\left(\frac{r}{r^*}\right)^{\frac{n}{2}}\int_{-\infty}^{\infty}\frac{d\nu}{\nu^2+\frac{n^2}{4}}\,|r|^{2i\nu}\,\Phi_{\mathrm{Reg}}(\nu,n)\left(-(1-u_1)\sqrt{\tilde{u}_2\tilde{u}_3}\right)^{-\omega(\nu,n)}$$

We see that both at weak and strong coupling, the remainder function shows a Regge power-law dependence $\sim (1-u_1)^{\omega}$. Furthermore, the phase $\delta_{6,--}$ we find in Eq.(6.51) nicely matches the expression in [76] once the strong coupling expansion of γ_K is taken into account and the phase $(-1)^{-\omega}$ shows up correctly.

However, there is a striking difference. While the weak coupling expression contains an integration and a summation over the conformal quantum numbers ν and n, only one term appears at strong coupling. The result Eq.(6.50) therefore suggests that at strong coupling the integral is dominated by a saddle point, which lies at $\nu = 0$, because we see

no factor of $|r|$ when comparing our strong coupling result Eq.(6.50) with Eq.(6.52). The exponent e_2 we find in Eq.(6.50) can then be interpreted as the strong coupling limit of the BFKL eigenvalue. In fact, also at weak coupling the remainder function is dominated by a saddle point at $n = 1$, $\nu = 0$. While we are not sensitive to the n-dependence on the strong coupling side as it is subleading in $\sqrt{\lambda}$, the strong coupling result shows that the dominant saddle point is located at $\nu = 0$ at strong coupling, as well.

The above speculations are supported by [131], where the author proposes all-loop expressions for the BFKL eigenvalue and the impact factor. Taking the strong coupling limit, he indeed finds a dominant saddle point with the BFKL eigenvalue e_2.

Before closing this chapter, let us remark that the strong coupling results are in very nice agreement with the analytic structure predicted at weak coupling [25] - we see a Regge cut-like contribution the region $P_{6,--}$ and no contributions in the other regions. We now move on to the 7-point amplitude to see whether this nice matching also holds for more external gluons.

7. The 7-point amplitude

In this chapter, we study the 7-gluon amplitude. The result of the last chapter nurtured the hope expressed in the introduction that the analytic structure imposed by Regge theory at weak coupling is preserved even in the strong coupling limit. The calculation of the 7-point amplitude will provide crucial input because we know from weak coupling predictions that the same BFKL eigenvalue is probed (i.e. the same number e_2 should appear in our remainder function) and there are four Regge regions where this number should show up. Confirming these predictions would provide very non-trivial support for our hypothesis.

We begin this chapter by highlighting the differences to the 6-point amplitude. This includes a study of the Regge regions and the analytic continuations of the driving terms, which will naturally lead us to the discussion of conformal Gram relations. We then go on to study the crossing solutions for the four relevant Regge regions and calculate the remainder function for the respective configurations. The 7-point amplitude in the multi-Regge limit has also been investigated at weak coupling recently, see [136–138]. Beyond the Regge limit, the two-loop symbol of the 7-point amplitude is determined in [139] and the part of the remainder function containing the highest-weight functions is found in [140] based on motivic amplitudes and the classification of the combinations of cross ratios which appear in the remainder function [141].

7.1. Cross ratios

In the 7-point case we have six independent cross ratios,

$$\begin{aligned} u_{11} &= \frac{x_{2,6}^2 x_{3,5}^2}{x_{3,6}^2 x_{2,5}^2} = \frac{Y_{2,2}^{[2]}}{1+Y_{2,2}^{[2]}}, \quad u_{21} = \frac{x_{4,7}^2 x_{1,3}^2}{x_{3,7}^2 x_{1,4}^2} = \frac{Y_{2,2}^{[-2]}}{1+Y_{2,2}^{[-2]}}, u_{31} = \frac{x_{2,4}^2 x_{1,5}^2}{x_{1,4}^2 x_{2,5}^2} = \frac{Y_{2,2}^{[0]}}{1+Y_{2,2}^{[0]}}, \\ u_{12} &= \frac{x_{3,7}^2 x_{4,6}^2}{x_{4,7}^2 x_{3,6}^2} = \frac{Y_{2,1}^{[-3]}}{1+Y_{2,1}^{[-3]}}, u_{22} = \frac{x_{5,7}^2 x_{1,4}^2}{x_{4,7}^2 x_{1,5}^2} = \frac{Y_{2,1}^{[-1]}}{1+Y_{2,1}^{[-1]}}, u_{32} = \frac{x_{2,5}^2 x_{1,6}^2}{x_{1,5}^2 x_{2,6}^2} = \frac{Y_{2,1}^{[1]}}{1+Y_{2,1}^{[1]}}, \end{aligned} \tag{7.1}$$

which we parametrise as

$$\begin{aligned} u_{11} &= 1 - \left(w_2 + \frac{1}{w_2} + 2\cosh C_2\right)\varepsilon_2, \quad u_{21} = w_2\varepsilon_2, \quad u_{31} = \frac{\varepsilon_2}{w_2}, \\ u_{12} &= 1 - \left(w_1 + \frac{1}{w_1} + 2\cosh C_1\right)\varepsilon_1, \quad u_{22} = w_1\varepsilon_1, \quad u_{32} = \frac{\varepsilon_1}{w_1}, \end{aligned} \tag{7.2}$$

via the quantities ε_s and w_s defined in Eq.(4.33).

However, starting from seven points, there are actually more cross ratios than independent ones. In particular, for the case at hand

$$\tilde{u} = \frac{x_{2,7}^2 x_{3,6}^2}{x_{2,6}^2 x_{3,7}^2} = \frac{Y_{2,2}^{[-4]}}{1 + Y_{2,2}^{[-4]}} \tag{7.3}$$

is another cross ratio which is not part of our basis Eq.(3.4). Since there are only six independent cross ratios, $\tilde{u}$ must be a function of the cross ratios of our basis. The equation relating our basis to $\tilde{u}$ is a conformal Gram identity whose full form and derivation we show in detail in appendix E. Here we just spell out the relation in the multi-Regge limit setting all small cross ratios $u_{2s} = u_{3s} = 0$,

$$0 = (\tilde{u} - 1)(1 - u_{11} - u_{12} + u_{11}u_{12}\tilde{u}) \tag{7.4}$$

for which the non-trivial solution is given by

$$\tilde{u} = -\frac{1 - u_{11} - u_{12}}{u_{11}u_{12}}. \tag{7.5}$$

However, just like the other cross ratios, $\tilde{u}$ is a combination of Mandelstam invariants and can have a non-trivial behaviour during the analytic continuations. We therefore have to make sure that we find paths of continuation that are consistent with the Gram relation.

7.2. Regge regions

Following our general discussion in section 5.4, we have $2^{7-4} = 8$ possible Regge regions. However, we will ignore those Regge regions in which only one leg is flipped. As in the 6-point case, these involve only rotations of the small cross ratios and will not lead to a non-trivial remainder function. This leaves us with five regions, of which the Euclidean region again leads to a trivial result, as we show in section 7.4.1. We present the interesting Regge regions in figure 7.1, for which the calculation of the phases for the cross ratios gives us the following paths:

$$\begin{aligned}
P_{7,+--}: &u_{11}(\varphi) = u_{11}, && u_{21}(\varphi) = e^{i\varphi}u_{21}, && u_{31}(\varphi) = e^{-i\varphi}u_{31}, \\
&u_{12}(\varphi) = e^{-2i\varphi}u_{12}, && u_{22}(\varphi) = u_{22}, && u_{32}(\varphi) = u_{32}, && \tilde{u}(\varphi) = \tilde{u} \\
P_{7,-+-}: &u_{11}(\varphi) = e^{2i\varphi}u_{11}, && u_{21}(\varphi) = e^{-i\varphi}u_{21}, && u_{31}(\varphi) = e^{i\varphi}u_{31}, \\
&u_{12}(\varphi) = e^{2i\varphi}u_{12}, && u_{22}(\varphi) = e^{i\varphi}u_{22}, && u_{32}(\varphi) = e^{-i\varphi}u_{32}, && \tilde{u}(\varphi) = e^{-2i\varphi}\tilde{u} \\
P_{7,--+}: &u_{11}(\varphi) = e^{-2i\varphi}u_{11}, && u_{21}(\varphi) = u_{21}, && u_{31}(\varphi) = u_{31}, \\
&u_{12}(\varphi) = u_{12}, && u_{22}(\varphi) = e^{-i\varphi}u_{22}, && u_{32}(\varphi) = e^{i\varphi}u_{32}, && \tilde{u}(\varphi) = \tilde{u} \\
P'_{7,---}: &u_{11}(\varphi) = u_{11}, && u_{21}(\varphi) = u_{21}, && u_{31}(\varphi) = u_{31}, \\
&u_{12}(\varphi) = u_{12}, && u_{22}(\varphi) = u_{22}, && u_{32}(\varphi) = u_{32}, && \tilde{u}(\varphi) = e^{-2i\varphi}\tilde{u}.
\end{aligned}$$

While the first three paths look reasonable, the last path is rather odd. All cross ratios of our basis remain fixed, while the dependent cross ratio $\tilde{u}$ has to do a full rotation. This is impossible, of course. The reason for this behaviour lies in our assumption stated in

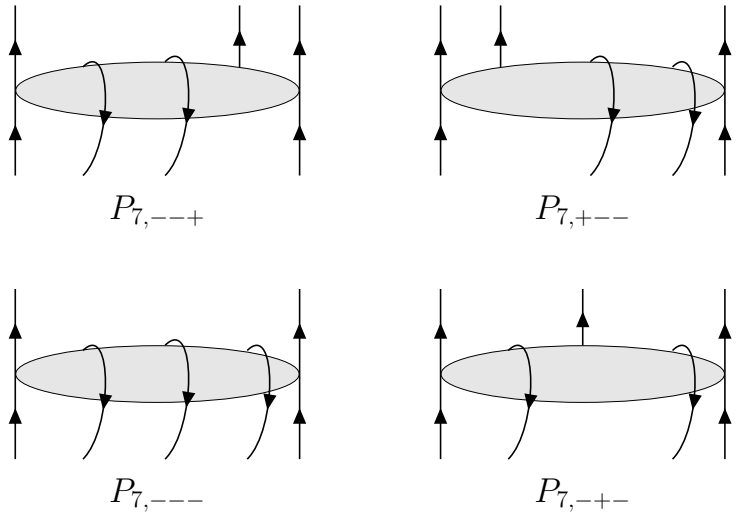

Figure 7.1.: Interesting Regge regions for the 7-point amplitude.

section 5.4 that we can always perform the continuation along (semi-)circles. We now see that this is too naive. Instead, we should choose paths that both have the same winding number around $u_{as} = 0$ as the naive paths using circles and are consistent with the Gram relation Eq.(7.4).

Let us illustrate this for the path $P'_{7,---}$. In the multi-Regge limit, we can use the Gram relation in the approximation $u_{12} = u_{11} =: u_1$ with all small cross ratios set to zero, Eq.(7.5). Inverting this relation for u_1, we find

$$u_1 = \frac{1}{\tilde{u}}\left(1 \pm \sqrt{1-\tilde{u}}\right). \tag{7.6}$$

This Gram relation has two solutions for u_1, of which we choose the one that has winding number zero around $u_1 = 0$. This specifies a path that fulfils both our requirements. Explicitly, it is given by:

$$\begin{aligned} P_{7,---} : u_{11}(\varphi) &= e^{2i\varphi}\left(1-\sqrt{1-e^{-2i\varphi}}\right) u_{11},\ u_{12}(\varphi) = e^{2i\varphi}\left(1-\sqrt{1-e^{-2i\varphi}}\right) u_{12} \\ \tilde{u}(\varphi) &= e^{-2i\varphi}\tilde{u},\ u_{2s}(\varphi) = u_{2s},\ u_{3s}(\varphi) = u_{3s}. \end{aligned} \tag{7.7}$$

We can now study the crossing solutions for the given paths and calculate the remainder functions. It should be kept in mind that our assumption that only the winding number and consistency with the Gram relations and no further details of the paths are relevant is a hypothesis.

7.3. Predictions from weak coupling

Before we begin the explicit calculation of the remainder functions at strong coupling, let us briefly review the predictions for the analytic structure of the 7-point amplitude in the MRL as derived in [137]. The approach taken in [137] is similar to the method outlined in section 3.4 for the 6-point amplitude. Analysing the factorisation properties of the BDS

Region	Cuts	Relevant variables	Conformal phase δ
$P_{7,--+}$	t_2	u_{a1}	$\frac{\pi}{4}\gamma_K \log\left(\sqrt{\tilde{u}_{21}\tilde{u}_{31}}\right)$
$P_{7,+--}$	t_3	u_{a2}	$\frac{\pi}{4}\gamma_K \log\left(\sqrt{\tilde{u}_{22}\tilde{u}_{32}}\right)$
$P_{7,---}$	t_2+t_3	$u_{a1}\cdot u_{a2}$	$\frac{\pi}{4}\gamma_K \log\left(\frac{(1-u_{11})(1-u_{12})}{1-\tilde{u}}\sqrt{\tilde{u}_{21}\tilde{u}_{31}\tilde{u}_{22}\tilde{u}_{32}}\right)$
$P_{7,-+-}$	t_2, t_3, t_2+t_3	u_{a1}, u_{a2}	$\frac{\pi}{4}\gamma_K \log\left(\frac{(1-u_{11})(1-u_{12})}{1-\tilde{u}}\sqrt{\frac{\tilde{u}_{21}}{\tilde{u}_{31}}\frac{\tilde{u}_{32}}{\tilde{u}_{22}}}\right)$

Table 7.1.: Predictions for the structure of the 7-point remainder function in the multi-Regge limit.

ansatz, the authors of [137] find that in some Regge regions unphysical poles appear which need to be cancelled by a Regge cut contribution. In that way, the Regge regions in which Regge cuts show up can be identified. In particular, for the $2 \to 5$ amplitude, the four Regge regions of figure 7.1 are shown to receive the following cut contributions:

- $P_{7,--+}$: 'short' Regge cut in t_2-channel
- $P_{7,+--}$: 'short' Regge cut in t_3-channel
- $P_{7,---}$: 'long' Regge cut in t_2+t_3-channel
- $P_{7,-+-}$: both short cuts and the long cut contribute

The Regge cuts in the 7-point amplitude still arise from a bound state of two Reggeons. Therefore, it is to be expected that the universal quantities governing the 6-point case reappear in the 7-point amplitude and the remainder function should have the same structure as Eq.(6.50). Of course, we have twice as many variables as in the 6-point case. However, the relevant variables can be identified from the cut structure. For example, in the region $P_{7,--+}$ a cut should appear in the t_2-channel, which is connected with the energy variable s_2. This variable, in turn, appears only in the triplet u_{a1} and we expect the remainder function to be a function of these three variables only. Similarly, the remainder function in the region $P_{7,+--}$ should only depend on the triplet u_{a2}. The long Regge cut in the region $P_{7,---}$ is connected with the energy variable s_{234} in the notation of section 3.1. As we know from Eq.(3.21) we have $s_{234} \sim s_2 s_3$ in the multi-Regge limit and therefore we expect the remainder function to be a function of the products $u_{a1}u_{a2}$.

As we have already seen in the 6-point amplitude, the Regge cut contribution is connected with a conformal phase δ. These phases are also obtained in [137]. We spell them out, together with the other weak-coupling predictions, in table 7.1. Note that $1-\tilde{u} = \mathcal{O}(\varepsilon^2)$ in the multi-Regge limit so that all conformal phases are constants in the MRL.

The structure of the cut contributions is studied in [138]. Like in the 6-point case, every cut contribution gives rise to a dispersion relation-like integral. In analogy with Eq.(3.49), the remainder function in the region $P_{7,--+}$ is given by

$$e^{R_{7,--+}+i\delta_{7,--+}}\Big|_{\text{MRL}} = \tag{7.8}$$
$$\cos\pi\omega_{ab} + i\frac{\lambda}{2}\sum_n (-1)^n \left(\frac{r_1}{r_1^*}\right)^{\frac{n}{2}} \int_{-\infty}^{+\infty} \frac{d\nu}{\nu^2+\frac{n^2}{4}} \Phi_{\text{reg}}(\nu,n)|r_1|^{2i\nu} \left(-(1-u_{11})\sqrt{\tilde{u}_{21}\tilde{u}_{31}}\right)^{-\omega(\nu,n)},$$

with the phase $\delta_{7,--+}$ spelled out in table 7.1 and a Regge pole contribution ω_{ab}. Note that the quantities $\Phi_{\text{Reg}}(\nu,n)$ and $\omega(\nu,n)$ are the same quantities governing the 6-point case. The form of the remainder function in the region $P_{7,+--}$ can be obtained from Eq.(7.8) by applying target-projectile symmetry. This leaves us with the regions involving the long cuts. For the region $P_{7,---}$ one obtains

$$e^{R_{7,---}+i\delta_{7,---}}\Big|_{\text{MRL}} = \tag{7.9}$$
$$i\frac{\lambda}{2}\sum_{n_1,n_2}(-1)^{n_1+n_2}\left(\frac{r_1}{r_1^*}\right)^{\frac{n_1}{2}}\left(\frac{r_2}{r_2^*}\right)^{\frac{n_2}{2}}\int_{-\infty}^{+\infty}\frac{d\nu_1 d\nu_2}{(2\pi)^2}\Phi^*(\nu_1,n_1)C(\nu_1,n_1,\nu_2,n_2)\Phi(\nu_2,n_2)$$
$$\times|r_1|^{2i\nu_1}|r_2|^{2i\nu_2}\left(-(1-u_{11})\sqrt{\tilde{u}_{21}\tilde{u}_{31}}\right)^{-\omega(\nu_1,n_1)}\left(-(1-u_{12})\sqrt{\tilde{u}_{22}\tilde{u}_{32}}\right)^{-\omega(\nu_2,n_2)}+\cdots$$

Again, the quantities $\Phi(\nu,n)$ and $\omega(\nu,n)$ are the same quantities as in the 6-point case. However, a new vertex $C(\nu_1,n_1,\nu_2,n_2)$ appears, which is calculated to leading order in [136] and reads

$$\Phi^*C\Phi = \frac{\Gamma\left(-i\nu_1-\frac{n_1}{2}\right)}{\Gamma\left(1+i\nu_1-\frac{n_1}{2}\right)}\frac{\Gamma\left(i\nu_2+\frac{n_2}{2}\right)}{\Gamma\left(1-i\nu_2+\frac{n_2}{2}\right)}\frac{\Gamma\left(i(\nu_1-\nu_2)+\frac{1}{2}(n_2-n_1)\right)}{\Gamma\left(1-i(\nu_1-\nu_2)+\frac{1}{2}(n_2-n_1)\right)}. \tag{7.10}$$

In addition to the nicely factorised expression in Eq.(7.9) further Regge pole and subtraction terms should appear, as indicated by the dots. These, however, are not relevant for our discussion and are explained in [137, 138].

The region $P_{7,-+-}$ should also be governed by a factorised ansatz as in Eq.(7.9). In fact, the only difference in the dispersion relation should be that the complex conjugate of the new production vertex appears. To leading order this vertex C is real-valued in momentum space, therefore differences between the two regions can only appear starting from the NLLA. Furthermore, the subtraction terms for the region $P_{7,-+-}$ are different from those in the region $P_{7,---}$.

7.4. Contributions to the remainder function

Let us begin our investigations by spelling out the explicit formulas for the contributions to the remainder function. As in the 6-point case, the remainder function consists of three terms

$$R_7 = -\frac{\sqrt{\lambda}}{2\pi}\left(\Delta + A_{\text{per}} + A_{\text{free}}\right). \tag{7.11}$$

The free energy part A_{free} has standard form,

$$\text{A}_{\text{free}} = \sum_{s=1}^{2}\frac{|m_s|}{2\pi}\int_{\mathbb{R}}d\theta\cosh\theta\left[\left(1+\tilde{\text{Y}}_{1,s}(\theta)\right)\left(1+\tilde{\text{Y}}_{3,s}(\theta)\right)\left(1+\tilde{\text{Y}}_{2,s}(\theta)\right)^{\sqrt{2}}\right]. \tag{7.12}$$

Recall that $\tilde{\text{Y}}_{a,s}(\theta) = \text{Y}_{a,s}(\theta+i\phi_s)$. The periods part A_{per} is more complicated than in the 6-point case and the phases explicitly enter:

$$\text{A}_{\text{per}} = \frac{|m_1|^2}{2}+\frac{|m_2|^2}{2}+\frac{1}{\sqrt{2}}|m_1||m_2|\left(\cos\phi_1\cos\phi_2+\sin\phi_1\sin\phi_2\right). \tag{7.13}$$

This leaves us with Δ, which is a function of the cross ratios and is written down in [142],

$$\begin{aligned}\Delta :=&\mathrm{A}_{\mathrm{BDS-like}} - \mathrm{A}_{\mathrm{BDS}} = -\frac{1}{4}\sum_{i=1}^{7}\left(\log^2 u_i + \mathrm{Li}_2(1-u_i)\right) + \frac{1}{8}\log u_{11}\log\left(\frac{u_{21}u_{22}}{\tilde{u}\,u_{32}}\right)\\ &+\frac{1}{8}\log u_{12}\log\left(\frac{u_{32}u_{31}}{\tilde{u}\,u_{21}}\right)+\frac{1}{8}\log u_{21}\log\left(\frac{u_{11}u_{32}}{u_{12}u_{22}}\right)+\frac{1}{8}\log u_{22}\log\left(\frac{u_{11}\,\tilde{u}}{u_{21}u_{31}}\right)\\ &+\frac{1}{8}\log u_{31}\log\left(\frac{u_{12}\,\tilde{u}}{u_{22}u_{32}}\right)+\frac{1}{8}\log u_{32}\log\left(\frac{u_{12}u_{21}}{u_{11}u_{31}}\right)+\frac{1}{8}\log\tilde{u}\log\left(\frac{u_{22}u_{31}}{u_{11}u_{12}}\right). \quad (7.14)\end{aligned}$$

7.4.1. The remainder function in the Euclidean regime

As a quick check that the above expressions are correct, let us compute the remainder function in the Euclidean regime. We will drop the integral contributions and thereby A_{free} from the beginning, since we know that their contribution is negligible (cf. section 6.2). To calculate the contributions of the other two terms, we use the parametrisation Eq.(4.33) and the multi-Regge limit expressions Eq.(7.2). After expanding in ε_s and keeping only the leading terms we find

$$\begin{aligned}\mathrm{A}_{\mathrm{per}} =&\frac{1}{2}\left(\log^2\varepsilon_1+\log^2 w_1+\log^2\varepsilon_2+\log^2 w_2\right.\\ &\left.+\log\varepsilon_1\log\varepsilon_2+\log w_1\log w_2+\log\varepsilon_2\log w_1-\log\varepsilon_1\log w_2\right)+\mathcal{O}(\varepsilon). \quad (7.15)\end{aligned}$$

as well as

$$\begin{aligned}\Delta =&-\frac{\pi^2}{6}-\frac{1}{2}\left(\log^2\varepsilon_1+\log^2 w_1+\log^2\varepsilon_2+\log^2 w_2\right)\\ &-\frac{1}{2}\left(\log\varepsilon_1\log\varepsilon_2-\log\varepsilon_1\log w_2+\log\varepsilon_2\log w_1+\log w_1\log w_2\right)+\mathcal{O}(\varepsilon). \quad (7.16)\end{aligned}$$

Summing both terms, we see that only a constant remains, which actually cancels with a constant appearing in the BDS-part of the full amplitude. Consequently, the remainder function is trivial in the Euclidean regime, as it should.

7.5. Region $P_{7,--+}$

We now discuss the calculation of the remainder function in the region $P_{7,--+}$ for which we identified the path

$$\begin{aligned}&u_{11}(\varphi)=e^{-2i\varphi}u_{11}, \quad u_{21}(\varphi)=u_{21}, \qquad u_{31}(\varphi)=u_{31},\\ &u_{12}(\varphi)=u_{12}, \qquad u_{22}(\varphi)=e^{-i\varphi}u_{22}, \quad u_{32}(\varphi)=e^{i\varphi}u_{32}, \quad \tilde{u}(\varphi)=\tilde{u}. \quad (7.17)\end{aligned}$$

Before we present the results, let us make a remark. The Y-system we use for the numerical investigations Eqs.(5.18-5.20) was derived under the assumption that the phases are fixed during the continuation, as described in section 5.2. This choice amounts to setting $u_{2s} = u_{3s}$ during the continuation. Looking at the prescribed path $P_{7,--+}$ in Eq.(7.17) we see that this condition is not satisfied, because $\frac{u_{21}}{u_{31}}$ is not a constant during the continuation but rather rotates along a full circle. We can estimate the size of the error we are making

by allowing a small shift in the phases $\phi_s = (1-s)\frac{\pi}{4} + \delta\phi_s$. We keep the index s variable as the same discussion applies to the path $P_{7,+--}$. This leads to

$$\frac{u_{2n-4-s}}{u_{3n-4-s}} = w_s^2 = e^{2|m_s|\sin(\phi_s-(1-s)\frac{\pi}{4})} = e^{2|m_s|\delta\phi_s} = e^{2i\varphi}, \tag{7.18}$$

which translates into

$$\delta\phi_s = \frac{i\varphi}{|m_s|} \sim \mathcal{O}\left(\frac{1}{\log\varepsilon_s}\right) \tag{7.19}$$

for the size of the phase deviation. Since the mass parameters $|m_s|$ stay very large during the continuation, the error we are making is negligibly small and we conclude that we can still use the Y-system for fixed phases without making a mistake. This is consistent with the observation that in our numerical analysis of crossing solutions the rotation of the small cross ratios has practically no effect as compared to the rotation of the large cross ratios.

7.5.1. Continuation of the driving terms

To determine the driving terms, we solve the recursion relations Eq.(2.68) numerically for the driving terms of the modified Y-system Eqs.(5.18-5.20), imposing the behaviour Eq.(7.17) for the cross ratios. We find the results shown in figure 7.2.

7.5.2. Crossing solutions

We now study how the locations of the solutions $\tilde{\mathrm{Y}}_{a,s}(\theta) = -1$ move in the θ-plane during the continuation, using the algorithm described in section 5.3 and find the behaviour shown in figure 7.3. We see that the crossing behaviour looks very similar to the one studied in the 6-point case in section 6.4.1. We have one pair of crossing solutions of $\tilde{\mathrm{Y}}_{3,2}$ and one pair of solutions of $\tilde{\mathrm{Y}}_{2,2}$ which approaches the origin towards the end of the calculation. All other $\tilde{\mathrm{Y}}$-functions do not come close to the real axis. We can then spell out the set of equations at the end of the continuation by picking up the appropriate S-matrices,

$$\begin{aligned}\log\tilde{\mathrm{Y}}'_{1,s}(\theta) &= -|m_s|'\cosh\theta - C'_s + \sum_{a',s'}\int d\theta' K^{1,a'}_{s,s'}\left(\theta-\theta'+i\phi'_s-i\phi'_{s'}\right)\log\left(1+\tilde{\mathrm{Y}}'_{a',s'}(\theta')\right)\\ &\quad + \log\frac{S^{1,3}_{s,2}(\theta-\theta_- + i\phi'_s - i\phi'_2)}{S^{1,3}_{s,2}(\theta-\theta_+ + i\phi'_s - i\phi'_2)},\end{aligned} \tag{7.20}$$

$$\begin{aligned}\log\tilde{\mathrm{Y}}'_{2,s}(\theta) &= -\sqrt{2}|m_s|'\cosh\theta + \sum_{a',s'}\int d\theta' K^{2,a'}_{s,s'}\left(\theta-\theta'+i\phi'_s-i\phi'_{s'}\right)\log\left(1+\tilde{\mathrm{Y}}'_{a',s'}(\theta')\right)\\ &\quad + \log\frac{S^{2,3}_{s,2}(\theta-\theta_- + i\phi'_s - i\phi'_2)}{S^{2,3}_{s,2}(\theta-\theta_+ + i\phi'_s - i\phi'_2)},\end{aligned} \tag{7.21}$$

$$\begin{aligned}\log\tilde{\mathrm{Y}}'_{3,s}(\theta) &= -|m_s|'\cosh\theta + C'_s + \sum_{a',s'}\int d\theta' K^{3,a'}_{s,s'}\left(\theta-\theta'+i\phi'_s-i\phi'_{s'}\right)\log\left(1+\tilde{\mathrm{Y}}'_{a',s'}(\theta')\right)\\ &\quad + \log\frac{S^{3,3}_{s,2}(\theta-\theta_- + i\phi'_s - i\phi'_2)}{S^{3,3}_{s,2}(\theta-\theta_+ + i\phi'_s - i\phi'_2)}.\end{aligned} \tag{7.22}$$

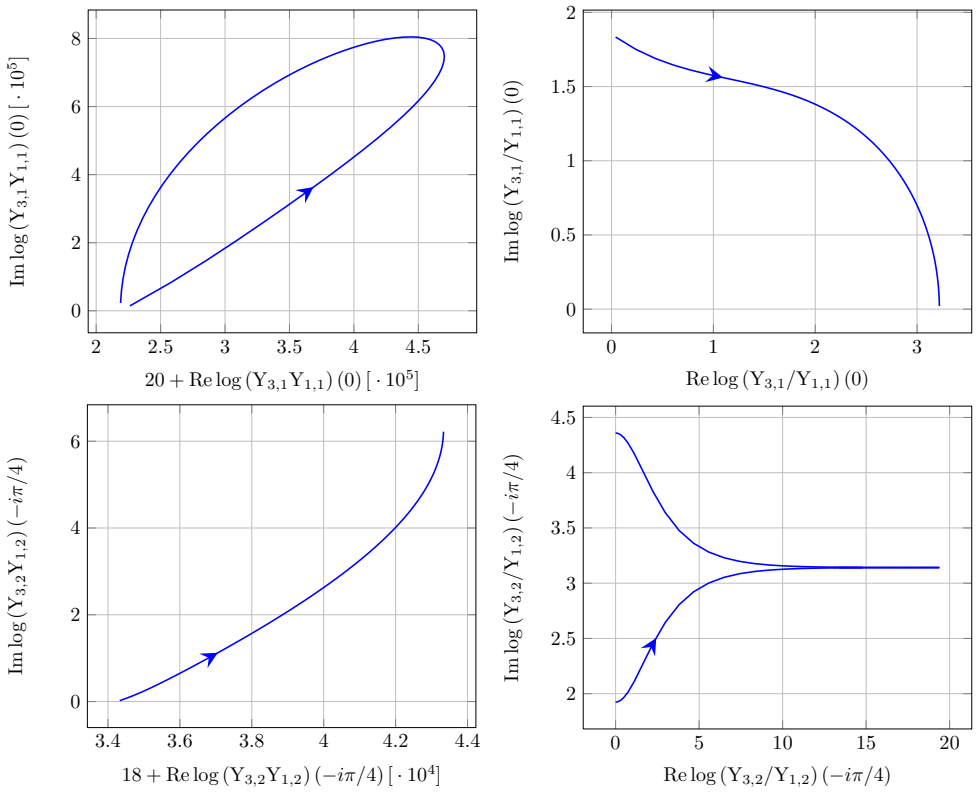

Figure 7.2.: Paths of the driving terms during the analytic continuation for the path Eq.(7.17). For this plot, the specific starting values for the parameters are $|m_1| = 10$, $|m_2| = 9$, $C_1 = \operatorname{arccosh}\left(\frac{3}{5}\right)$, $C_2 = \operatorname{arccosh}\left(\frac{4}{7}\right)$. Note that some axes have been shifted and rescaled. The direction of growing φ is indicated by the arrows.

Note that, despite the fact that the numerical analysis was performed for fixed phases, we keep the phases ϕ' general in Eqs.(7.20-7.22). This is consistent because the crossing picture does not change for small deviations of the phases. One should, however, be careful about taking collinear limits of our results, as explained in section 6.4.3.

After neglecting the integrals, the functions above for the triplet $\tilde{\mathrm{Y}}_{a,2}$ in which the Y-functions with crossing solutions live are the same as in the 6-point case for fixed phase $\phi' = 0$. This means that the endpoint conditions are the same, as well, and we can conclude without any further calculation that

$$\theta_\pm = \pm i\frac{\pi}{4} \tag{7.23}$$

are the endpoints for the crossing solutions of $\tilde{\mathrm{Y}}_{3,2}$ and the solutions of $\tilde{\mathrm{Y}}_{2,2}$ pinch the contour but never cross. Note that the second triplet $\tilde{\mathrm{Y}}_{a,1}$ plays no role in the determination of the endpoints because no solutions of Y-functions in that triplet cross. For completeness, we also show the behaviour of the original Y-system parameters during the continuation in figure 7.4.

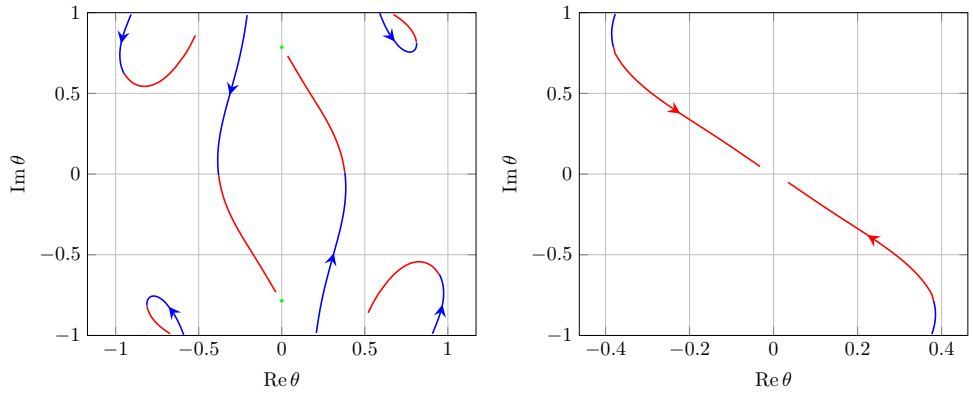

Figure 7.3.: Left: Crossing solutions of $\tilde{\mathrm{Y}}_{3,2}(\theta) = -1$ during the continuation Eq.(7.17). One pair of solutions crosses the real axis and approaches $\pm i\frac{\pi}{4}$. Right: One pair of solutions of $\tilde{\mathrm{Y}}_{2,2}(\theta) = -1$ approaches the origin, but does not contribute to the remainder function. The direction of growing φ is indicated by the arrows.

7.5.3. Calculation of the remainder function $R_{7,--+}$

Now that we know the endpoints of the crossing solutions, we can use the expressions given in section 7.4 to calculate the remainder function in this region. First, let us determine the cross ratios at the end of the continuation by evaluating the Y′-functions at the appropriate values of θ (cf. Eq.(7.1)). Neglecting the integrals and shifting the argument, we find the relevant formulas for the Y′-functions from Eqs.(7.20-7.22):

$$\mathrm{Y}'_{1,s}(\theta) = \left(e^{-|m_s|'\cosh(\theta - i\phi'_s) - C'_s}\right) \frac{S^{1,3}_{s,2}(\theta + i\frac{\pi}{4} - i\phi'_2)}{S^{1,3}_{s,2}(\theta - i\frac{\pi}{4} - i\phi'_2)}, \tag{7.24}$$

$$\mathrm{Y}'_{2,s}(\theta) = \left(e^{-\sqrt{2}|m_s|'\cosh(\theta - i\phi'_s)}\right) \frac{S^{2,3}_{s,2}(\theta + i\frac{\pi}{4} - i\phi'_2)}{S^{2,3}_{s,2}(\theta - i\frac{\pi}{4} - i\phi'_2)}, \tag{7.25}$$

$$\mathrm{Y}'_{3,s}(\theta) = \left(e^{-|m_s|'\cosh(\theta - i\phi'_s) + C'_s}\right) \frac{S^{3,3}_{s,2}(\theta + i\frac{\pi}{4} - i\phi'_2)}{S^{3,3}_{s,2}(\theta - i\frac{\pi}{4} - i\phi'_2)}. \tag{7.26}$$

From these equations, we calculate the cross ratios and find[1]

$$\begin{aligned} u'_{11} &= 1 - \gamma\varepsilon'_2\left(w'_2 + \frac{1}{w'_2} - 2\cosh C'_2\right), & u'_{21} &= \gamma w'_2\varepsilon'_2, & u'_{31} &= \gamma\frac{\varepsilon'_2}{w'_2}, \\ u'_{12} &= 1 + \varepsilon'_1\left(\frac{1}{\gamma}w'_1 + \frac{1}{w'_1} + 2\frac{1}{\sqrt{-\gamma}}\sinh C'_1\right), & u'_{22} &= -\frac{1}{\gamma}w'_1\varepsilon'_1, & u'_{32} &= -\frac{\varepsilon'_1}{w'_1}, \end{aligned} \tag{7.27}$$

where $\gamma = -3 - 2\sqrt{2}$, and all above expressions are valid up to corrections of $\mathcal{O}(\varepsilon'^2)$. As before, we define

$$\varepsilon'_s = e^{-|m_s|'\cos\left((s-1)\frac{\pi}{4} + \phi'_s\right)},\ w'_s = e^{|m_s|'\sin\left((s-1)\frac{\pi}{4} + \phi'_s\right)}. \tag{7.28}$$

[1]Note that in evaluating the cross ratios, we set $\phi'_s = \phi_s$ in the S-matrices because any small deviation from the strict value in the multi-Regge limit would lead to a subleading contribution (cf. Eq.(7.19) and the discussion in section 6.4.2).

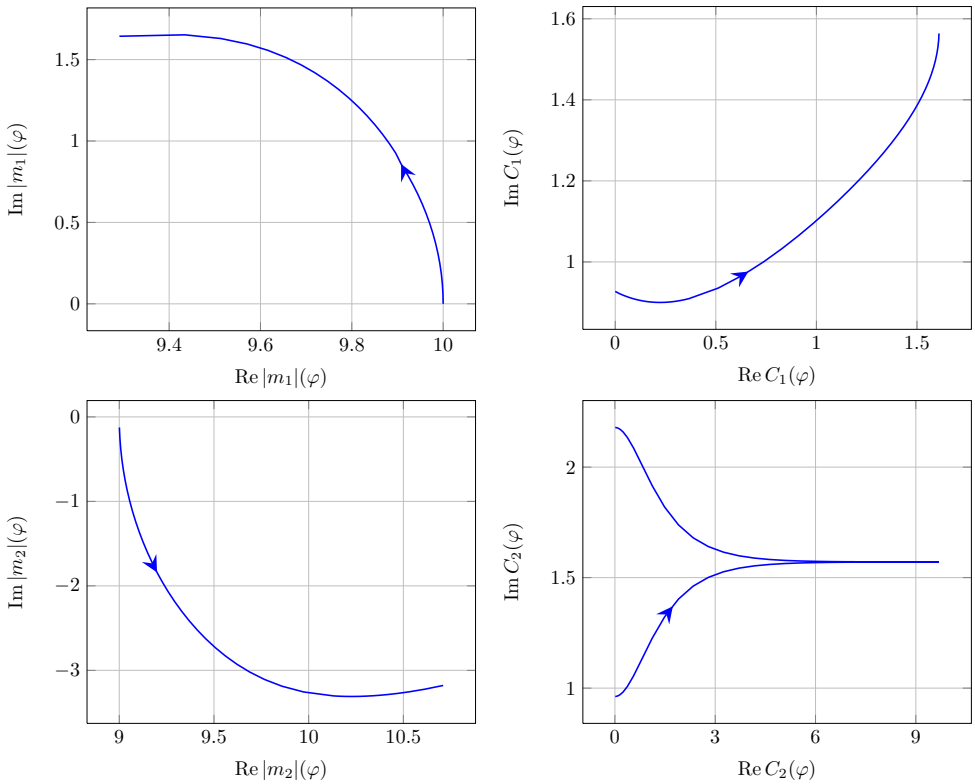

Figure 7.4.: Behaviour of the original Y-system parameters during the continuation Eq.(7.17). Note that C_2 starts and ends on the imaginary axis and quickly attains a large real part, as in the 6-point case (cf. figure 6.5), while C_1 is considerably smaller. The mass parameters $|m_s|$ stay large throughout the continuation. The direction of growing φ is indicated by the arrows.

By our choice of the path Eq.(7.17), we have to identify $u'_{22} = -u_{22}$, $u'_{32} = -u_{32}$ and $u'_{as} = u_{as}$ for all other cross ratios. This identification relates the primed parameters with the original parameters and gives

$$\begin{aligned} \varepsilon'_1 &= \sqrt{\gamma}\varepsilon_1, \quad w'_1 = \sqrt{\gamma} w_1, \quad \cosh C'_1 = \sqrt{1 - \left(w_1 + \frac{1}{w_1} + \cosh C_1\right)^2}, \\ \varepsilon'_2 &= \frac{1}{\gamma}\varepsilon_2, \qquad w'_2 = w_2, \qquad\quad \cosh C'_2 = -\cosh C_2. \end{aligned} \tag{7.29}$$

Using Eq.(4.33) we can analytically calculate the $|m_s|'$, which are nicely consistent with our numerical results in figure 7.4. We now turn to the individual terms of the remainder function, beginning with A'_{per},

$$\begin{aligned} \mathrm{A}'_{\text{per}} =& \frac{1}{2}\left(\log^2 \varepsilon'_1 + \log^2 w'_1 + \log^2 \varepsilon'_2 + \log^2 w'_2 \right. \\ &\left. + \log \varepsilon'_1 \log \varepsilon'_2 + \log w'_1 \log w'_2 + \log \varepsilon'_2 \log w'_1 - \log \varepsilon'_1 \log w'_2\right), \end{aligned} \tag{7.30}$$

Using Eq.(7.29) we obtain

$$\mathrm{A}'_{\text{per}} - \mathrm{A}_{\text{per}} = \frac{1}{4}\log^2 \gamma - \frac{1}{2}\log \gamma \log \varepsilon_2. \tag{7.31}$$

As always, the free energy part A'_{free} is dominated by the residue contributions, which we worked out in section 7.5.2. Inserting the information that one pair of solutions of $\tilde{\text{Y}}_{3,2}$ crosses and approaches $\pm i\frac{\pi}{4}$, we find

$$\begin{aligned}\text{A}'_{\text{free}} &\cong -\frac{|m_2|'}{2\pi}\left(2\pi i\sinh\left(-i\frac{\pi}{4}\right)-2\pi i\sinh\left(i\frac{\pi}{4}\right)\right)\\ &= -\sqrt{2}|m_2|' = -\sqrt{2}\sqrt{\log^2\varepsilon'_2+\log^2 w'_2}\\ &\cong +\sqrt{2}\log\varepsilon'_2 = +\sqrt{2}\left(\log\varepsilon_2-\log\gamma\right).\end{aligned} \tag{7.32}$$

Note that in going from the second to the third line in Eq.(7.32) it is important to choose the correct sign in the square root. The last missing piece is Δ' which is a function of the cross ratios and therefore is easy to obtain. Performing the rotation in the cross ratios we have to pick up some cut contributions and end up with

$$\begin{aligned}\Delta' =&\Delta + i\frac{\pi}{4}\left(2\log u_{11}+\log u_{12}+\log\tilde{u}-2\log(1-u_{11})\right)\\ &+\frac{1}{4}\left(\text{Li}_2(1-u_{22})-\text{Li}_2(1+u_{22})+\text{Li}_2(1-u_{32})-\text{Li}_2(1+u_{32})\right)+\text{const.}\\ \cong& -i\frac{\pi}{2}\log\varepsilon_2 - i\frac{\pi}{2}\log\left(w_2+\frac{1}{w_2}+2\cosh C_2\right)+\text{const.}\end{aligned} \tag{7.33}$$

Adding up all pieces, we find

$$A'_{\text{free}}+A'_{\text{per}}+\Delta'+i\delta'_{7,--+}\cong -e_2\log\varepsilon_2 - i\pi e_2+\text{const.}, \tag{7.34}$$

where $\delta'_{7,--+}=\frac{\pi}{2}\log\left(w_2+\frac{1}{w_2}+2\cosh C_2\right)$ is a phase similar to the one we found in the 6-point case and $e_2=-\sqrt{2}+\frac{1}{2}\log\left(3+2\sqrt{2}\right)$, as before. We rewrite this result using the relations

$$\varepsilon_2=\sqrt{\tilde{u}_{21}\tilde{u}_{31}}(1-u_{11}),\quad w_2=\sqrt{\frac{u_{21}}{u_{31}}}, \tag{7.35}$$

which of course only hold in the multi-Regge limit. After exponentiation, we obtain our final result

$$e^{\text{R}_{7,--+}+i\delta_{7,--+}}\Big|_{\text{MRL}}\sim\left(-(1-u_{11})\sqrt{\tilde{u}_{21}\tilde{u}_{31}}\right)^{\frac{\sqrt{\lambda}}{2\pi}e_2}. \tag{7.36}$$

Rewriting the phase in terms of the cross ratios we find

$$\delta_{7,--+}=\frac{\sqrt{\lambda}}{4}\log\left(\sqrt{\tilde{u}_{21}\tilde{u}_{31}}\right)=\frac{\pi}{4}\gamma_K\log\left(\sqrt{\tilde{u}_{21}\tilde{u}_{31}}\right), \tag{7.37}$$

where we again used the leading strong coupling behaviour $\gamma_K=\frac{\sqrt{\lambda}}{\pi}$. A closer look at our result Eq.(7.36) shows a remarkable similarity with the 6-point result. In fact, the only difference is that in the region $P_{7,--+}$, the 6-point result is evaluated on one triplet only,

$$R_{7,--+}(u_{as})=R_{6,--}(u_{11},u_{21},u_{31}). \tag{7.38}$$

Furthermore, the phases match nicely, as well. In this section we have only considered the region $P_{7,--+}$. Yet it is clear that the region $P_{7,+--}$ should be related to the region

studied here, by target-projectile symmetry Eq.(3.5). This is indeed true and we show by explicit calculation in appendix F that

$$R_{7,+--}(u_{as}) = R_{6,--}(u_{12}, u_{22}, u_{32}), \tag{7.39}$$

and the conformal phase is given by

$$\delta_{7,+--} = \frac{\sqrt{\lambda}}{4} \log\left(\sqrt{\tilde{u}_{22}\tilde{u}_{32}}\right) = \frac{\pi}{4}\gamma_K \log\left(\sqrt{\tilde{u}_{22}\tilde{u}_{32}}\right). \tag{7.40}$$

We have now determined the remainder function for the regions in which two legs are bend down. As we saw, the crossing picture is very similar to the 6-point case and so is the result, although the intermediate calculations are somewhat different. We now turn to the region $P_{7,---}$ in which new effects start to appear.

7.6. Region $P_{7,---}$

In this section, we investigate the region with all three produced particles flipped, for which we identified the path

$$\begin{aligned} u_{11}(\varphi) &= e^{2i\varphi}\left(1-\sqrt{1-e^{-2i\varphi}}\right)u_{11}, \quad u_{21}(\varphi) = u_{21}, \quad u_{31}(\varphi) = u_{31}, \\ u_{12}(\varphi) &= e^{2i\varphi}\left(1-\sqrt{1-e^{-2i\varphi}}\right)u_{12}, \quad u_{22}(\varphi) = u_{22}, \quad u_{32}(\varphi) = u_{32}, \quad \tilde{u}(\varphi) = e^{-2i\varphi}\tilde{u}, \end{aligned} \tag{7.41}$$

in section 7.2.

7.6.1. Continuation of the driving terms

This region differs from the two studied before in that it is invariant under target-projectile symmetry, Eq.(3.5). Due to that symmetry, we can actually find analytic formulas for the driving terms which are approximately correct and which generate the desired winding behaviour. The formulas read

$$\begin{aligned} \mathrm{Y}_{2\pm1,1}(0) =& \frac{1}{2}\frac{1}{1-u_{11}-u_{12}-u_{31}}\big(-1+u_{12}+u_{11}u_{32}+u_{22} \\ & \mp\sqrt{-4u_{12}u_{22}u_{32}(-1+2u_{11}+u_{31})+(-1+u_{22}+u_{12}+u_{11}u_{32})^2}\big). \end{aligned} \tag{7.42}$$

A similar formula holds for $\mathrm{Y}_{2\pm1,2}\left(-i\frac{\pi}{4}\right)$, which can be obtained by applying target-projectile symmetry to the right-hand side of Eq.(7.42). We obtain Eq.(7.42) by solving the recursion relation Eq.(2.68) for the special kinematical point $u_{11} = u_{12}$, $u_{21} = u_{32}$, $u_{31} = u_{22}$. We then reconstruct which of the cross ratios appears by demanding that taking the strict multi-Regge limit, i.e. $u_{1s} = 1$, $u_{2s} = 0$, $u_{3s} = 0$, in one triplet should reduce to the 6-point formulas Eqs.(6.4-6.6) for the other triplet. For example, the strict multi-Regge limit for the triplet u_{a1} reduces Eq.(7.42) to the 6-point case Eqs.(6.4-6.6). This leaves some ambiguities in the above formulas, which, however, are subleading. From this result, we obtain the behaviour of the driving terms shown in figure 7.5.

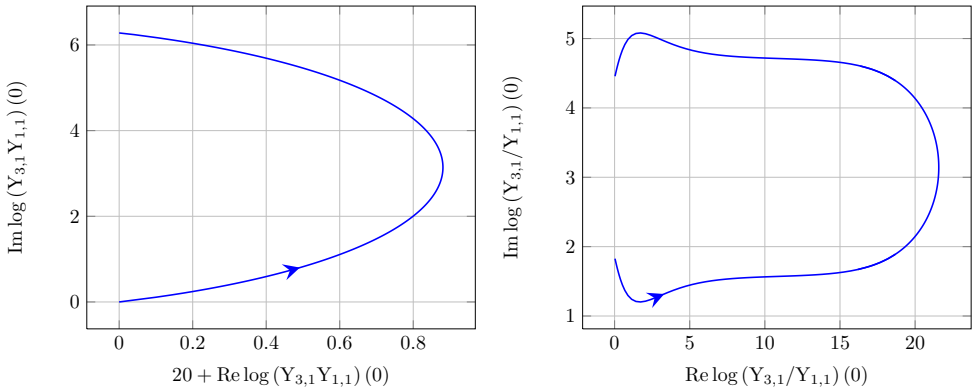

Figure 7.5.: Paths of the driving terms during the analytic continuation for the path Eq.(7.41). The direction of growing φ is indicated by the arrows. The curves shown correspond to the specific choice $|m| = |m_1| = |m_2| = 10$, $C = C_1 = -C_2 = \operatorname{arccosh}\left(\frac{3}{5}\right)$ at the starting point.

7.6.2. Crossing solutions

Let us now perform the analytic continuation and study the crossing solutions. We choose to study the crossing behaviour mostly for the specific case

$$|m| := |m_1| = |m_2|, \quad C := C_1 = -C_2, \tag{7.43}$$

which gives rise to an additional exact symmetry

$$\tilde{\mathrm{Y}}_{a,1}(\theta) = \tilde{\mathrm{Y}}_{4-a,2}(-\theta). \tag{7.44}$$

We choose this special kinematical point for convenience and have made sure that the crossing picture presented below persists for the non-symmetric case $|m_1| \neq |m_2|$, $C_1 \neq -C_2$. The analytic arguments which determine the endpoints of the crossing solutions will be valid for the non-symmetric case, as well.

We present our results in figure 7.6. For the first time, we see crossing solutions for more than one Y-function. In fact, we have two pairs of crossing solutions, one from $\tilde{\mathrm{Y}}_{1,2}$ and one from $\tilde{\mathrm{Y}}_{3,1}$, whose positions we denote by $\theta_{12\pm}$ and $\theta_{31\pm}$, respectively. Note that the solutions of the $\tilde{\mathrm{Y}}$-functions do not cross simultaneously, which introduces some numerical complications. Since no other solutions cross the real axis, we can write down the $\tilde{\mathrm{Y}}$-equations at the endpoint of the continuation:

$$\begin{aligned}\log \tilde{\mathrm{Y}}'_{1,s}(\theta) = &- |m_s|' \cosh\theta - C'_s + \sum_{a',s'} \int d\theta' K^{1,a'}_{s,s'}\left(\theta - \theta' + i\phi'_s - i\phi'_{s'}\right) \log\left(1 + \tilde{\mathrm{Y}}'_{a',s'}(\theta')\right) \\ &+ \log \frac{S^{1,1}_{s,2}(\theta - \theta_{12-} + i\phi'_s - i\phi'_2)}{S^{1,1}_{s,2}(\theta - \theta_{12+} + i\phi'_s - i\phi'_2)} \frac{S^{1,3}_{s,1}(\theta - \theta_{31-} + i\phi'_s - i\phi'_1)}{S^{1,3}_{s,1}(\theta - \theta_{31+} + i\phi'_s - i\phi'_1)},\end{aligned} \tag{7.45}$$

$$\begin{aligned}\log \tilde{\mathrm{Y}}'_{2,s}(\theta) = &- \sqrt{2}|m_s|' \cosh\theta + \sum_{a',s'} \int d\theta' K^{2,a'}_{s,s'}\left(\theta - \theta' + i\phi'_s - i\phi'_{s'}\right) \log\left(1 + \tilde{\mathrm{Y}}'_{a',s'}(\theta')\right) \\ &+ \log \frac{S^{2,1}_{s,2}(\theta - \theta_{12-} + i\phi'_s - i\phi'_2)}{S^{2,1}_{s,2}(\theta - \theta_{12+} + i\phi'_s - i\phi'_2)} \frac{S^{2,3}_{s,1}(\theta - \theta_{31-} + i\phi'_s - i\phi'_1)}{S^{2,3}_{s,1}(\theta - \theta_{31+} + i\phi'_s - i\phi'_1)},\end{aligned} \tag{7.46}$$

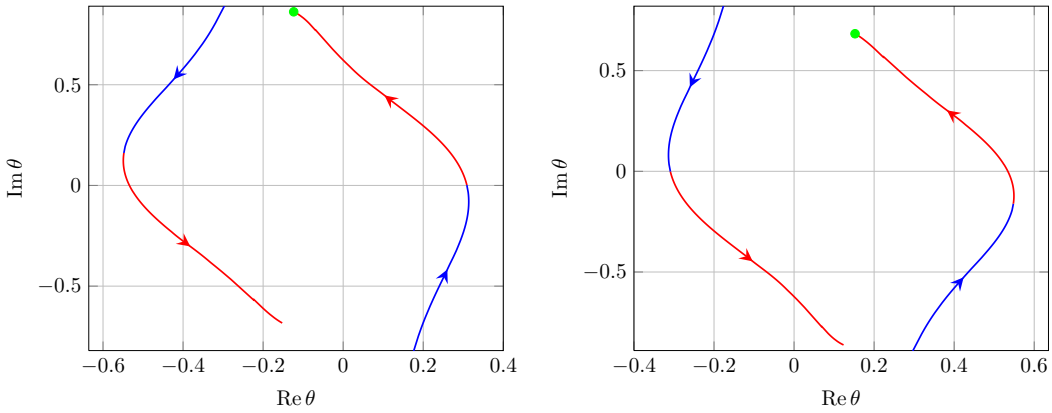

Figure 7.6.: Crossing solutions for the function $\tilde{\mathrm{Y}}_{1,2}(\theta)$ (left) and $\tilde{\mathrm{Y}}_{3,1}(\theta)$ (right) during the continuation Eq.(7.41). The mirror symmetry is due to our choice of parameters, cf. Eq.(7.44). The arrows indicate the direction in which the solutions move. We change colours once the first solution crosses the real axis. The plots correspond to the specific choice $|m| = 10$ and $C = \operatorname{arccosh}\left(\frac{3}{5}\right)$ at the starting point.

$$\begin{aligned}\log \tilde{\mathrm{Y}}'_{3,s}(\theta) = &- |m_s|' \cosh\theta + C'_s + \sum_{a',s'} \int d\theta' K^{3,a'}_{s,s'}\left(\theta - \theta' + i\phi'_s - i\phi'_{s'}\right) \log\left(1 + \tilde{\mathrm{Y}}'_{a',s'}(\theta')\right) \\ &+ \log \frac{S^{3,1}_{s,2}(\theta - \theta_{12-} + i\phi'_s - i\phi'_2)}{S^{3,1}_{s,2}(\theta - \theta_{12+} + i\phi'_s - i\phi'_2)} \frac{S^{3,3}_{s,1}(\theta - \theta_{31-} + i\phi'_s - i\phi'_1)}{S^{3,3}_{s,1}(\theta - \theta_{31+} + i\phi'_s - i\phi'_1)}. \end{aligned} \tag{7.47}$$

We now need to understand the endpoints of the crossed solutions. Due to the symmetry Eq.(7.44) we know that $\theta_{12\pm} = -\theta_{31\mp}$. Furthermore, it seems obvious from figure 7.6 that the differences of the locations of the solutions satisfy

$$\theta_{12+} - \theta_{12-} = i\frac{\pi}{2}, \quad \theta_{31+} - \theta_{31-} = i\frac{\pi}{2}, \tag{7.48}$$

but their absolute position does not seem to correspond to a special position in the θ-plane. This problem is due to the fact that our choice of the mass parameter $|m|$ is still too far away from the multi-Regge limit $|m| \to \infty$. For all other paths studied so far, this was not an issue as only one triplet contained a crossing solution. The fact that we now find two large $\tilde{\mathrm{Y}}$-functions seems to spoil the fast convergence we see for the other paths. Nevertheless, since we have control over the driving terms at the endpoint via Eq.(7.42),

$$\log\left(\hat{\mathrm{Y}}_{1,s} \cdot \hat{\mathrm{Y}}_{3,s}\right)(0)\Big|_{\varphi=\pi} = -2|m_s| + 2\pi i, \tag{7.49}$$

we can study the solutions of the Bethe ansatz at the endpoint numerically as a function of the initial mass parameters, which explicitly enter in Eq.(7.49). Indeed, we find that both θ_{12+} and θ_{31+} approach $i\frac{\pi}{4}$, as shown in figure 7.7. The paths of the original Y-system parameters $|m|$ and C during the continuation is shown in figure 7.8. Let us now try to understand the endpoints analytically. We begin by writing out the usual endpoint conditions

$$-1 = \tilde{\mathrm{Y}}_{1,2}(\theta_{12\pm}) = \tilde{\mathrm{Y}}_{3,1}(\theta_{31\pm}), \tag{7.50}$$

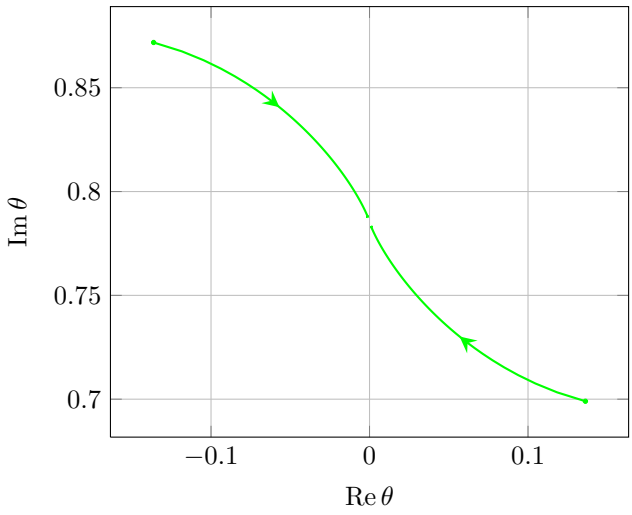

Figure 7.7.: Convergence of the crossing solutions θ_{12+} and θ_{31+} against $i\frac{\pi}{4}$. The green dots indicate the position of the endpoints in figure 7.6. The starting point corresponds to an initial value for the mass parameter of $m = 10$. We then increase the initial mass parameter up to $m = 2000$ to see the convergence against $i\frac{\pi}{4}$.

which, however, only enforce the constraints Eq.(7.48). To find the absolute endpoints, note that for the case of four crossing solutions we have the possibility to construct non-trivial quotients of Bethe ansatz equations,

$$\begin{aligned} 1 = \frac{\tilde{\mathrm{Y}}_{1,2}(\theta_{12-})}{\tilde{\mathrm{Y}}_{1,2}(\theta_{12+})} &= e^{|m_2|'(\cosh\theta_{12+}+i\sinh\theta_{12+})}\left(\frac{1+\cosh(\theta_{12+}-\theta_{31+})+i\sinh(\theta_{12+}-\theta_{31+})}{-1+\cosh(\theta_{12+}-\theta_{31+})+i\sinh(\theta_{12+}-\theta_{31+})}\right) \\ = \frac{\tilde{\mathrm{Y}}_{3,1}(\theta_{31-})}{\tilde{\mathrm{Y}}_{3,1}(\theta_{31+})} &= e^{|m_1|'(\cosh\theta_{31+}+i\sinh\theta_{31+})}\left(\frac{-1+\cosh(\theta_{12+}-\theta_{31+})+i\sinh(\theta_{12+}-\theta_{31+})}{1+\cosh(\theta_{12+}-\theta_{31+})+i\sinh(\theta_{12+}-\theta_{31+})}\right), \end{aligned} \tag{7.51}$$

where we already used Eq.(7.48). They, too, give rise to endpoint conditions. We see that the S-matrix factors in Eq.(7.51) are inverses of each other. Since the S-matrix factors have to either diverge or go to zero in the infinite mass limit, this means that the S-matrix factors of one of the equations (7.51) diverge while the S-matrix factors for the other equation go to zero. This is fulfilled for

$$\theta_{12+} = \theta_{31+}. \tag{7.52}$$

This still leaves us with one undetermined position. We can, however, take the product of both equations in Eq.(7.51) and use Eq.(7.52) to find

$$1 = e^{(|m_1|+|m_2|)(\cosh\theta_{12+}+i\sinh\theta_{12+})}, \tag{7.53}$$

from which we conclude that the driving term has to vanish. This finally gives

$$\theta_{12+} = i\frac{\pi}{4} \tag{7.54}$$

and we conclude that all pole positions lie on $\pm i\frac{\pi}{4}$.

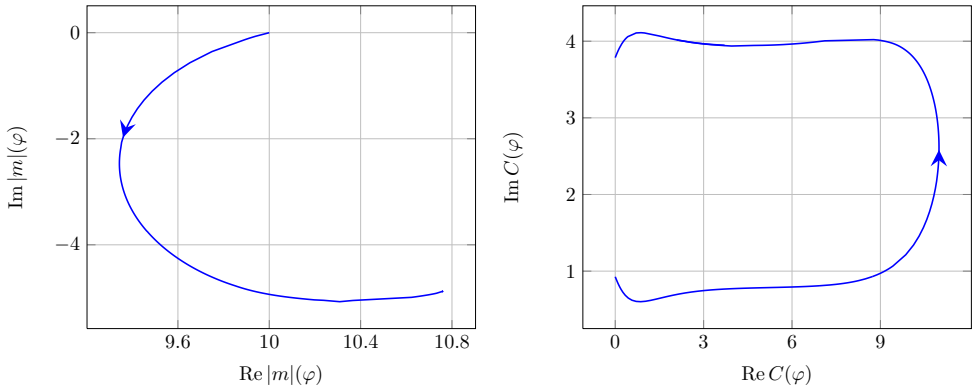

Figure 7.8.: Paths of the original Y-system parameters $|m|$ and C during the analytic continuation Eq.(7.41). The direction of growing φ is indicated by the arrows. The curves shown correspond to the specific choice $|m| = |m_1| = |m_2| = 10$, $C = C_1 = -C_2 = \operatorname{arccosh}\left(\frac{3}{5}\right)$ at the starting point.

7.6.3. Calculation of the remainder function $R_{7,---}$

While the determination of the endpoints and the numerical investigation was much more difficult for this region, the calculation of the remainder function is as simple as for the other regions. We start from the Y′-equations at the endpoint of the continuation,

$$\mathrm{Y}'_{1,s} = \left(e^{-|m_s|'\cosh(\theta - i\phi'_s) - C'_s}\right) \frac{S^{1,1}_{s,2}(\theta + i\frac{\pi}{4} - i\phi'_2)}{S^{1,1}_{s,2}(\theta - i\frac{\pi}{4} - i\phi'_2)} \frac{S^{1,3}_{s,1}(\theta + i\frac{\pi}{4} - i\phi'_1)}{S^{1,3}_{s,1}(\theta - i\frac{\pi}{4} - i\phi'_1)}, \tag{7.55}$$

$$\mathrm{Y}'_{2,s} = \left(e^{-\sqrt{2}|m_s|'\cosh(\theta - i\phi'_s)}\right) \frac{S^{2,1}_{s,2}(\theta + i\frac{\pi}{4} - i\phi'_2)}{S^{2,1}_{s,2}(\theta - i\frac{\pi}{4} - i\phi'_2)} \frac{S^{2,3}_{s,1}(\theta + i\frac{\pi}{4} - i\phi'_1)}{S^{2,3}_{s,1}(\theta - i\frac{\pi}{4} - i\phi'_1)}, \tag{7.56}$$

$$\mathrm{Y}'_{3,s} = \left(e^{-|m_s|'\cosh(\theta - i\phi'_s) + C'_s}\right) \frac{S^{3,1}_{s,2}(\theta + i\frac{\pi}{4} - i\phi'_2)}{S^{3,1}_{s,2}(\theta - i\frac{\pi}{4} - i\phi'_2)} \frac{S^{3,3}_{s,1}(\theta + i\frac{\pi}{4} - i\phi'_1)}{S^{3,3}_{s,1}(\theta - i\frac{\pi}{4} - i\phi'_1)}, \tag{7.57}$$

which, evaluated at the corresponding values of θ, give us the cross ratios

$$u'_{11} = 1 + \varepsilon'_2\left(\frac{1}{w'_2} + \gamma w'_2 + 2\sqrt{-\gamma}\sinh C'_2\right), \quad u'_{21} = -\gamma w'_2 \varepsilon'_2, \quad u'_{31} = -\frac{\varepsilon'_2}{w'_2}, \tag{7.58}$$

$$u'_{12} = 1 + \varepsilon'_1\left(w'_1 + \frac{\gamma}{w'_1} + 2\sqrt{-\gamma}\sinh C'_1\right), \quad u'_{22} = -w'_1\varepsilon'_1, \quad u'_{31} = -\gamma\frac{\varepsilon'_1}{w'_1}. \tag{7.59}$$

For the path under consideration Eq.(7.41), we impose $u'_{as} = u_{as}$ at the endpoint and obtain the new parameters

$$\varepsilon'_1 = \frac{\varepsilon_1}{\sqrt{\gamma}}, \quad w'_1 = -\sqrt{\gamma}w_1, \quad \cosh C'_1 = -\sinh C_1, \tag{7.60}$$

$$\varepsilon'_2 = \frac{\varepsilon_2}{\sqrt{\gamma}}, \quad w'_2 = -\frac{w_2}{\sqrt{\gamma}}, \quad \cosh C'_2 = \sinh C_2, \tag{7.61}$$

where again $\gamma = -3-2\sqrt{2}$. This gives rise to the following contributions to the remainder function:

$$A'_{\text{free}} \cong \sqrt{2}\log\varepsilon_1 + \sqrt{2}\log\varepsilon_2 - \sqrt{2}\log\gamma, \tag{7.62}$$

$$A'_{\text{per}} - A_{\text{per}} \cong -\frac{1}{2}\left(i\pi + \log\gamma\right)\log\left(\varepsilon_1\varepsilon_2\right) - \frac{i\pi}{2}\log\left(\frac{w_1}{w_2}\right) + \text{const.} \tag{7.63}$$

For Δ', a small subtlety appears due to the non-trivial rotation of $\tilde{u}$, which gives rise to contributions $\sim \log(1-\tilde{u})$ and $\sim \log\tilde{u}$. $\tilde{u}$ appears explicitly in the answer. However, we will not replace it with an expression in terms of the ε_s and w_s, but just use the fact that $1-\tilde{u} \sim \mathcal{O}(\varepsilon^2)$ as can be seen from Eq.(7.5). This allows us to drop the term $\sim \log\tilde{u}$ and we obtain

$$\Delta' - \Delta \cong -i\frac{\pi}{2}\log\left(\varepsilon_1\varepsilon_2\right) + \frac{i\pi}{2}\log\left(\frac{w_2}{w_1}\right) - i\frac{\pi}{2}\log\left(1-\tilde{u}\right) + \text{const.}$$

From figure 7.8 we see that the ambiguity for $\log\gamma$ for this path is resolved by

$$\log\gamma = \log(3+2\sqrt{2}) - 3i\pi, \tag{7.64}$$

see also the discussion around Eq.(6.43) in the 6-point case. Adding all contributions, we find

$$A'_{\text{free}} + A'_{\text{per}} + \Delta' + i\delta'_{7,---} \cong -e_2\log\left(\varepsilon_1\varepsilon_2\right) + \text{const.}, \tag{7.65}$$

where $e_2 = -\sqrt{2} + \frac{1}{2}\log(3+2\sqrt{2})$, as before. After using the relations

$$\varepsilon_1 = \sqrt{\tilde{u}_{22}\tilde{u}_{32}}(1-u_{12}), \quad w_1 = \sqrt{\frac{u_{22}}{u_{32}}} \tag{7.66}$$

and the corresponding relations for the other triplet we find the remainder function to be given by

$$e^{R_{7,---}+i\delta_{7,---}}\Big|_{\text{MRL}} \sim \left((1-u_{11})(1-u_{12})\sqrt{\tilde{u}_{21}\tilde{u}_{31}\tilde{u}_{22}\tilde{u}_{32}}\right)^{\frac{\sqrt{\lambda}}{2\pi}e_2}, \tag{7.67}$$

where

$$\delta_{7,---} = \frac{\sqrt{\lambda}}{4}\log\left(\frac{(1-u_{11})(1-u_{12})}{1-\tilde{u}}\sqrt{\tilde{u}_{21}\tilde{u}_{31}\tilde{u}_{22}\tilde{u}_{32}}\right) + \frac{\sqrt{\lambda}}{4}\log\left(\frac{\tilde{u}_{21}}{\tilde{u}_{31}}\frac{\tilde{u}_{32}}{\tilde{u}_{22}}\right). \tag{7.68}$$

Remarkably, we find that the remainder function for the region $P_{7,---}$ is just the sum of the remainder functions for the regions $P_{7,--+}$ and $P_{7,+--}$,

$$R_{7,---}(u_{as}) = R_{7,--+}(u_{as}) + R_{7,+--}(u_{as}). \tag{7.69}$$

This ends our study of this path and we turn to the last remaining region for the 7-point amplitude.

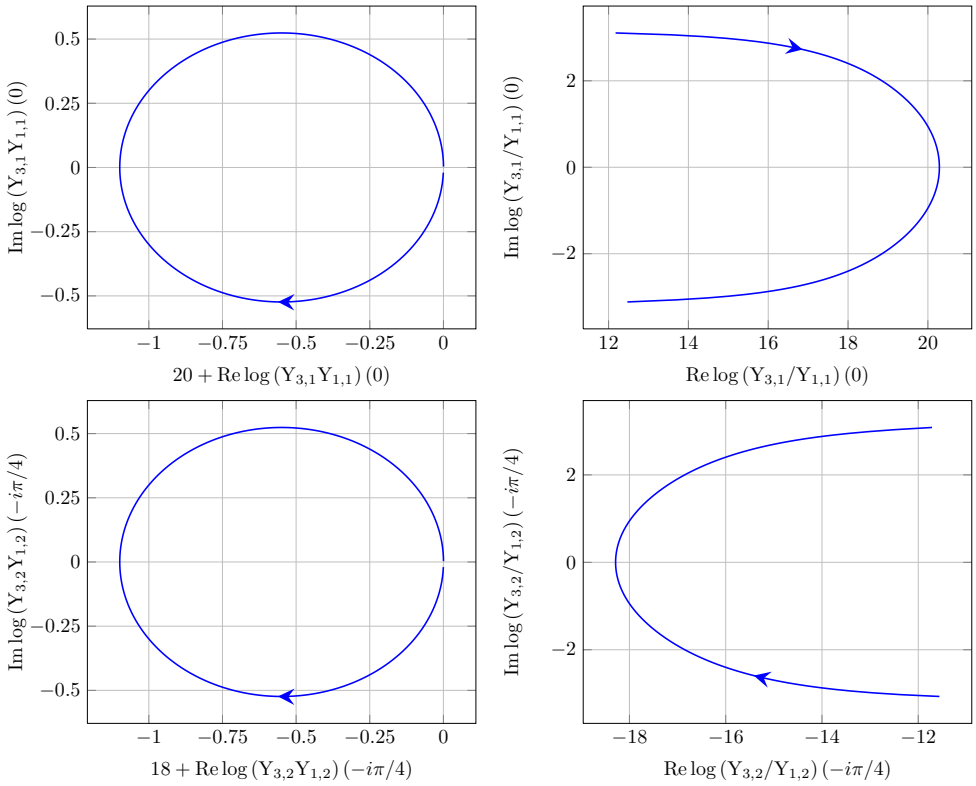

Figure 7.9.: Paths of the driving terms during the analytic continuation Eq.(7.70). Note that some axes have been shifted. The direction of growing φ is indicated by the arrows.

7.7. Region $P_{7,-+-}$

7.7.1. Continuation of the driving terms

The remaining Regge region we want to investigate is $P_{7,-+-}$, for which we identified the path

$$\begin{aligned} &u_{11}(\varphi) = e^{2i\varphi}u_{11}, \quad u_{21}(\varphi) = e^{-i\varphi}u_{21}, \quad u_{31}(\varphi) = e^{i\varphi}u_{31}, \\ &u_{12}(\varphi) = e^{2i\varphi}u_{12}, \quad u_{22}(\varphi) = e^{i\varphi}u_{22}, \quad u_{32}(\varphi) = e^{-i\varphi}u_{32}, \quad \tilde{u}(\varphi) = e^{-2i\varphi}\tilde{u}. \end{aligned} \tag{7.70}$$

This again is a path which is target-projectile symmetric and we can use the analytic formulas Eq.(7.42) to describe the driving terms. We find the results depicted in figure 7.9.

7.7.2. Crossing solutions

Studying the movement of the solutions to $\tilde{\mathrm{Y}}_{a,s}(\theta) = -1$ during the continuation, we find that no solution crosses the real axis, as shown in figure 7.10.

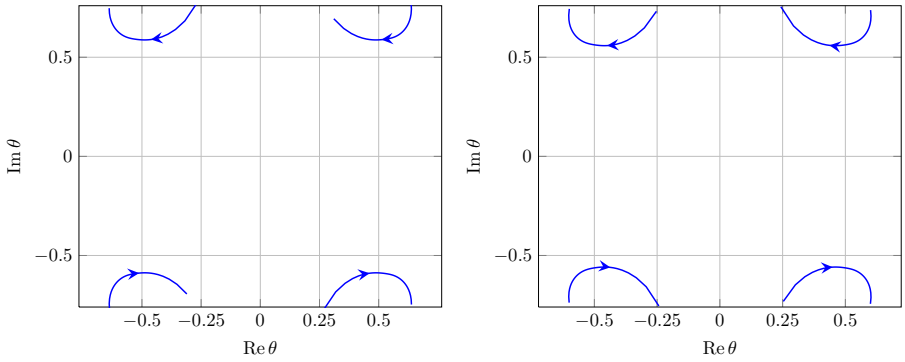

Figure 7.10.: Movement of the solutions $\tilde{Y}_{a,s}(\theta) = -1$ for the path Eq.(7.70). Specifically, we show the results for $\tilde{Y}_{1,2}(\theta)$ (left) and $\tilde{Y}_{3,1}(\theta)$ (right). The solutions $Y_{a,s}(\theta) = -1$ of all other Y-functions do not approach the vicinity of the real axis. The direction of growing φ is indicated by the arrows.

7.7.3. Calculation of the remainder function $R_{7,-+-}$

The fact that we see no crossing solutions means that the Y-system equations at the endpoint of the continuation are just given by the original equations. Since this is the same situation as in the Euclidean regime, we conclude that the remainder function is almost trivial in this Regge region. The only difference stems from the fact that we have followed a non-trivial path in the cross ratios which can give rise to cut contributions in Δ. To be precise, we find

$$\Delta' \cong \Delta + i\frac{\pi}{2}\log\left(\frac{(1-u_{11})(1-u_{12})}{u_{22}u_{31}(1-\tilde{u})}\right) + \text{const.} \tag{7.71}$$

This gives rise to a phase contribution

$$\delta_{7,-+-} = \frac{\pi}{4}\gamma_K \log\left(\frac{1}{(1-\tilde{u})}\frac{1}{\tilde{u}_{22}\tilde{u}_{31}}\right), \tag{7.72}$$

which combines with the otherwise trivial remainder function,

$$e^{R_{7,-+-}+i\delta_{7,-+-}}\Big|_{\text{MRL}} \sim 1. \tag{7.73}$$

7.8. Comparison with weak coupling predictions

We have finished the calculation in all relevant Regge regions. Let us therefore now compare our results to the weak coupling predictions presented in section 7.3. For the regions $P_{7,--+}$ and $P_{7,+--}$ we find full consistency with the weak coupling predictions. The remainder function in these Regge regions has the same structure as the 6-point result presented in chapter 6. Furthermore, the strong coupling analogue of the BFKL eigenvalue shows up with the same value and all phases match perfectly. It should be noted that this is non-trivial, as the contributions to the remainder function have a more complex dependence on the kinematical variables, of which we have twice as many as in the 6-point case. The additional variables also show a non-negligible movement during the

analytic continuation (cf. figure 7.4), which, however, does not lead to a crossing solution and allows us to obtain the same structure as in the 6-point case.

Turning to the region $P_{7,---}$ we faced a new situation with two pairs of crossing solutions and more complicated paths for the cross ratios. Still we are able to confirm the weak coupling prediction that a product of 6-point structures shows up also at strong coupling. Comparing Eq.(7.68) and table 7.1 we see that we do not find the same conformal phase $\delta_{7,---}$. In fact, we find an additional conformally invariant contribution. This, however, is not necessarily a problem, as the Regge cut piece at weak coupling, which is still not fully known, can contain additional phases through prefactors (see e.g. Eq.(4.59) of [137]) or the production vertex C.

In region $P_{7,-+-}$ the weak coupling analysis predicts that all three cuts contribute. Alas, at strong coupling we find no crossing solutions and the remainder function is a pure phase. The origin of this discrepancy is not understood. The strong coupling result looks like there is a cancellation between the three cut pieces we expect, since they all come with the same prefactor e_2 in $\log R_{7,-+-}$ and the long cut is given by the product of the two short cuts. Furthermore, the rotation sense of the u_{1s} is opposite to that of $\tilde{u}$. However, such a cancellation would be difficult to accommodate from the weak coupling perspective, where we expect a sum of terms which exponentiate as we go to strong coupling, not an exponential of a sum. It may well be that the choice of our path is too naive. For example, the right prescription might be to approach the relevant region in a stepwise process $P_{7,+++} \to P_{7,---} \to P_{7,-+-}$. It would certainly be interesting to see whether the crossed solutions found in the transition to the region $P_{7,---}$ cross back over the real axis. Furthermore, this process would test our hypothesis that the transition between Regge regions is defined by the winding numbers and the Gram relations only, and not by details of the path. This interesting question will be explored in future work.

8. Conclusions and outlook

Let us summarise our results. In this thesis we have studied the remainder function of scattering amplitudes in strongly coupled $\mathcal{N} = 4\,\mathrm{SYM}$. As the general prescription in terms of the Y-system is too difficult to solve analytically, we specialised to the multi-Regge limit.

A central result we found was that the non-linear integral equations simplify drastically in this kinematical limit. In fact, all integral contributions can be dropped and the multi-Regge limit is governed by algebraic equations. This simplification is necessary to obtain analytic expressions for the remainder function. We then developed an algorithm for the computation of the remainder function in the multi-Regge limit in various Regge regions with the result that in each region there exists a set of algebraic Bethe ansatz equations which contain all necessary information to calculate the remainder function. The identification of the correct solution of the Bethe ansatz equations, however, requires a numerical analysis.

We applied this algorithm to the 6- and 7-point amplitude and found that the analytic structure predicted from field theory calculations also holds in the strong coupling limit. The results we find have exactly the structure expected from the dispersion relation-like results at weak coupling and suggest that at strong coupling a saddle point dominates the integrals appearing at weak coupling. Remarkably, we find that the universal quantities governing the 6-point case show up in the 7-point case, as well, exactly as predicted by Regge theory. Furthermore, our results suggest that there is a nice dictionary between Regge cut contributions at weak coupling and crossing solutions at strong coupling. For every triplet of variables appearing in the dispersion relation of the Regge cut contribution, we find a pair of crossing solutions and in Regge regions where no cut contributions is present, there are no crossing solutions.

From our results, many interesting new questions emerge: For a better understanding of the connection between Regge cut contributions and crossing solutions, it would be interesting to study the 8-point amplitude. In this case, a Regge cut which is generated from a bound state of three Reggeons appears for the first time. Studying this cut contribution from the strong coupling side would provide the analogue of the new BFKL eigenvalue at strong coupling and is amenable to an analysis very much similar to the cases studies in this thesis. It would be very interesting to see whether this quantity is somehow related to the BFKL eigenvalue we determined in this thesis and if speculations about the strong coupling BFKL eigenvalue for a bound state of n Reggeons can be made. Furthermore, this contribution is still unknown at weak coupling and would serve to show that the difficulty of the computation grows less with the number of gluons at strong coupling as compared to a weak coupling analysis.

We also found a discrepancy of the weak coupling prediction with our strong coupling result for the Regge region $P_{7,-+-}$. This region is more complicated than the other three Regge regions of the 7-point case since it is expected to contain contributions from all three possible Regge cuts. A full analysis at weak coupling is still missing, but on general

grounds one would expect the difference between $P_{7,---}$ and $P_{7,-+-}$ to be given only by a different phase for the production vertex of the central gluon. It may well be that the choice of our path for this region is too naive and it would certainly be interesting to study more sophisticated paths for this region.

As we mentioned before, our result for the 6-point amplitude does not vanish in the collinear limit and we have also identified a potential reason for this discrepancy in the way we obtain our numerical results. Understanding this phenomenon will require new methods as our numerical investigations are not suitable for taking limits, since they are always carried out for finite parameters. This is a very interesting question to investigate as it would open a connection with the Wilson loop OPE programme of [61] from which an all-loop proposal for the universal quantities in the multi-Regge limit emerged recently [131]. Understanding this connection properly might help to introduce $\mathcal{N} = 4$ integrability in the description of the dispersion relation Eq.(3.49), which, in turn, might lead to an understanding for intermediate couplings and for any number of gluons. As our results crucially depend on the existence of a gravity dual and the planar limit, understanding it from a field theory perspective would be very relevant for potential generalisations to less symmetric theories. All this is left for future work.

We hope it has become clear throughout this thesis that the major virtues of the multi-Regge limit lie in the fact that the perturbative expansion is not just an expansion in the coupling constant but that every logarithmic order contains all-loop order information in the coupling constant and therefore probes the structure of the theory at all couplings. Furthermore, the scaling to higher-point amplitudes is accessible, as some of the universal quantities can be lifted to cases with more gluons. This serves to show that the multi-Regge limit is a rich and important kinematical regime which is and will continue to be an essential ingredient in the programme of determining all scattering amplitudes in $\mathcal{N} = 4$ SYM.

A. Acknowledgements

First and foremost, I would like to express my sincere gratitude to my supervisors. I'd like to thank Volker Schomerus for offering me this project, which allowed me to enter the beautiful research area of scattering amplitudes. Furthermore, I thank Volker for his constant help and interest in our project and for his support in sending me to numerous conferences and schools. Likewise, I am thankful to Jochen Bartels who was always available for discussions and explanations and for his continuous interest in the project. The discussions I had with both were always extremely helpful and I could not have hoped for a better supervision. Also, I would like to thank Yasuyuki Hatsuda and Andrey Kormilitzin who often joined our discussions.

Thanks to everyone in the DESY theory string group for discussions and many nice lunch breaks. Furthermore, I thank the amplitudes group of Rutger Boels for the nice seminars, discussions and conference trips. Most of all, thanks to Reinke (although in exile) for the many helpful discussions, collaboration on various unfinished projects (I am sure THIS one is going to work out) and the running trips. I'd like to thank Matthias Kaminski for collaboration and everyone I had the pleasure to meet and discuss physics with at various conferences and schools. I am very grateful to the SFB 676 'Particles, Strings and the Early Universe' for funding me.

Thanks to my office mates Andi, Carlos, Falk, Javier, Marcos and Stefano for the nice working atmosphere. A big thanks to Francisco, Maikel, Marco^2, Paolo, Sara and Stefano for many coffee breaks and evenings out and for making the time in Hamburg so much nicer - *grazie a tutti, seguite le regole.*

Furthermore, I'd like to thank David for discussions, collaboration and many nice hiking trips. Last, but certainly not least, I would like to thank my family, without who my studies would not have been possible, and Anne for her constant support and love and for bearing with me and my moods while I was writing this thesis. This thesis is dedicated to them.

B. Determination of the phases ϕ_s for the 7-point amplitude

In this appendix, we provide the formulas for the constraints on the Y-system parameters in the 7-point case which are left out in the main text in section 4.2.2. As for the formulas presented in the main text, we indicate the desired behaviour of the cross ratio along with the behaviour of the Y-function that is needed and the constraints on the Y-system parameters this entails. For those cross ratios related to a Y-function in the fundamental strip, we easily find:

$$u_{31} \to 0 \implies Y_{2,2}^{[0]} \cong e^{-\sqrt{2}|m_2|\cos\phi_2} \to 0 \qquad \Rightarrow \boxed{\phi_2 \in \left(-\frac{\pi}{2}, \frac{\pi}{2}\right)}$$

$$u_{32} \to 0 \implies Y_{2,1}^{[1]} \cong e^{-\sqrt{2}|m_1|\cos\left(\frac{\pi}{4}-\phi_1\right)} \to 0 \quad \Rightarrow \boxed{\phi_1 \in \left(-\frac{\pi}{4}, \frac{3\pi}{4}\right)}$$

$$u_{22} \to 0 \implies Y_{2,1}^{[-1]} \cong e^{-\sqrt{2}|m_1|\cos\left(\frac{\pi}{4}+\phi_1\right)} \to 0 \Rightarrow \boxed{\phi_1 \in \left(-\frac{3\pi}{4}, \frac{\pi}{4}\right)}$$

Since the remaining cross ratios involve values of the Y-functions outside the fundamental strip we must use the recursion relations Eq.(2.68). This gives:

$$\begin{aligned} u_{21} \to 0 \implies Y_{2,2}^{[-2]} &= \frac{1 + Y_{2,1}^{[-1]}}{Y_{2,2}^{[0]}\left(1+\frac{1}{Y_{3,2}^{[-1]}}\right)\left(1+\frac{1}{Y_{1,2}^{[-1]}}\right)} \\ &\cong \frac{e^{\sqrt{2}|m_2|\cos\phi_2}\left(1+e^{-\sqrt{2}|m_1|\cos\left(\frac{\pi}{4}+\phi_1\right)}\right)}{\left(1+e^{|m_2|\cos\left(\frac{\pi}{4}+\phi_2\right)-C_2}\right)\left(1+e^{|m_2|\cos\left(\frac{\pi}{4}+\phi_2\right)+C_2}\right)} \to 0 \\ &\Rightarrow \boxed{\phi_2 \in (-\pi, 0) \cup \left(\frac{\pi}{2}, \pi\right)} \end{aligned}$$

$$\begin{aligned} u_{11} \to 1 \implies Y_{2,2}^{[2]} &= \frac{1 + Y_{2,1}^{[1]}}{Y_{2,2}^{[0]}\left(1+\frac{1}{Y_{3,2}^{[1]}}\right)\left(1+\frac{1}{Y_{1,2}^{[1]}}\right)} \\ &\cong \frac{e^{\sqrt{2}|m_2|\cos\phi_2}\left(1+e^{-\sqrt{2}|m_1|\cos\left(\frac{\pi}{4}-\phi_1\right)}\right)}{\left(1+e^{|m_2|\cos\left(\frac{\pi}{4}-\phi_2\right)-C_2}\right)\left(1+e^{|m_2|\cos\left(\frac{\pi}{4}-\phi_2\right)+C_2}\right)} \to \infty \\ &\Rightarrow \boxed{\phi_2 \in \left(-\frac{\pi}{2}, 0\right)} \end{aligned}$$

To determine the precise values of ϕ_s in the multi-Regge limit, we look at the finite ratios:

$$\frac{u_{22}}{u_{32}} \to \text{const.} \implies \frac{Y_{2,1}^{[-1]}}{Y_{2,1}^{[1]}} = \frac{e^{-\sqrt{2}|m_1|\cos\left(\frac{\pi}{4}+\phi_1\right)}}{e^{-\sqrt{2}|m_1|\cos\left(\frac{\pi}{4}-\phi_1\right)}} = e^{2|m_1|\sin\phi_1} \to \text{const.} \Rightarrow \boxed{\phi_1 \to 0}$$

$$\frac{u_{21}}{u_{31}} \to \text{const.} \implies \frac{Y_{2,2}^{[-2]}}{Y_{2,2}^{[0]}} = \frac{e^{2\sqrt{2}|m_2|\cos\phi_2}\left(1+e^{-\sqrt{2}|m_1|\cos\left(\frac{\pi}{4}-\phi_1\right)}\right)}{\left(1+e^{|m_2|\cos\left(\frac{\pi}{4}+\phi_2\right)-C_2}\right)\left(1+e^{|m_2|\cos\left(\frac{\pi}{4}+\phi_2\right)+C_2}\right)} \to \text{const.}$$

$$\Rightarrow \boxed{\phi_2 \to -\frac{\pi}{4} \,||\, \phi_2 \to \frac{\pi}{2}}$$

Taking all constraints into account, we see that the phases have to attain the values $\phi_1 \to 0$, $\phi_2 \to -\frac{\pi}{4}$.

C. Residue structure for the large cross ratios in the MRL

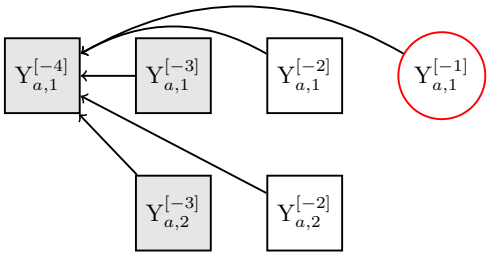

Figure C.1.: Graphical representation of the residue structure of $Y_{a,1}^{[-4]}$, cf. Eq.(C.1). All Y-functions which are not contributing are hidden for simplicity.

A central issue in finding the multi-Regge limit in the Y-system parameters is the residue structure of the Y-functions. In the main text, we concentrated on those Y-functions with a simple residue structure. However, to establish the correct expressions for the $u_{1\sigma}$ we need to understand the residue structures of the grey boxes in the first row of figure 4.2, too.

As a specific example, we present the residue structure of $Y_{2,1}^{[-4]}$ for the $n \geq 7$-amplitude. As in the main text, we start from the equivalent calculation of $\tilde{Y}_{2,1}^{[-4]}$ and consider the equation for $\theta = 0$, which receives no residue contributions. We then move θ towards $-i\pi$. In this process, we cross the lines $\operatorname{Im}\theta = -3i\frac{\pi}{4}, -i\frac{\pi}{2}, -i\frac{\pi}{4}$, as well as $\operatorname{Im}(\theta + i\phi_1 - i\phi_2) = -i\frac{\pi}{2}, -i\frac{\pi}{4}$, on which poles lie. Shifting back to the Y-function, this gives rise to

$$Y_{2,1}^{[-4]} = \epsilon_1^{-\sqrt{2}} \cdot \underbrace{\frac{\left(1 + Y_{2,2}^{[-3]}\right)}{\left(1 + Y_{3,1}^{[-3]}\right)\left(1 + Y_{1,1}^{[-3]}\right)}}_{\text{Residues at } -i\frac{\pi}{4}} \cdot \underbrace{\frac{\left(1 + Y_{3,2}^{[-2]}\right)\left(1 + Y_{1,2}^{[-2]}\right)}{\left(1 + Y_{2,1}^{[-2]}\right)^2}}_{\text{Residues at } -i\frac{\pi}{2}} \cdot \underbrace{\frac{1}{\left(1 + Y_{3,1}^{[-1]}\right)\left(1 + Y_{1,1}^{[-1]}\right)}}_{\text{Residues at } -i\frac{3}{4}\pi} \cdot \tag{C.1}$$

This shows that there is a simple graphical representation of the residue structure of the grey boxes, as well. For our specific example, this is shown in figure C.1 - all Y-functions in the same row and the row below to the right of the function we want to determine can give rise to a residue contribution, with the rightmost Y-functions being those that do not receive any residue contribution themselves. A subtle point is that the Y-functions which

appear in residue contributions can receive residue corrections themselves. In the example given above, $Y_{2,2}^{[-3]}$ would be such a function. However, note that residue contributions always come from Y-functions that are to the right and/or below the Y-function we are interested in. This means that the Y-function with the highest s' that can influence a given Y-function $Y_{a,s}^{[k]}$ with k negative lies on the intersection point of the two diagonals $Y_{a,s+i}^{[k+i]}$ and $Y_{a,j}^{[-j]}$.

D. Kernels and S-matrices

D.1. Kernels

In this appendix we list the explicit expressions for the Y-system kernels $\mathcal{K}_{s,s'}^{a,a'}$ of the rewritten version Eqs.(5.18-5.20) used in the numerics in terms of the kernels of the original Y-system Eqs.(2.64) for the 7-point case. In the following, $s\pm1$ denotes the unique possible choice for s' in a given kernel. Furthermore, if a formula holds for both $a'=1$ and $a'=3$ we just write $a'=2\pm1$.

$$
\begin{aligned}
\mathcal{K}_{s,s}^{1,2\pm1}(\theta,\theta') &= K_1(\theta')\cosh\theta - K_1(\theta-\theta')\\
\mathcal{K}_{s,s}^{1,2}(\theta,\theta') &= K_2(\theta')\cosh\theta - K_2(\theta-\theta')\\
\mathcal{K}_{s,s\pm1}^{1,2}(\theta,\theta') &= -K_1(-\theta'+i\phi_s-i\phi_{s\pm1})\cosh\theta + K_1(\theta-\theta'+i\phi_s-i\phi_{s\pm1})\\
\mathcal{K}_{s,s\pm1}^{1,1}(\theta,\theta') &= \frac{1}{2}\left(K_2(\theta-\theta'+i\phi_s-i\phi_{s\pm1}) - K_2(-\theta'+i\phi_s-i\phi_{s\pm1})\cosh\theta\right)\\
&\quad+\frac{1}{2}(-1)^{s+1}\left(K_3(\theta-\theta'+i\phi_s-i\phi_{s\pm1}) - K_3(-\theta'+i\phi_s-i\phi_{s\pm1})\right)\\
\mathcal{K}_{s,s\pm1}^{1,3}(\theta,\theta') &= \frac{1}{2}\left(K_2(\theta-\theta'+i\phi_s-i\phi_{s\pm1}) - K_2(-\theta'+i\phi_s-i\phi_{s\pm1})\cosh\theta\right)\\
&\quad+\frac{1}{2}(-1)^{s}\left(K_3(\theta-\theta'+i\phi_s-i\phi_{s\pm1}) - K_3(-\theta'+i\phi_s-i\phi_{s\pm1})\right)\\
\mathcal{K}_{s,s}^{2,2\pm1}(\theta,\theta') &= \sqrt{2}K_1(\theta')\cosh\theta - K_2(\theta-\theta')\\
\mathcal{K}_{s,s}^{2,2}(\theta,\theta') &= \sqrt{2}K_2(\theta')\cosh\theta - 2K_1(\theta-\theta')\\
\mathcal{K}_{s,s\pm1}^{2,2}(\theta,\theta') &= -\sqrt{2}K_1(-\theta'+i\phi_s-i\phi_{s\pm1})\cosh\theta + K_2(\theta-\theta'+i\phi_s-i\phi_{s\pm1})\\
\mathcal{K}_{s,s\pm1}^{2,2\pm1}(\theta,\theta') &= -\frac{1}{\sqrt{2}}K_2(-\theta'+i\phi_s-i\phi_{s\pm1})\cosh\theta + K_1(\theta-\theta'+i\phi_s-i\phi_{s\pm1})\\
\mathcal{K}_{s,s}^{3,2\pm1}(\theta,\theta') &= K_1(\theta')\cosh\theta - K_1(\theta-\theta')\\
\mathcal{K}_{s,s}^{3,2}(\theta,\theta') &= K_2(\theta')\cosh\theta - K_2(\theta-\theta')\\
\mathcal{K}_{s,s\pm1}^{3,2}(\theta,\theta') &= -K_1(-\theta'+i\phi_s-i\phi_{s\pm1})\cosh\theta + K_1(\theta-\theta'+i\phi_s-i\phi_{s\pm1})\\
\mathcal{K}_{s,s\pm1}^{3,1}(\theta,\theta') &= \frac{1}{2}\left(K_2(\theta-\theta'+i\phi_s-i\phi_{s\pm1}) - K_2(-\theta'+i\phi_s-i\phi_{s\pm1})\cosh\theta\right)\\
&\quad+\frac{1}{2}(-1)^{s}\left(K_3(\theta-\theta'+i\phi_s-i\phi_{s\pm1}) - K_3(-\theta'+i\phi_s-i\phi_{s\pm1})\right)\\
\mathcal{K}_{s,s\pm1}^{3,3}(\theta,\theta') &= \frac{1}{2}\left(K_2(\theta-\theta'+i\phi_s-i\phi_{s\pm1}) - K_2(-\theta'+i\phi_s-i\phi_{s\pm1})\cosh\theta\right)\\
&\quad+\frac{1}{2}(-1)^{s+1}\left(K_3(\theta-\theta'+i\phi_s-i\phi_{s\pm1}) - K_3(-\theta'+i\phi_s-i\phi_{s\pm1})\right)
\end{aligned}
$$

D.2. S-matrices

Corresponding to the new set of kernels written out above, we also have a new set of S-matrices. Since the kernels presented above are linear combinations of the original kernels, possibly with prefactors, the S-matrices too should be constructable from the original S-matrices Eqs.(5.6). Recall the definition of the S-matrices,

$$-2\pi i K(\theta,\theta') =: \partial_{\theta'} \log S(\theta,\theta'). \tag{D.1}$$

Using this definition, we see that for a kernel of the schematic form

$$K(\theta,\theta') = f(\theta)K_1(\theta,\theta') + g(\theta)K_2(\theta,\theta') + \dots \tag{D.2}$$

the S-matrix is given by

$$S(\theta,\theta') = S_1(\theta,\theta')^{f(\theta)} \cdot S_2(\theta,\theta')^{g(\theta)} \cdot \dots \tag{D.3}$$

As explicit examples, we write out the S-matrices for a crossed solution of $\tilde{\mathrm{Y}}_{3,1}$ in the rewritten Y-system:

$$S_{1,1}^{2,3}(\theta,\theta') = S_1(\theta')^{\sqrt{2}\cosh(\theta)} S_2(\theta-\theta') \tag{D.4}$$

$$S_{1,1}^{2\pm1,3}(\theta,\theta') = S_1(\theta')^{\cosh(\theta)} S_1(\theta-\theta') \tag{D.5}$$

$$S_{2,1}^{1,3}(\theta,\theta') = \frac{S_2(-\theta'+i\phi_2-i\phi_1)^{\frac{1}{2}\cosh(\theta)} S_3(-\theta'+i\phi_2-i\phi_1)^{\frac{1}{2}}}{S_2(\theta-\theta'+i\phi_2-i\phi_1)^{\frac{1}{2}} S_3(\theta-\theta'+i\phi_2-i\phi_1)^{\frac{1}{2}}} \tag{D.6}$$

$$S_{2,1}^{2,3}(\theta,\theta') = S_2(\theta'-i\phi_2+i\phi_1)^{-\frac{1}{\sqrt{2}}\cosh(\theta)} S_1(\theta-\theta'+i\phi_2-i\phi_1)^{-1} \tag{D.7}$$

$$S_{2,1}^{3,3}(\theta,\theta') = \frac{S_2(-\theta'+i\phi_2-i\phi_1)^{\frac{1}{2}\cosh(\theta)} S_3(\theta-\theta'+i\phi_2-i\phi_1)^{\frac{1}{2}}}{S_2(\theta-\theta'+i\phi_2-i\phi_1)^{\frac{1}{2}} S_3(-\theta'+i\phi_2-i\phi_1)^{\frac{1}{2}}} \tag{D.8}$$

Since the remaining expressions are lengthy and can be easily obtained from the expressions for the kernels in section D.1, we refrain from spelling out the other S-matrices.

E. Conformal Gram relations

In this appendix we describe the construction of the conformal Gram relations. Gram relations are not only available for conformal theories, but appear already on the level of the Mandelstam invariants. Since the latter are simpler, we describe them first. We start from a very simple, but powerful fact: there are at most four linearly independent vectors in four dimensions. Choosing $p_1,\ldots,\ p_4$ to be a basis, this means that for a n-particle amplitude we have $n-4$ relations

$$\sum_{i}^{1,\ldots,4,k} c_{ki}p_i = 0 \tag{E.1}$$

for some non-vanishing coefficients c_{ki}. Multiplying Eq.(E.1) with p_j, we obtain a linear relation between the Lorentz invariants p_ip_j. Choosing $j = 1,\ldots,4,l$ for $l > 4$ we obtain a set of five linear relations for the five variables c_{ki}. This set of equations has a non-trivial solution for the c_{ki} only if the determinant of the coefficient matrix

$$\begin{vmatrix} 0 & p_1p_2 & p_1p_3 & p_1p_4 & p_1p_k \\ p_2p_1 & 0 & p_2p_3 & p_2p_4 & p_2p_k \\ p_3p_1 & p_3p_2 & 0 & p_3p_4 & p_3p_k \\ p_4p_1 & p_4p_2 & p_4p_3 & 0 & p_4p_k \\ p_lp_1 & p_lp_2 & p_lp_3 & p_lp_4 & p_lp_k \end{vmatrix} = 0. \tag{E.2}$$

The zeros along the diagonal are a consequence of the fact that we are scattering gluons. Since Eq.(E.2) is symmetric in l and k we get $\frac{1}{2}(n-4)(n-5)$ relations, which, together with momentum conservation[1], reduce the number of independent Lorentz invariants p_ip_j to

$$\frac{1}{2}n(n-1) - n - \frac{1}{2}(n-4)(n-5) = 3n-10, \tag{E.3}$$

which indeed is the correct number of independent variables.

We now follow a similar argument to find the Gram relations for the conformal cross ratios. This discussion follows [143]. The essential trick is to lift the four-dimensional momenta to six-dimensional objects, which in light-cone coordinates are given in terms of the dual variables x_i (cf. Eq.(3.1)) by

$$X_i^A := (1, x_i^2, x_i^\mu). \tag{E.4}$$

The four-dimensional dual conformal symmetry group $SO(2,4)$ simply acts linearly as a rotation symmetry on these objects. For the X_i^A we can now repeat our above argument

[1] Momentum conservation counts as n relations below because we have a relation $p_ip_n = -\sum_{k\neq n} p_ip_k$ for every i.

by saying that at most six vectors can be linearly independent. Choosing $X_1, \ldots, X_6$ as a basis, this leads to relations

$$\sum_i^{1,\ldots,6,k} c_{ki} X_i = 0. \tag{E.5}$$

Observing that

$$X_i^2 = 2(1 \cdot x_i^2) - 2x_i^\mu x_{i\mu} = 0, \tag{E.6}$$

as well as

$$X_i \cdot X_j = x_j^2 + x_i^2 - 2x_i \cdot x_j = (x_i - x_j)^2 = x_{i,j}^2, \tag{E.7}$$

this translates into the statement that the determinant of the matrices

$$\begin{pmatrix} 0 & x_{1,2}^2 & x_{1,3}^2 & x_{1,4}^2 & x_{1,5}^2 & x_{1,6}^2 & x_{1,k}^2 \\ x_{1,2}^2 & 0 & x_{2,3}^2 & x_{2,4}^2 & x_{2,5}^2 & x_{2,6}^2 & x_{2,k}^2 \\ x_{1,3}^2 & x_{2,3}^2 & 0 & x_{3,4}^2 & x_{3,5}^2 & x_{3,6}^2 & x_{3,k}^2 \\ x_{1,4}^2 & x_{2,4}^2 & x_{3,4}^2 & 0 & x_{4,5}^2 & x_{4,6}^2 & x_{4,k}^2 \\ x_{1,5}^2 & x_{2,5}^2 & x_{3,5}^2 & x_{4,5}^2 & 0 & x_{5,6}^2 & x_{5,k}^2 \\ x_{1,6}^2 & x_{2,6}^2 & x_{3,6}^2 & x_{4,6}^2 & x_{5,6}^2 & 0 & x_{6,k}^2 \\ x_{1,l}^2 & x_{2,l}^2 & x_{3,l}^2 & x_{4,l}^2 & x_{5,l}^2 & x_{6,l}^2 & x_{k,l}^2 \end{pmatrix} \tag{E.8}$$

has to vanish, for a total of $\frac{1}{2}(n-5)(n-6)$ relations among the $x_{i,j}^2$. These relations are invariant under dual conformal symmetry by construction and can easily be converted into expressions involving only the cross ratios. For the 7-point case, the unique Gram relation in arbitrary kinematics is given by

$$a\tilde{u}^2 + b\tilde{u} + c = 0 \tag{E.9}$$

with lengthy coefficients

$$a = u_{11}u_{12}\left(-1 + u_{12}u_{21} + u_{11}u_{32}\right), \tag{E.10}$$

$$\begin{aligned} b = &-\frac{1}{2} + u_{11} + \frac{1}{2}u_{11}u_{12} + u_{12}u_{21} - 2u_{11}u_{12}u_{21} - u_{12}^2u_{21} + u_{22} - u_{11}u_{22} \\ &- 2u_{12}u_{21}u_{22} + u_{11}u_{12}u_{21}u_{22} + u_{12}^2u_{21}^2u_{22} - \frac{1}{2}u_{22}u_{31} + u_{12}u_{21}u_{22}u_{31} \\ &+ \frac{1}{2}u_{11}u_{12}u_{21}u_{32} + \frac{1}{2}u_{11}u_{12}u_{21}u_{22}u_{31}u_{32} + (\text{target} \leftrightarrow \text{projectile}), \end{aligned} \tag{E.11}$$

$$\begin{aligned} c = &\frac{1}{2} - u_{11} - u_{21} + u_{11}u_{21} + u_{12}u_{21} - u_{22} + u_{11}u_{22} + u_{21}u_{22} - u_{11}u_{21}u_{22} \\ &+ u_{12}u_{21}u_{22} - u_{12}u_{21}^2u_{22} + \frac{1}{2}u_{22}u_{31} + u_{21}u_{22}u_{31} - 2u_{12}u_{21}u_{22}u_{31} \\ &- u_{21}u_{22}^2u_{31} + u_{12}u_{21}^2u_{22}^2u_{31} + \frac{1}{2}u_{21}u_{32} - u_{11}u_{21}u_{32} - u_{21}u_{22}u_{31}u_{32} \\ &+ u_{11}u_{21}u_{22}u_{31}u_{32} + \frac{1}{2}u_{21}u_{22}^2u_{31}^2u_{32} + (\text{target} \leftrightarrow \text{projectile}), \end{aligned} \tag{E.12}$$

where (target $\leftrightarrow$ projectile) means that the same expression after applying a target-projectile transformation, including the constant terms, should be added.

F. The remainder function $R_{7,+--}$

In this appendix, we briefly spell out the results for the region $P_{7,+--}$. Since practically everything works as for the region $P_{7,--+}$, we will be brief. The path of continuation for the region $P_{7,+--}$ is defined via

$$\begin{aligned} &u_{11}(\varphi) = u_{11}, && u_{21}(\varphi) = e^{i\varphi}u_{21}, && u_{31}(\varphi) = e^{-i\varphi}u_{31}, \\ &u_{12}(\varphi) = e^{-2i\varphi}u_{12}, && u_{22}(\varphi) = u_{22}, && u_{32}(\varphi) = u_{32}, \qquad \tilde{u}(\varphi) = \tilde{u}. \end{aligned} \tag{F.1}$$

The numerical solution for the driving terms is shown in figure F.1. By comparison with figure 7.2 for the path $P_{7,--+}$, we see that the two triplets have changed their roles. From this observation it is clear that the crossing solutions will appear in the other triplet, as well. Indeed, we find a pair of crossing solutions for the function $\tilde{\mathrm{Y}}_{3,1}$ which approaches $\pm i\frac{\pi}{4}$, as shown in figure F.2. Furthermore, a pair of solutions of $\tilde{\mathrm{Y}}_{2,1}$ approaches the origin, which do not contribute, as before. We can then spell out the equations at the endpoint of the analytic continuation, after dropping the integrals:

$$\mathrm{Y}'_{1,s}(\theta) = \left(e^{-|m_s|'\cosh(\theta - i\phi'_s) - C'_s}\right) \frac{S^{1,3}_{s,1}(\theta + i\frac{\pi}{4} - i\phi'_1)}{S^{1,3}_{s,1}(\theta - i\frac{\pi}{4} - i\phi'_1)}, \tag{F.2}$$

$$\mathrm{Y}'_{2,s}(\theta) = \left(e^{-\sqrt{2}|m_s|'\cosh(\theta - i\phi'_s)}\right) \frac{S^{2,3}_{s,1}(\theta + i\frac{\pi}{4} - i\phi'_1)}{S^{2,3}_{s,1}(\theta - i\frac{\pi}{4} - i\phi'_1)}, \tag{F.3}$$

$$\mathrm{Y}'_{3,s}(\theta) = \left(e^{-|m_s|'\cosh(\theta - i\phi'_s) + C'_s}\right) \frac{S^{3,3}_{s,1}(\theta + i\frac{\pi}{4} - i\phi'_1)}{S^{3,3}_{s,1}(\theta - i\frac{\pi}{4} - i\phi'_1)}, \tag{F.4}$$

Using these equations, we determine the cross ratios and find

$$\begin{aligned} &u'_{11} = 1 + \varepsilon'_2\left(w'_2 + \frac{1}{\gamma w'_2} + 2\frac{1}{\sqrt{-\gamma}}\sinh C'_2\right), \quad u'_{21} = -w'_2\varepsilon'_2, \quad u'_{31} = -\frac{1}{\gamma}\frac{\varepsilon'_2}{w'_2}, \\ &u'_{12} = 1 - \gamma\varepsilon'_1\left(w'_1 + \frac{1}{w'_1} - 2\cosh C'_1\right), \qquad u'_{22} = \gamma w'_1\varepsilon'_1, \quad u'_{32} = \gamma\frac{\varepsilon'_1}{w'_1}. \end{aligned} \tag{F.5}$$

Setting $u'_{21} = -u_{21}$, $u'_{31} = -u_{31}$ and $u'_{as} = u_{as}$ for the remaining cross ratios we find

$$\begin{aligned} &\varepsilon'_1 = \frac{1}{\gamma}\varepsilon_1, \quad w'_1 = w_1, \qquad \cosh C'_1 = -\cosh C_1, \\ &\varepsilon'_2 = \sqrt{\gamma}\varepsilon_2, \quad w'_2 = \frac{1}{\sqrt{\gamma}}w_2, \quad \cosh C'_2 = \sqrt{1 - \left(w_2 + \frac{1}{w_2} + \cosh C_2\right)^2} \end{aligned} \tag{F.6}$$

By comparison with the corresponding equations for the path $P_{7,--+}$ in Eqs.(7.27,7.28), we see that the results are related by target-projectile symmetry. Since the terms appearing

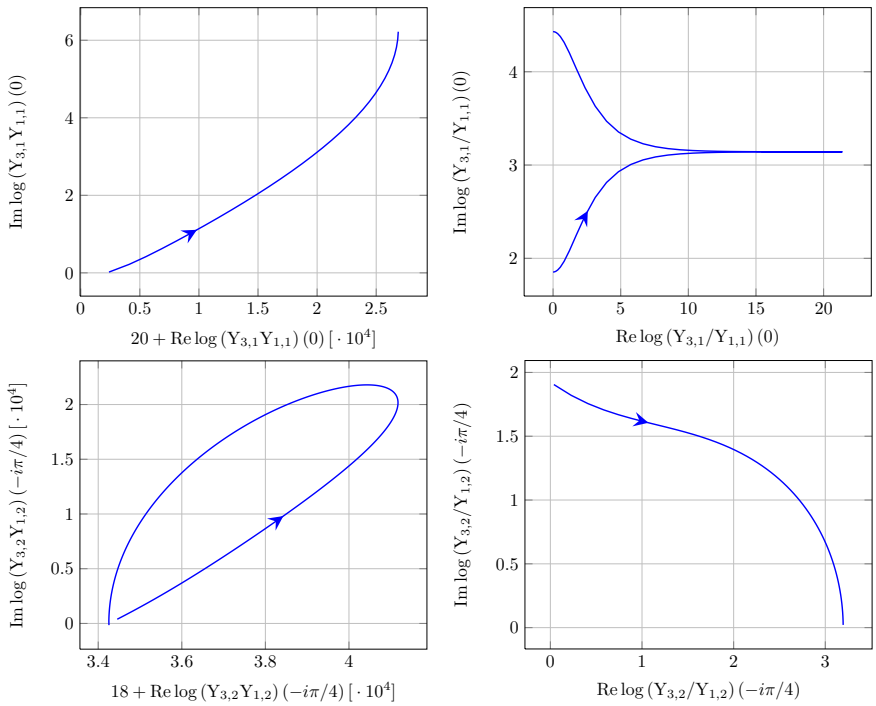

Figure F.1.: Paths of the driving terms during the analytic continuation for the path Eq.(F.1). Note that some axes have been rescaled and shifted. The direction of growing φ is indicated by the arrows. The plots were generated for the specific choice $|m_1| = 10$, $|m_2| = 9$, $C_1 = \operatorname{arccosh}\left(\frac{3}{5}\right)$, $C_2 = \operatorname{arccosh}\left(\frac{4}{7}\right)$ at the starting point.

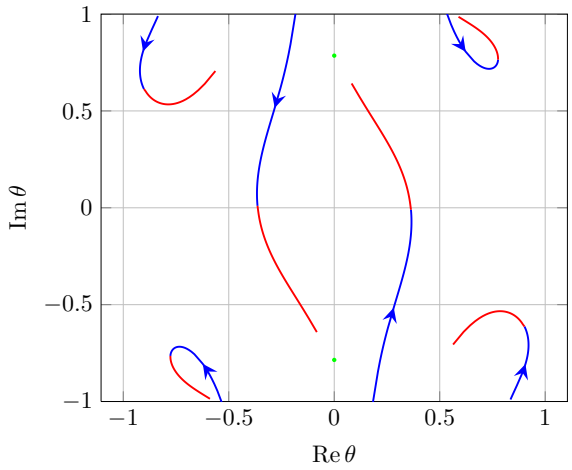

Figure F.2.: Movement of the solutions to $\tilde{\mathrm{Y}}_{3,1}(\theta) = -1$ during the continuation Eq.(F.1). We find one pair of crossing solutions. The direction of movement is indicated by arrows on the plot. For convenience, we change the colour when the pair of solutions crosses the real axis.

in the remainder function are all invariant under this symmetry, the rest of the calculation is exactly the same as for the path $P_{7,--+}$ and we can immediately conclude that

$$e^{\mathrm{R}_{7,+--}+i\delta_{7,+--}}\Big|_{\mathrm{MRL}} \sim \left(-(1-u_{12})\sqrt{\tilde{u}_{22}\tilde{u}_{32}}\right)^{\frac{\sqrt{\lambda}}{2\pi}e_2} \tag{F.7}$$

where

$$\delta_{7,+--} = \frac{\sqrt{\lambda}}{4}\log\left(\sqrt{\tilde{u}_{22}\tilde{u}_{32}}\right) = \frac{\pi}{4}\gamma_K \log\left(\sqrt{\tilde{u}_{22}\tilde{u}_{32}}\right). \tag{F.8}$$

G. Zusammenfassung

Zusammenfassung

Die vorliegende Arbeit befasst sich mit der analytischen Struktur von Streuamplituden in stark gekoppelter $\mathcal{N} = 4$ super Yang-Mills-Theorie (kurz $\mathcal{N} = 4\,\mathrm{SYM}$) im multi-Regge Limes. Dank der AdS/CFT-Korrespondenz können Observablen in stark gekoppelter $\mathcal{N} = 4\,\mathrm{SYM}$ durch duale Rechnungen in einer schwach gekoppelten, und daher mit normaler Störungstheorie beschreibbaren, Stringtheorie auf einer $\mathrm{AdS}_5 \times \mathrm{S}^5$-Geometrie berechnet werden. Insbesondere entspricht die Berechnung der führenden Ordnung der n-Gluon Amplitude in $\mathcal{N} = 4\,\mathrm{SYM}$ bei starker Kopplung so der Berechnung einer Minimalfläche in AdS_5, wobei die Fläche auf der Aneinanderreihung der Gluonimpulse, und daher auf einer lichtartigen Kurve, enden muss. Die Berechnung der Minimalfläche kann auf die Lösung eines Satzes von nichtlinearen, gekoppelten Integralgleichungen zurückgeführt werden. Diese Gleichungen haben jedoch keine analytische Lösung in allgemeiner Kinematik. Wir untersuchen sie in dieser Arbeit daher im multi-Regge Limes, der n-Teilchen Verallgemeinerung des Regge-Limes. Dieser Limes ist besonders relevant, da selbst in der Beschreibung von Streuamplituden in schwach gekoppelter $\mathcal{N} = 4\,\mathrm{SYM}$ in diesem Limes eine bestimmte Klasse von Feynman-Diagrammen resummiert werden muss. Diese Beschreibung organisiert sich in Ordnungen von Logarithmen der im Streuprozess vorhandenen Energie. Jede Ordnung in Logarithmen enthält dabei Terme aus allen Ordnungen in der Kopplungskonstante und damit auch spezifische Informationen über das Regime starker Kopplung der Theorie. In dieser Arbeit untersuchen wir daher die Frage, inwiefern die Struktur der Streuamplitude im multi-Regge Limes erhalten bleibt, wenn wir in den Limes starker Kopplung gehen. Wir zeigen, dass sich die Gleichungen, die die Minimalfläche beschreiben, im multi-Regge Limes für eine beliebige Anzahl von Gluonen stark vereinfachen, was eine analytische Auswertung der Streuamplituden ermöglicht. Wir entwickeln einen Algorithmus zur Berechnung von Streuamplituden im multi-Regge Limes und wenden diesen auf die 6- und 7-Gluon Amplitude an. Unsere Ergebnisse zeigen, dass die von Regge-Theorie vorhergesagte Faktorisierung der Amplitude für die betrachteten Fälle auch bei starker Kopplung gilt.

Summary

This thesis concerns itself with the analytic structure of scattering amplitudes in strongly coupled $\mathcal{N} = 4$ super Yang-Mills theory (abbreviated $\mathcal{N} = 4\,\mathrm{SYM}$) in the multi-Regge limit. Through the AdS/CFT-correspondence observables in strongly coupled $\mathcal{N} = 4\,\mathrm{SYM}$ are accessible via dual calculations in a weakly coupled string theory on an $\mathrm{AdS}_5 \times \mathrm{S}^5$-geometry, in which observables can be calculated using standard perturbation theory. In particular, the calculation of the leading order of the n-gluon amplitude in $\mathcal{N} = 4\,\mathrm{SYM}$ at strong coupling corresponds to the calculation of a minimal surface embedded into AdS_5. This surface ends on the concatenation of the gluon momenta, which is a light-like curve. The calculation of the minimal surface area can be reduced to finding the solution of a set of non-linear, coupled integral equations, which have no analytic solution in arbitrary kinematics. In this thesis, we therefore specialise to the multi-Regge limit, the n-particle generalisation of the Regge limit. This limit is especially interesting as even in the description of scattering amplitudes in weakly coupled $\mathcal{N} = 4\,\mathrm{SYM}$ in this limit a certain set of Feynman diagrams has to be resummed. This description organises itself into orders of logarithms of the energy involved in the scattering process. In this expansion each order in logarithms includes terms from every order in the coupling constant and therefore contains information about the strong coupling sector of the theory, albeit in a very specific way. This raises the central question of this thesis, which is how much of the analytic structure of the scattering amplitudes in the multi-Regge limit is preserved as we go to the strong coupling regime. We show that the equations governing the area of the minimal surface simplify drastically in the multi-Regge limit, which allows us to obtain analytic results for the scattering amplitudes. We develop an algorithm for the calculation of scattering amplitudes in the multi-Regge limit and apply it to the special cases of the 6- and 7-gluon amplitude. Our results show that for the cases under study the factorisation of the amplitude as predicted by Regge theory is also preserved in the strong coupling limit.

This thesis is based on the following publications:

- J. Bartels, V. Schomerus and M. Sprenger, *Heptagon Amplitude in the Multi-Regge Regime*, arXiv:1405.3658, submitted to JHEP.
- J. Bartels, J. Kotanski, V. Schomerus and M. Sprenger, *The Excited Hexagon Reloaded*, arXiv:1311.1512, submitted to JHEP as erratum to JHEP 1101 (2011) 069.
- J. Bartels, V. Schomerus and M. Sprenger, *Multi-Regge Limit of the n-Gluon Bubble Ansatz*, JHEP 1211 (2012) 145.

Bibliography

[1] **ATLAS** Collaboration, G. Aad et al., *Observation of a new particle in the search for the Standard Model Higgs boson with the ATLAS detector at the LHC*, *Phys.Lett.* **B716** (2012) 1–29, [arXiv:1207.7214].

[2] **CMS** Collaboration, S. Chatrchyan et al., *Observation of a new boson at a mass of* 125 *GeV with the CMS experiment at the LHC*, *Phys.Lett.* **B716** (2012) 30–61, [arXiv:1207.7235].

[3] S. J. Parke and T. Taylor, *An Amplitude for n Gluon Scattering*, *Phys.Rev.Lett.* **56** (1986) 2459.

[4] H. Elvang and Y.-t. Huang, *Scattering Amplitudes*, arXiv:1308.1697.

[5] N. Gromov, V. Kazakov, and P. Vieira, *Exact Spectrum of Anomalous Dimensions of Planar $N = 4$ Supersymmetric Yang-Mills Theory*, *Phys.Rev.Lett.* **103** (2009) 131601, [arXiv:0901.3753].

[6] N. Gromov, V. Kazakov, A. Kozak, and P. Vieira, *Exact Spectrum of Anomalous Dimensions of Planar $N = 4$ Supersymmetric Yang-Mills Theory: TBA and excited states*, *Lett.Math.Phys.* **91** (2010) 265–287, [arXiv:0902.4458].

[7] D. Bombardelli, D. Fioravanti, and R. Tateo, *Thermodynamic Bethe Ansatz for planar AdS/CFT: A Proposal*, *J.Phys.* **A42** (2009) 375401, [arXiv:0902.3930].

[8] G. Arutyunov and S. Frolov, *Thermodynamic Bethe Ansatz for the $AdS_5 \times S^5$ Mirror Model*, *JHEP* **0905** (2009) 068, [arXiv:0903.0141].

[9] N. Gromov, F. Levkovich-Maslyuk, G. Sizov, and S. Valatka, *Quantum Spectral Curve at Work: From Small Spin to Strong Coupling in $\mathcal{N} = 4$ SYM*, arXiv:1402.0871.

[10] N. Gromov, V. Kazakov, S. Leurent, and D. Volin, *Quantum spectral curve for arbitrary state/operator in AdS_5/CFT_4*, arXiv:1405.4857.

[11] W. van Neerven, *Infrared Behavior of On-shell Form-factors in a $N = 4$ Supersymmetric Yang-Mills Field Theory*, *Z.Phys.* **C30** (1986) 595.

[12] A. Brandhuber, B. Spence, G. Travaglini, and G. Yang, *Form Factors in $\mathcal{N} = 4$ Super Yang-Mills and Periodic Wilson Loops*, *JHEP* **1101** (2011) 134, [arXiv:1011.1899].

[13] L. Bork, D. Kazakov, and G. Vartanov, *On form factors in $\mathcal{N} = 4$ SYM*, *JHEP* **1102** (2011) 063, [arXiv:1011.2440].

[14] L. Bork, D. Kazakov, and G. Vartanov, *On MHV Form Factors in Superspace for $\mathcal{N} = 4$ SYM Theory*, *JHEP* **1110** (2011) 133, [arXiv:1107.5551].

[15] A. Brandhuber, O. Gurdogan, R. Mooney, G. Travaglini, and G. Yang, *Harmony of Super Form Factors*, *JHEP* **1110** (2011) 046, [arXiv:1107.5067].

[16] J. M. Henn, S. Moch, and S. G. Naculich, *Form factors and scattering amplitudes in $\mathcal{N} = 4$ SYM in dimensional and massive regularizations*, *JHEP* **1112** (2011) 024, [arXiv:1109.5057].

[17] T. Gehrmann, J. M. Henn, and T. Huber, *The three-loop form factor in $\mathcal{N} = 4$ super Yang-Mills*, *JHEP* **1203** (2012) 101, [arXiv:1112.4524].

[18] A. Brandhuber, G. Travaglini, and G. Yang, *Analytic two-loop form factors in $\mathcal{N} = 4$ SYM*, *JHEP* **1205** (2012) 082, [arXiv:1201.4170].

[19] R. H. Boels, B. A. Kniehl, O. V. Tarasov, and G. Yang, *Color-kinematic Duality for Form Factors*, *JHEP* **1302** (2013) 063, [arXiv:1211.7028].

[20] B. Penante, B. Spence, G. Travaglini, and C. Wen, *On super form factors of half-BPS operators in $\mathcal{N} = 4$ super Yang-Mills*, arXiv:1402.1300.

[21] Z. Bern, L. J. Dixon, and V. A. Smirnov, *Iteration of planar amplitudes in maximally supersymmetric Yang-Mills theory at three loops and beyond*, *Phys.Rev.* **D72** (2005) 085001, [hep-th/0505205].

[22] N. Beisert, B. Eden, and M. Staudacher, *Transcendentality and Crossing*, *J.Stat.Mech.* **0701** (2007) P01021, [hep-th/0610251].

[23] J. Drummond, J. Henn, G. Korchemsky, and E. Sokatchev, *The hexagon Wilson loop and the BDS ansatz for the six-gluon amplitude*, *Phys.Lett.* **B662** (2008) 456–460, [arXiv:0712.4138].

[24] L. F. Alday and J. Maldacena, *Comments on gluon scattering amplitudes via AdS/CFT*, *JHEP* **0711** (2007) 068, [arXiv:0710.1060].

[25] J. Bartels, L. Lipatov, and A. Sabio Vera, *BFKL Pomeron, Reggeized gluons and Bern-Dixon-Smirnov amplitudes*, *Phys.Rev.* **D80** (2009) 045002, [arXiv:0802.2065].

[26] J. Drummond, J. Henn, V. Smirnov, and E. Sokatchev, *Magic identities for conformal four-point integrals*, *JHEP* **0701** (2007) 064, [hep-th/0607160].

[27] L. F. Alday and J. Maldacena, *Gluon scattering amplitudes at strong coupling*, *JHEP* **0706** (2007) 064, [arXiv:0705.0303].

[28] J. Drummond, J. Henn, G. Korchemsky, and E. Sokatchev, *Conformal Ward identities for Wilson loops and a test of the duality with gluon amplitudes*, *Nucl.Phys.* **B826** (2010) 337–364, [arXiv:0712.1223].

[29] V. Del Duca, C. Duhr, and V. A. Smirnov, *An Analytic Result for the Two-Loop Hexagon Wilson Loop in $\mathcal{N} = 4$ SYM*, *JHEP* **1003** (2010) 099, [arXiv:0911.5332].

[30] L. J. Dixon, J. M. Drummond, M. von Hippel, and J. Pennington, *Hexagon functions and the three-loop remainder function*, *JHEP* **1312** (2013) 049, [arXiv:1308.2276].

[31] L. J. Dixon, J. M. Drummond, C. Duhr, and J. Pennington, *The four-loop remainder function and multi-Regge behavior at NNLLA in planar $\mathcal{N} = 4$ super-Yang-Mills theory*, arXiv:1402.3300.

[32] Z. Bern, J. Carrasco, and H. Johansson, *New Relations for Gauge-Theory Amplitudes*, *Phys.Rev.* **D78** (2008) 085011, [arXiv:0805.3993].

[33] Z. Bern, T. Dennen, Y.-t. Huang, and M. Kiermaier, *Gravity as the Square of Gauge Theory*, *Phys.Rev.* **D82** (2010) 065003, [arXiv:1004.0693].

[34] R. H. Boels, R. S. Isermann, R. Monteiro, and D. O'Connell, *Colour-Kinematics Duality for One-Loop Rational Amplitudes*, *JHEP* **1304** (2013) 107, [arXiv:1301.4165].

[35] N. E. J. Bjerrum-Bohr, T. Dennen, R. Monteiro, and D. O'Connell, *Integrand Oxidation and One-Loop Colour-Dual Numerators in N=4 Gauge Theory*, *JHEP* **1307** (2013) 092, [arXiv:1303.2913].

[36] R. H. Boels and R. S. Isermann, *On powercounting in perturbative quantum gravity theories through color-kinematic duality*, *JHEP* **1306** (2013) 017, [arXiv:1212.3473].

[37] Z. Bern, J. Carrasco, L. J. Dixon, H. Johansson, and R. Roiban, *The Ultraviolet Behavior of $\mathcal{N} = 8$ Supergravity at Four Loops*, *Phys.Rev.Lett.* **103** (2009) 081301, [arXiv:0905.2326].

[38] Z. Bern, J. Carrasco, L. Dixon, H. Johansson, and R. Roiban, *Simplifying Multiloop Integrands and Ultraviolet Divergences of Gauge Theory and Gravity Amplitudes*, *Phys.Rev.* **D85** (2012) 105014, [arXiv:1201.5366].

[39] Z. Bern, J. Carrasco, H. Johansson, and R. Roiban, *The Five-Loop Four-Point Amplitude of $\mathcal{N} = 4$ super-Yang-Mills Theory*, *Phys.Rev.Lett.* **109** (2012) 241602, [arXiv:1207.6666].

[40] J. M. Maldacena, *The Large N limit of superconformal field theories and supergravity*, *Adv.Theor.Math.Phys.* **2** (1998) 231–252, [hep-th/9711200].

[41] L. F. Alday and J. Maldacena, *Minimal surfaces in AdS and the eight-gluon scattering amplitude at strong coupling*, arXiv:0903.4707.

[42] L. F. Alday and J. Maldacena, *Null polygonal Wilson loops and minimal surfaces in Anti-de-Sitter space*, *JHEP* **0911** (2009) 082, [arXiv:0904.0663].

[43] L. F. Alday, D. Gaiotto, and J. Maldacena, *Thermodynamic Bubble Ansatz*, *JHEP* **1109** (2009) 032, [arXiv:0911.4708].

[44] L. F. Alday, J. Maldacena, A. Sever, and P. Vieira, *Y-system for Scattering Amplitudes*, *J.Phys.* **A43** (2010) 485401, [arXiv:1002.2459].

[45] I. Bena, J. Polchinski, and R. Roiban, *Hidden symmetries of the $AdS_5 \times S^5$ superstring*, *Phys.Rev.* **D69** (2004) 046002, [hep-th/0305116].

[46] J. Maldacena and A. Zhiboedov, *Form factors at strong coupling via a Y-system*, *JHEP* **1011** (2010) 104, [arXiv:1009.1139].

[47] Z. Gao and G. Yang, *Y-system for form factors at strong coupling in AdS_5 and with multi-operator insertions in AdS_3*, *JHEP* **1306** (2013) 105, [arXiv:1303.2668].

[48] O. Aharony, O. Bergman, D. L. Jafferis, and J. Maldacena, *$\mathcal{N} = 6$ superconformal Chern-Simons-matter theories, M2-branes and their gravity duals*, *JHEP* **0810** (2008) 091, [arXiv:0806.1218].

[49] E. O Colgain, *Fermionic T-duality: A snapshot review*, *Int.J.Mod.Phys.* **A27** (2012) 1230032, [arXiv:1210.5588].

[50] P. Heslop and V. V. Khoze, *Analytic Results for MHV Wilson Loops*, *JHEP* **1011** (2010) 035, [arXiv:1007.1805].

[51] T. Goddard, P. Heslop, and V. V. Khoze, *Uplifting Amplitudes in Special Kinematics*, *JHEP* **1210** (2012) 041, [arXiv:1205.3448].

[52] M. A. C. Torres, *Cluster algebras in scattering amplitudes with special $2D$ kinematics*, arXiv:1310.6906.

[53] Y. Hatsuda, K. Ito, K. Sakai, and Y. Satoh, *Six-point gluon scattering amplitudes from Z_4-symmetric integrable model*, *JHEP* **1009** (2010) 064, [arXiv:1005.4487].

[54] Y. Hatsuda, K. Ito, K. Sakai, and Y. Satoh, *g-functions and gluon scattering amplitudes at strong coupling*, *JHEP* **1104** (2011) 100, [arXiv:1102.2477].

[55] Y. Hatsuda, K. Ito, and Y. Satoh, *T-functions and multi-gluon scattering amplitudes*, *JHEP* **1202** (2012) 003, [arXiv:1109.5564].

[56] Y. Hatsuda, K. Ito, and Y. Satoh, *Null-polygonal minimal surfaces in AdS_4 from perturbed W minimal models*, *JHEP* **1302** (2013) 067, [arXiv:1211.6225].

[57] L. F. Alday, D. Gaiotto, J. Maldacena, A. Sever, and P. Vieira, *An Operator Product Expansion for Polygonal null Wilson Loops*, *JHEP* **1104** (2010) 088, [arXiv:1006.2788].

[58] D. Gaiotto, J. Maldacena, A. Sever, and P. Vieira, *Bootstrapping Null Polygon Wilson Loops*, *JHEP* **1103** (2011) 092, [arXiv:1010.5009].

[59] D. Gaiotto, J. Maldacena, A. Sever, and P. Vieira, *Pulling the straps of polygons*, *JHEP* **1112** (2011) 011, [arXiv:1102.0062].

[60] A. Sever, P. Vieira, and T. Wang, *OPE for Super Loops*, *JHEP* **1111** (2011) 051, [arXiv:1108.1575].

[61] B. Basso, A. Sever, and P. Vieira, *Space-time S-matrix and Flux-tube S-matrix at Finite Coupling*, *Phys.Rev.Lett.* **111** (2013) 091602, [arXiv:1303.1396].

[62] B. Basso, A. Sever, and P. Vieira, *Space-time S-matrix and Flux tube S-matrix II. Extracting and Matching Data*, *JHEP* **1401** (2013) 008, [arXiv:1306.2058].

[63] B. Basso, A. Sever, and P. Vieira, *Space-time S-matrix and Flux-tube S-matrix III. The two-particle contributions*, arXiv:1402.3307.

[64] B. Basso, *Exciting the GKP string at any coupling*, *Nucl.Phys.* **B857** (2012) 254–334, [arXiv:1010.5237].

[65] B. Basso and A. Rej, *Bethe ansätze for GKP strings*, *Nucl.Phys.* **B879** (2014) 162–215, [arXiv:1306.1741].

[66] Y. V. Kovchegov and E. Levin, *Quantum Chromodynamics at High Energy*. Cambridge University Press, 2012.

[67] L. Lipatov, *High-energy asymptotics of multicolor QCD and exactly solvable lattice models*, hep-th/9311037.

[68] L. Lipatov, *Asymptotic behavior of multicolor QCD at high energies in connection with exactly solvable spin models*, *JETP Lett.* **59** (1994) 596–599.

[69] L. Faddeev and G. Korchemsky, *High-energy QCD as a completely integrable model*, *Phys.Lett.* **B342** (1995) 311–322, [hep-th/9404173].

[70] L. J. Dixon, C. Duhr, and J. Pennington, *Single-valued harmonic polylogarithms and the multi-Regge limit*, *JHEP* **1210** (2012) 074, [arXiv:1207.0186].

[71] V. Del Duca, L. J. Dixon, C. Duhr, and J. Pennington, *The BFKL equation, Mueller-Navelet jets and single-valued harmonic polylogarithms*, *JHEP* **1402** (2014) 086, [arXiv:1309.6647].

[72] S. Caron-Huot, *When does the gluon reggeize?*, arXiv:1309.6521.

[73] H. Johansson, A. Sabio Vera, E. Serna Campillo, and M. A. Vazquez-Mozo, *Color-Kinematics Duality in Multi-Regge Kinematics and Dimensional Reduction*, *JHEP* **1310** (2013) 215, [arXiv:1307.3106].

[74] H. Johansson, A. Sabio Vera, E. Serna Campillo, and M. A. Vazquez-Mozo, *Color-kinematics duality and dimensional reduction for graviton emission in Regge limit*, arXiv:1310.1680.

[75] J. Bartels, L. Lipatov, and A. Sabio Vera, *N=4 supersymmetric Yang Mills scattering amplitudes at high energies: The Regge cut contribution*, *Eur.Phys.J.* **C65** (2010) 587–605, [arXiv:0807.0894].

[76] L. N. Lipatov and A. Prygarin, *BFKL approach and six-particle MHV amplitude in $\mathcal{N} = 4$ super Yang-Mills*, *Phys.Rev.* **D83** (2010) 125001, [arXiv:1011.2673].

[77] J. Bartels, V. Schomerus, and M. Sprenger, *Multi-Regge Limit of the n-Gluon Bubble Ansatz*, *JHEP* **11** (2012) 145, [arXiv:1207.4204].

[78] J. Bartels, J. Kotanski, and V. Schomerus, *Excited Hexagon Wilson Loops for Strongly Coupled $\mathcal{N} = 4$ SYM*, *JHEP* **1101** (2010) 096, [arXiv:1009.3938].

[79] J. Bartels, J. Kotanski, V. Schomerus, and M. Sprenger, *The Excited Hexagon Reloaded*, arXiv:1311.1512.

[80] J. Bartels, V. Schomerus, and M. Sprenger, *Heptagon Amplitude in the Multi-Regge Regime*, arXiv:1405.3658.

[81] M. Sohnius, *Introducing Supersymmetry*, *Phys.Rept.* **128** (1985) 39–204.

[82] J. M. Henn and J. C. Plefka, *Scattering Amplitudes in Gauge Theories*, *Lect.Notes Phys.* **883** (2014).

[83] S. Mandelstam, *Light Cone Superspace and the Ultraviolet Finiteness of the $N = 4$ Model*, *Nucl.Phys.* **B213** (1983) 149–168.

[84] L. Brink, O. Lindgren, and B. E. Nilsson, *The Ultraviolet Finiteness of the $N = 4$ Yang-Mills Theory*, *Phys.Lett.* **B123** (1983) 323.

[85] S. Gubser, I. R. Klebanov, and A. M. Polyakov, *Gauge theory correlators from noncritical string theory*, *Phys.Lett.* **B428** (1998) 105–114, [hep-th/9802109].

[86] E. Witten, *Anti-de Sitter space and holography*, *Adv.Theor.Math.Phys.* **2** (1998) 253–291, [hep-th/9802150].

[87] O. Aharony, S. S. Gubser, J. M. Maldacena, H. Ooguri, and Y. Oz, *Large N field theories, string theory and gravity*, *Phys.Rept.* **323** (2000) 183–386, [hep-th/9905111].

[88] E. D'Hoker and D. Z. Freedman, *Supersymmetric gauge theories and the AdS / CFT correspondence*, hep-th/0201253.

[89] N. Beisert, C. Ahn, L. F. Alday, Z. Bajnok, J. M. Drummond, et al., *Review of AdS/CFT Integrability: An Overview*, *Lett.Math.Phys.* **99** (2012) 3–32, [arXiv:1012.3982].

[90] L. F. Alday, *Review of AdS/CFT Integrability, Chapter V.3: Scattering Amplitudes at Strong Coupling*, *Lett.Math.Phys.* **99** (2010) 507–528, [arXiv:1012.4003].

[91] D. J. Gross and P. F. Mende, *The High-Energy Behavior of String Scattering Amplitudes*, *Phys.Lett.* **B197** (1987) 129.

[92] D. J. Gross and P. F. Mende, *String theory beyond the Planck scale*, *Nucl.Phys.* **B303** (1988) 407–454.

[93] N. Berkovits and J. Maldacena, *Fermionic T-Duality, Dual Superconformal Symmetry, and the Amplitude/Wilson Loop Connection*, *JHEP* **0809** (2008) 062, [arXiv:0807.3196].

[94] N. Beisert, R. Ricci, A. Tseytlin, and M. Wolf, *Dual Superconformal Symmetry from $AdS_5 \times S^5$ Superstring Integrability*, *Phys.Rev.* **D78** (2008) 126004, [arXiv:0807.3228].

[95] T. H. Buscher, *Path Integral Derivation of Quantum Duality in Nonlinear Sigma Models*, *Phys.Lett.* **B201** (1987) 466.

[96] J. McGreevy and A. Sever, *Quark scattering amplitudes at strong coupling*, *JHEP* **0802** (2008) 015, [arXiv:0710.0393].

[97] S. Forste, D. Ghoshal, and S. Theisen, *Stringy Corrections to the Wilson Loop in $\mathcal{N} = 4$ Super Yang-Mills Theory*, *JHEP* **9908** (1999) 013, [hep-th/9903042].

[98] J. M. Maldacena, *Wilson loops in large N field theories*, *Phys.Rev.Lett.* **80** (1998) 4859–4862, [hep-th/9803002].

[99] S.-J. Rey and J.-T. Yee, *Macroscopic strings as heavy quarks in large N gauge theory and anti-de Sitter supergravity*, *Eur.Phys.J.* **C22** (2001) 379–394, [hep-th/9803001].

[100] S. Caron-Huot, *Notes on the scattering amplitude / Wilson loop duality*, *JHEP* **1107** (2011) 058, [arXiv:1010.1167].

[101] L. Mason and D. Skinner, *The Complete Planar S-matrix of $\mathcal{N} = 4$ SYM as a Wilson Loop in Twistor Space*, *JHEP* **1012** (2010) 018, [arXiv:1009.2225].

[102] A. Belitsky, G. Korchemsky, and E. Sokatchev, *Are scattering amplitudes dual to super Wilson loops?*, *Nucl.Phys.* **B855** (2012) 333–360, [arXiv:1103.3008].

[103] L. F. Alday, B. Eden, G. P. Korchemsky, J. Maldacena, and E. Sokatchev, *From correlation functions to Wilson loops*, *JHEP* **1109** (2011) 123, [arXiv:1007.3243].

[104] B. Eden, G. P. Korchemsky, and E. Sokatchev, *From correlation functions to scattering amplitudes*, *JHEP* **1112** (2011) 002, [arXiv:1007.3246].

[105] B. Eden, G. P. Korchemsky, and E. Sokatchev, *More on the duality correlators/amplitudes*, *Phys.Lett.* **B709** (2012) 247–253, [arXiv:1009.2488].

[106] T. Adamo, M. Bullimore, L. Mason, and D. Skinner, *A Proof of the Supersymmetric Correlation Function / Wilson Loop Correspondence*, *JHEP* **1108** (2011) 076, [arXiv:1103.4119].

[107] B. Eden, P. Heslop, G. P. Korchemsky, and E. Sokatchev, *The super-correlator/super-amplitude duality: Part I*, *Nucl.Phys.* **B869** (2013) 329–377, [arXiv:1103.3714].

[108] B. Eden, P. Heslop, G. P. Korchemsky, and E. Sokatchev, *The super-correlator/super-amplitude duality: Part II*, *Nucl.Phys.* **B869** (2013) 378–416, [arXiv:1103.4353].

[109] Z. Komargodski and S. S. Razamat, *Planar quark scattering at strong coupling and universality*, *JHEP* **0801** (2007) 044, [arXiv:0707.4367].

[110] E. Barnes and D. Vaman, *Massive quark scattering at strong coupling from AdS/CFT*, *Phys.Rev.* **D81** (2009) 126007, [arXiv:0911.0010].

[111] K. Ito, H. Nastase, and K. Iwasaki, *Gluon scattering in $\mathcal{N} = 4$ Super Yang-Mills at finite temperature*, *Prog.Theor.Phys.* **120** (2007) 99–128, [arXiv:0711.3532].

[112] G. Georgiou and D. Giataganas, *Gluon Scattering Amplitudes in Finite Temperature Gauge/Gravity Dualities*, *JHEP* **1108** (2010) 045, [arXiv:1011.6339].

[113] Y. Oz, S. Theisen, and S. Yankielowicz, *Gluon Scattering in Deformed $N = 4$ SYM*, *Phys.Lett.* **B662** (2007) 297–301, [arXiv:0712.3491].

[114] A. Kuniba, T. Nakanishi, and J. Suzuki, *T-systems and Y-systems in integrable systems*, *J.Phys.* **A44** (2011) 103001, [arXiv:1010.1344].

[115] G. Yang, *Scattering amplitudes at strong coupling for $4K$ gluons*, *JHEP* **1012** (2010) 082, [arXiv:1004.3983].

[116] D. Gaiotto, G. W. Moore, and A. Neitzke, *Wall-crossing, Hitchin Systems, and the WKB Approximation*, arXiv:0907.3987.

[117] V. Del Duca, *An introduction to the perturbative QCD pomeron and to jet physics at large rapidities*, hep-ph/9503226.

[118] J. Bartels, L. N. Lipatov, and A. Prygarin, *Collinear and Regge behavior of $2 \to 4$ MHV amplitude in $N = 4$ super Yang-Mills theory*, arXiv:1104.4709.

[119] J. R. Forshaw and D. Ross, *Quantum chromodynamics and the pomeron*, *Cambridge Lect.Notes Phys.* **9** (1997) 1–248.

[120] R. Brower, C. E. DeTar, and J. Weis, *Regge Theory for Multiparticle Amplitudes*, *Phys.Rept.* **14** (1974) 257.

[121] E. A. Kuraev, L. N. Lipatov, and V. S. Fadin, *Multi - Reggeon Processes in the Yang-Mills Theory*, *Sov.Phys.JETP* **44** (1976) 443–450.

[122] J. Bartels, *High-Energy Behavior in a Nonabelian Gauge Theory. 1. $T_{n\to m}$ in the Leading ln s Approximation*, *Nucl.Phys.* **B151** (1979) 293.

[123] E. Kuraev, L. Lipatov, and V. S. Fadin, *The Pomeranchuk Singularity in Nonabelian Gauge Theories*, *Sov.Phys.JETP* **45** (1977) 199–204.

[124] I. Balitsky and L. Lipatov, *The Pomeranchuk Singularity in Quantum Chromodynamics*, *Sov.J.Nucl.Phys.* **28** (1978) 822–829.

[125] J. Bartels, *High-Energy Behavior in a Nonabelian Gauge Theory. 2. First Corrections to $T_{n\to m}$ Beyond the Leading ln s Approximation*, *Nucl.Phys.* **B175** (1980) 365.

[126] J. Kwiecinski and M. Praszalowicz, *Three Gluon Integral Equation and Odd c Singlet Regge Singularities in QCD*, *Phys.Lett.* **B94** (1980) 413.

[127] J. Weis, *Factorization of multi-regge amplitudes*, *Phys.Rev.* **D4** (1971) 1777–1787.

[128] J. Weis, *Factorization of multi-regge amplitudes. II*, *Phys.Rev.* **D5** (1972) 1043–1047.

[129] O. Steinmann, *Über den Zusammenhang zwischen den Wightmanfunktionen und den retardierten Kommutatoren*, *Helv. Phys. Acta* **33** (1960) 257.

[130] V. Fadin and L. Lipatov, *BFKL equation for the adjoint representation of the gauge group in the next-to-leading approximation at $N = 4$ SUSY*, *Phys.Lett.* **B706** (2012) 470–476, [arXiv:1111.0782].

[131] B. Basso, "*Flux-tube methods for scattering amplitudes in planar N=4 SYM theory*." Talk at the 'Scattering Amplitudes & the Multi-Regge Limit 2014' in Madrid, 2014.

[132] P. Dorey, "*Exact finite-size effects in relativistic field theories*." Talk at the 'IGST 2008' in Utrecht, slides available at http://testweb.science.uu.nl/IGST08/pdf/Dorey.pdf, 2008.

[133] P. Dorey and R. Tateo, *Excited states by analytic continuation of TBA equations*, *Nucl.Phys.* **B482** (1996) 639–659, [hep-th/9607167].

[134] P. Dorey and R. Tateo, *Excited states in some simple perturbed conformal field theories*, *Nucl.Phys.* **B515** (1998) 575–623, [hep-th/9706140].

[135] F. W. J. Olver, D. W. Lozier, R. F. Boisvert and C. W. Clark, ed., *NIST Handbook of Mathematical Functions*. Cambridge University Press, 2010.

[136] J. Bartels, A. Kormilitzin, L. Lipatov, and A. Prygarin, *BFKL approach and $2 \to 5$ maximally helicity violating amplitude in $\mathcal{N} = 4$ super-Yang-Mills theory*, *Phys.Rev.* **D86** (2012) 065026, [arXiv:1112.6366].

[137] J. Bartels, A. Kormilitzin, and L. Lipatov, *Analytic structure of the $n = 7$ scattering amplitude in $\mathcal{N} = 4$ SYM theory at multi-Regge kinematics: Conformal Regge pole contribution*, *Phys.Rev.* **D89** (2014) 065002, [arXiv:1311.2061].

[138] J. Bartels, A. Kormilitzin, and L. Lipatov, *in preparation*, .

[139] S. Caron-Huot, *Superconformal symmetry and two-loop amplitudes in planar N=4 super Yang-Mills*, *JHEP* **1112** (2011) 066, [arXiv:1105.5606].

[140] J. Golden, M. F. Paulos, M. Spradlin, and A. Volovich, *Cluster Polylogarithms for Scattering Amplitudes*, arXiv:1401.6446.

[141] J. Golden, A. B. Goncharov, M. Spradlin, C. Vergu, and A. Volovich, *Motivic Amplitudes and Cluster Coordinates*, *JHEP* **1401** (2014) 091, [arXiv:1305.1617].

[142] G. Yang, *A simple collinear limit of scattering amplitudes at strong coupling*, *JHEP* **1103** (2011) 087, [arXiv:1006.3306].

[143] B. Eden, P. Heslop, G. P. Korchemsky, and E. Sokatchev, *Constructing the correlation function of four stress-tensor multiplets and the four-particle amplitude in $\mathcal{N} = 4$ SYM*, *Nucl.Phys.* **B862** (2012) 450–503, [arXiv:1201.5329].

Eidesstattliche Erklärung
Hiermit erkläre ich an Eides statt, dass ich die vorliegende Dissertationsschrift selbst verfasst und keine anderen als die angegebenen Quellen und Hilfsmittel benutzt habe.

Hamburg, den 28. Mai 2014

Martin Sprenger